Exploring Ligand-Enabled Nickel-Catalyzed Cross-Coupling of Sulfur-based Nucleophiles

By

Connor M. Simon

Submitted in partial requirement

for the degree of Master of Science

at

Dalhousie University

Halifax, Nova Scotia

December 2022

© Copyright by Connor M. Simon, 2022

Table of Contents

List of Figures

Abstract

The catalytic synthesis of C(sp^2)-N linkages is of utmost significance in modern synthetic chemistry, predominantly due to their prevalence in active pharmaceutical ingredients and natural products. Pd-catalyzed cross-couplings of this type, known colloquially as Buchwald-Hartwig amination (BHA), represent a tremendously important class of reactions in research and industrial settings. The success achieved by BHA can largely be attributed to the rational design of ancillary ligands specifically configured to exploit the natural electronic characteristics of the Pd metal centre. Research efforts surrounding the BHA reaction have enabled the scope of suitable coupling partners to grow rapidly, encompassing a vast array of (hetero)aryl (pseudo)halides and NH couplings partners.

Notwithstanding the value of the BHA reaction, concerns over the rising costs of Pd and subsequent sustainability issues have prompted researchers to seek economical methods for accessing these linkages. One of the most promising alternatives to Pd-catalysis is the developing field of its 3*d* congener, Ni. However, given the relatively underdeveloped nature of Ni-catalyzed C-N bond formation, many questions regarding the mechanistic underpinnings and scope limitations remain unanswered. In this thesis, my contributions include experimental investigations into the elementary steps of a successful Ni-catalyzed cross-coupling. The successful synthesis and characterization of primary Ni-NHR catalytic intermediates reveal previously undocumented C-N bond-forming pathways, and the implementation of the mechanistic lessons learned from these studies allow for the discovery of new ligand-enabled Ni-catalyzed C-N cross-couplings.

List of Abbreviations Used

Ar	aryl
bpy	bipyridine
BHA	Buchwald-Hartwig amination
BINAP	2,2’-bis(diphenylphosphino)-1,1’-binaphthalene
BTPP	tert-Butylimino-tri(pyrrolidino)phosphorane
COD	1,5-cyclooctadiene
CgP	1,3,5,7-tetramethyl-2,4,8-trioxa-6-phosphaadamantane
δ	chemical shift
DBU	1,8-diazabicyclo[5.4.0]undec-7-ene
DCM	dichloromethane
dcype	1,1-bis(dicyclohexylphosphino)ethane
DFT	density functional theory
DPEPhos	bis[(2-diphenyphosphino)phenyl] ether
dppf	1,1’-bis(diphenylphosphino)ferrocene
ESI	electrospray ionization
EtOAc	ethyl acetate
GC	gas chromatography
HMDS	hexamethyldisilazane
HPLC	high-performance liquid chromatography
HRMS	high-resolution mass spectrometry
J	linear coupling constant
NMR	nuclear magnetic resonance

OMs	mesylate
OTs	tosylate
OTf	triflate
PTFE	polytetrafluoroethylene
RVC	reticulated vitreous carbon
SET	single electron transfer
S_NAr	nucleophilic aromatic substitution
TFA	trifluoroacetate
THF	tetrahydrofuran
UDEFT	uniform driven equilibrium Fourier transform
UV	ultraviolet
X	halide substituent

Acknowledgements

The pursuit of this MSc has at times been an arduous task, and I wish to extend my sincerest gratitude to the numerous people who have helped me over the course of my time here:

- My supervisor, Mark Stradiotto. I am enormously grateful for your support and guidance throughout this program. You are an exceptional mentor both in the lab and in life. Your dedication to both the success and well-being of your group is something to aspire to. Thank you for everything, Mark.
- Members of the Stradiotto group, including past (Dr. Joseph Tassone, Dr. Ryan McGuire, Dr. Travis Lundrigan, Dr. Karlee Bamford, and Dr. Casper Macaulay), and present (Kathleen, Nick, Josh, Sam F., Nicole, Dr. Tim Anderson, Peter, and Mike). I deeply appreciate the company, knowledge, and guidance offered by all of you during my time in the group. A special thank you to Ryan and Joseph for providing such a positive welcome to the group, your combined mentorship was instrumental in this process.
- My friends, here and back home. Thank you for your endless support, know that even though I don't say it enough, I am grateful for all of you.
- My partner, this would have been a much more difficult task without your boundless support, patience, and positivity. Thank you for everything that you do. I love you.
- Most importantly, to my family: Mom, Dad, Alyssa, and Katherine, thank you all for always being just a phone call away. I know I don't open up much, but please know that I love you and I truly appreciate the support provided by each of you.

Chapter 1. Introduction

1.1 Overview

The utility of homogeneous transition metal catalysts in the modern pharmaceutical and agrochemical industries cannot be overstated.[1] Given the often-complex structural nature of active pharmaceutical ingredients, the design of tailored ancillary ligands to enable intricate metal-catalyzed chemical transformations has become an area of great interest. The capacity of designer ligands to finely tune the steric and electronic properties of a given transition metal is perhaps most pervasive in cross-coupling reactivity involving C-X bond formation (X = C, N, O, S, P, etc.).[2] Cross-couplings of this type have found extensive use in the derivatization of diverse bio-active structural motifs, with several decades of research having established the chemical equivalent of a tool library for the synthetic chemist.[3]

From the growing field of pharmaceutical discovery, there is great interest in the development of practical synthetic methodology for the formation of C(sp^2)-N bonds, as the resulting hetero(aniline) moieties have shown promising bioactivities in many cases.[3,4] Traditionally synthesized through nucleophilic aromatic substitution (S_NAr) methods from (hetero)aryl halides,[5] or from well-established nitration-reduction reactions,[6] both techniques often require elevated temperatures and/or strongly basic/acidic conditions. These can introduce limitations with functional group tolerance and late-stage functionalization of complicated structures. The advent of Pd-catalyzed C(sp^2)-N cross-coupling (herein Buchwald-Hartwig Amination, BHA) between (hetero)aryl (pseudo)halides and suitably nucleophilic NH substrates has served to address the previously mentioned challenges associated with hetero(aniline) synthesis.[3,7] The notable

achievements of BHA, in particular the wide-reaching scope of NH coupling partners, can largely be attributed to intelligent ancillary ligand design.[8] The introduction of this cross-coupling methodology has inspired a family of highly efficient Pd catalysts.[3] However, concerns over the relatively low Earth-abundance of Pd and its consequential cost barriers have led to a dramatic shift in transition metal research. Contemporary research has shown that base metals such as Ni[9] and Cu[10] can offer comparable, complimentary, or even superior reactivity to Pd in some cases. Importantly, Ni-based catalysts have shown successful application in the activation of cheap and abundant (hetero)aryl chloride electrophiles, as well as (hetero)aryl (pseudo)halide electrophiles.[11]

1.2 Buchwald-Hartwig Amination

The Pd-catalyzed C(sp^2)-N cross-coupling reaction, now colloquially known as Buchwald-Hartwig amination (BHA), was independently invented in 1995 by the research groups of Stephen L. Buchwald and John F. Hartwig.[12,13] Beginning with the initial cross-coupling of aryl bromides with aliphatic amines, this reaction template rapidly expanded to cover a wide scope of both electrophiles and nucleophiles. In a BHA reaction, a ligated Pd species catalyzes the cross-coupling of a (hetero)aryl (pseudo)halide with a given NH partner in a well understood $Pd^{0/II}$ cycle.[7,14] The scope of electrophiles encompasses aryl chlorides, bromides, and iodides, as well as select pseudohalides such as aryl mesylates, tosylates, and triflates.[15] On the nucleophile side, a wide range of nitrogen containing compounds have been accommodated, including primary and secondary aliphatic amines, hydrazines, amides, and sulfinamides.[7,16]

The catalytic mechanism of BHA closely mirrors those of other well-known Pd cross-coupling reactions (**Figure 1.1**).[7] Beginning with either an ancillary ligand and Pd

source, or a ligated Pd precatalyst, the active catalytic species oxidatively adds the corresponding aryl electrophile, generating a Pd^{II}(aryl)(X) species. The nitrogen-containing nucleophile then coordinates to the metal centre and is subsequently deprotonated to yield a Pd^{II}(aryl)(amido) complex. From this intermediate, reductive elimination occurs, yielding the desired *N*-arylamine and regenerating the active Pd^0 complex, thus turning over the catalytic cycle. Given the mechanistic details that have been extracted from the BHA reaction, the design and implementation of ancillary ligands to optimize reactivity has been studied thoroughly. Oxidative addition is aided via the use of strongly electron-donating ligands, which increases the electron density around the metal centre. This, in turn, promotes the oxidative addition of challenging electrophiles such as (hetero)aryl chlorides. Sterically encumbering ligands are also often found in BHA chemistry, which promote the formation of the coordinatively unsaturated Pd^0 species active in catalysis. The use of bulky ligands also encourages reductive elimination via the driving force of steric relief.[8]

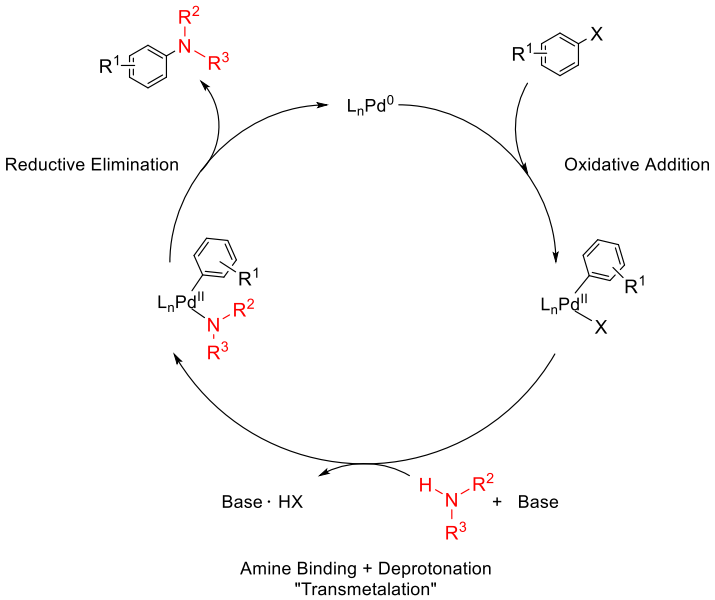

Figure 1.1. Established mechanism of the Buchwald-Hartwig amination reaction.

Dialkylmonophosphine ligands bearing a substituted biaryl backbone such as **XPhos**, **SPhos**, and **RuPhos,** are characteristic of the work from the Buchwald research group.[7,8] Complementarily, bisphosphine ligands featuring a ferrocenyl backbone, known broadly as the **JosiPhos** ligand family, have proven extremely effective in this chemistry, particularly in the Pd-precatalysts developed by the Hartwig group (**Figure 1.2**).[17] Monoligated Pd species have been shown to benefit the metal centre in two distinct ways: *i*) by providing stability to the active Pd^0 complex and allowing the aryl electrophile closer access to the metal; and *ii*) the dialkyl groups directly bound to the phosphorus atom provide increased electron density to the Pd centre, thus enabling oxidative addition. Bidentate Pd complexes benefit from reduced ligand dissociation, which discourages undesirable β-hydride elimination. Additionally, the increased steric bulk of bisphosphine ligands on a coordinatively saturated Pd centre can enforce a geometry resembling that of the reductive elimination transition state.[14]

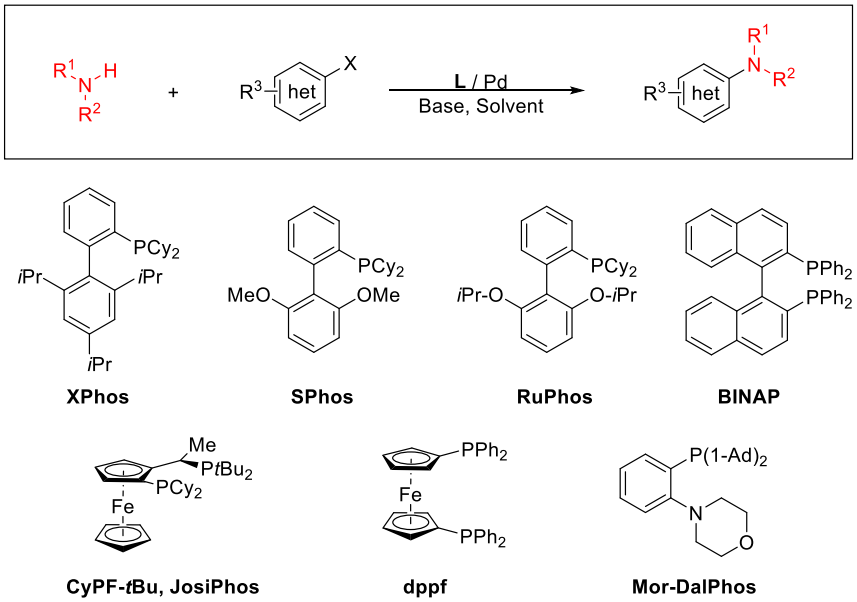

Figure 1.2. Select designer ligands in Buchwald-Hartwig Amination chemistry.

Another class of chelating ligands, known as hybrid ligands, utilize mixed P,N or P,O donor groups. These hybrid structures are complimentary in nature to the binding modes of monophosphine and bisphosphine ligands; wherein the harder N or O fragment can reversibly coordinate to the metal centre, which offers flexibility to the electronic structure of the catalyst throughout the course of the cycle. The Stradiotto group has had remarkable success implementing this strategy with **Mor-DalPhos** - a hybrid ligand that enables difficult reactivities such as the monoarylation of ammonia and the activation of aryl chlorides under diverse conditions.[18]

Notwithstanding the efficacy of Pd-based catalytic systems in the field of C-N cross-coupling, the prohibitive cost and limited abundance of Pd has prompted researchers to seek comparable reactivities from the more Earth-abundant base metals such as Ni and Cu. Cu-catalyzed alternatives to BHA, namely Ullmann reactions, demonstrate the possibility of accessible 3*d*-block metals enabling aryl amination.[19a] Though fundamentally different, the Cu-catalyzed Chan-Lam cross-coupling reaction has proven to be a very efficient method of accessing C-heteroatom bonds.[19b] However, these reactions often require high catalyst loadings and are limited in scope (i.e., poor compatibility with the (hetero)aryl chlorides and pseudohalides). Considering this, the 3*d* congener of Pd has emerged as a promising alternative in C-N cross-coupling. While research into Ni-catalyzed C-N bond formation is still relatively young, numerous advancements have been made displaying similar, or in some cases superior reactivity to Pd catalysis.[11]

1.3 Ni-catalyzed C-N Cross-Coupling

1.3.1 Overview of Ni-catalyzed C-N cross-coupling

Following the shift in research focus from heavier Pt group catalysts, Ni has proven to be one of the most promising candidates for broad-scope base metal reactivity - accommodating numerous NH substrates including ammonia, indoles, sulfonamides, and azoles.[20,21] The harder, more electropositive nature of the Ni centre also allows for more facile oxidative addition into difficult C(sp^2)-X bonds, therefore expanding the scope of available coupling partners to include phenol derivatives and (hetero)aryl chlorides which are often challenging in BHA. The mechanism of the BHA reaction is well understood to operate via a $Pd^{0/II}$ cycle; however, the mechanistic underpinnings of Ni-catalysis are often more complex. Experimental and computational evidence suggest the possibility of Ni operating in both "Pd-like" $Ni^{0/II}$ and $Ni^{I/III}$ catalytic cycles.[22] Furthermore, the propensity of Ni to undergo single electron transfer (SET) processes such as comproportionation and disproportionation present the possibility of both cycles being active during a single catalytic reaction (**Figure 1.3**).[9,22a]

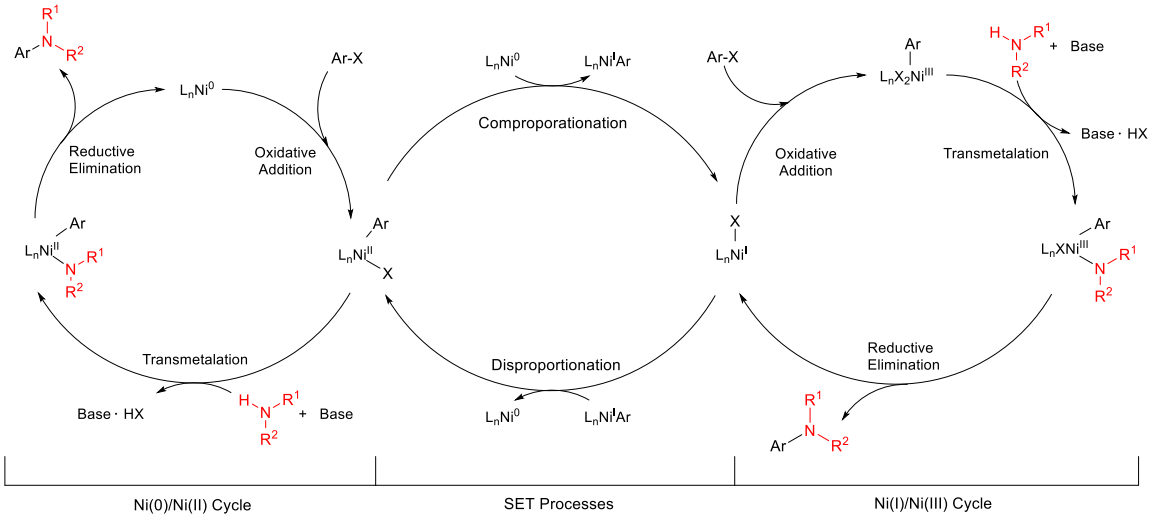

Figure 1.3. Proposed general mechanisms for Ni-catalyzed C-N cross coupling reactions showing the possible interplay between $Ni^{0/II}$ and $Ni^{I/III}$ catalytic cycles.

The inherent complexity of the Ni-catalyzed cross-coupling mechanism has generated numerous creative strategies designed to harness one, or in some cases both, of the primary catalytic cycles of Ni. For example, tailored ancillary ligands containing bulky, electron poor groups are capable of forcing the metal centre geometry into conformations consistent with $Ni^{0/II}$ reactivity,[11] whereas redox catalysis has demonstrated the power of accessing higher Ni oxidation states to facilitate reductive elimination.[23] These complementary processes have each contributed strongly to the evolution of Ni catalysis as a whole and will be discussed herein.

1.3.2 Redox-mediated Ni-catalyzed C-N cross-coupling

As discussed previously, redox chemistry can be an extremely effective methodology for enabling Ni-catalyzed C-N cross-coupling. Through electrochemical or photochemical stimulus, the susceptibility of Ni to undergo SET processes can be taken advantage of directly. Often, these methods target higher oxidation states (i.e., Ni^{III}) as a means of accelerating reductive elimination, which is commonly considered rate limiting in Ni catalysis. Both methods are generally capable of employing highly economical NiX_2 salts and comparatively simple N-donor ligands.[23,24]

The first popularization of photoredox-enabled C-N cross-coupling came from the research groups of MacMillan and Buchwald,[25] where they achieved the amination of (hetero)aryl bromides with a NiX_2·(glyme) catalyst and an iridium-based polypyridyl photocatalyst (**Figure 1.4A**). Since the advent of this technique, numerous groups have utilized the relatively accessible catalysts to enable transformations of a wide variety of NH substrates including sulfonamides, sulfoximines, and diverse primary aliphatic amines.[26] The current mechanistic understanding of these photoredox-enabled reactivities

points to a key SET process between the excited Ir photocatalyst and the transmetalated $Ni^{II}(aryl)(NR_2)$ species. This raises the oxidation state of the central metal to Ni^{III}, which is thought to undergo reductive elimination more readily than the corresponding Ni^{II} complex.[27]

A complementary process to photoredox catalysis is the direct use of electrochemical methods, popularized mainly by the research group of Phil S. Baran. In these reactions, the transmetalated $Ni^{II}(aryl)(NR_2)$ species is oxidized at the anode of an electrochemical cell, yielding the resultant Ni^{III} complex from which reductive elimination can readily occur. Analogous to the previously discussed photochemically enabled processes, the putative high-valent Ni intermediates are presumably supported by hard N-donor ligands (**Figure 1.4B**).[23]

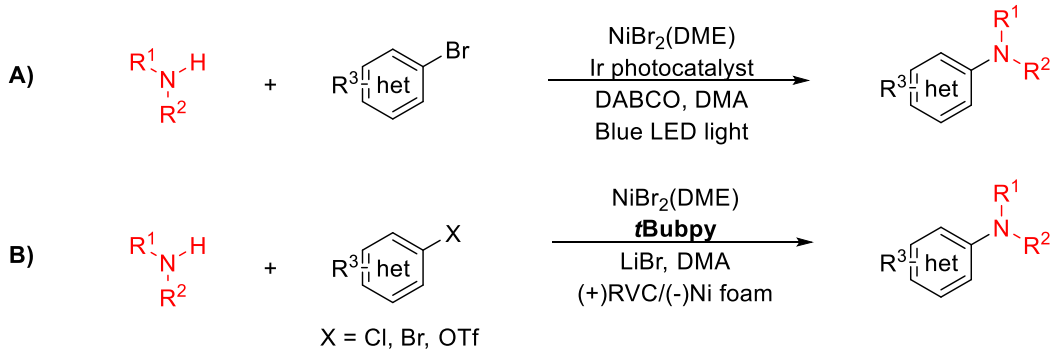

Figure 1.4. Examples of catalytic conditions for A) Ni/Ir photoredox catalyzed C-N cross-coupling, and B) electrochemically driven C-N cross-coupling.

While both redox methods have proven effective in C-N cross-coupling reactions, several limitations exist. For example, the precious Ir photocatalyst can present cost and sustainability issues, the activation of more difficult aryl-X electrophiles (X = Cl, OMs, OTs, OTf) is frequently not possible, and reactor design can be complex, leading to difficulties in scaling these reactions.[25,26] Interestingly, recent advancements in photoredox-enabled cross-coupling have revealed the possibility of promoting reactivity

without the need for exogenous Ir photocatalyst.[28] Nevertheless, several research groups including the Stradiotto group have sought alternative methods for effecting these difficult reactivities, primarily through the field of rational ligand design.

1.3.3 Ligand-enabled Ni-catalyzed C-N cross-coupling

An alternative approach to Ni-catalyzed C-N bond cross-coupling involves a method that closely mirrors what has been well-established in BHA chemistry. The coordination of relatively soft ancillary ligands (i.e., mono- or bisphosphines) to the metal centre is thought to promote reactivity that mimics the $Pd^{0/II}$ cycles discussed previously. This method has already shown best-in-class ability in regard to the activation of otherwise challenging aryl electrophiles (e.g., aryl chlorides, phenol derivatives), which has the immediate impact of broadening the available substrate scope.[11] However, given the mechanistic complexities that can arise from SET processes, the design and implementation of successful ancillary ligands has proven to be difficult.

Initial research into ligand-enabled Ni-catalyzed C-N cross-coupling often involved the repurposing of BHA ligands for use with a Ni metal centre. Standout bisphosphine Pd ligands such as **dppf**, **BINAP**, and **JosiPhos** ligands have all shown promising reactivities when applied to Ni-catalyzed cross-couplings (**Figure 1.2**).[29] However, a number a state-of-the-art BHA ligands such as Buchwald's biphenyl monophosphines (i.e., **SPhos**, **XPhos**, **RuPhos**), and Stradiotto's **Mor-DalPhos** have proven less efficient when applied to Ni catalysis.[11] This is likely due to the subtle, yet nonzero differences in electronic structure between Ni and Pd. As discussed in Section 1.2 of this chapter, Pd ligands are often strongly electron-donating mono- or bisphosphines, which electronically enrich the metal centre and improve the rate of oxidative addition. However, in the case of Ni, where

the metal itself is harder and more electropositive, oxidative addition proceeds much more readily.[9] Therefore, ligands designed specifically for use in Ni-catalyzed cross-couplings often feature relatively electron poor groups, as these can facilitate reductive elimination. Another prominent feature in Ni ligand design is a large degree of steric bulk. This has the dual effect of promoting reductive elimination via the relief of steric congestion, and the minimization of Ni-Ni SET interactions such as comproportionation or disproportionation (**Figure 1.3**).[11]

The Stradiotto group has spent recent years developing what are now a premier class of ligands specifically for use in Ni-catalysis, known as the **PAd-DalPhos** ligand family (**Figure 1.5**). The original **PAd-DalPhos** ligand featured a bisphosphine structure with a bulky, yet electron-poor "cage-phosphine" (CgP) group, which has proven to be highly effective in the Ni-catalyzed monoarylation of ammonia.[29] Using the CgP bisphosphine framework, several derivatives of the original ligand have also proven successful: using the CgP bisphosphine framework, several derivatives of the original ligand have also proven successful: **CyPAd-DalPhos** (**L1**), featuring a PCy_2 donor promotes the cross-coupling of cyclopropylamines and aliphatic alcohols; inclusion of a PPh_2 donor as in **PhPAd-DalPhos** (**L2**) enables the cross-coupling of bulky amines and sulfonamides; **PAd2-DalPhos** has shown stellar performance in the cross-couplings of primary heteroarylamines and fluoroalkylamines.[21,30] Successes have been found outside of the PCg fragment as well: *N*-heterocyclic phosphine-containing **NHP-DalPhos** enables the room-temperature cross-coupling of primary amines; and phosphonite-containing **Phen-DalPhos** can access heteroaniline and ammonia nucleophiles.[31] Interestingly, while unrelated to C-N cross-coupling, combining the bulky phosphonite donor with the bulky

PCg fragment generates a ligand (**CgPhen-DalPhos**) capable of cross-coupling tertiary aliphatic alcohols with (hetero)aryl (pseudo)halides, a notoriously difficult reaction.[32]

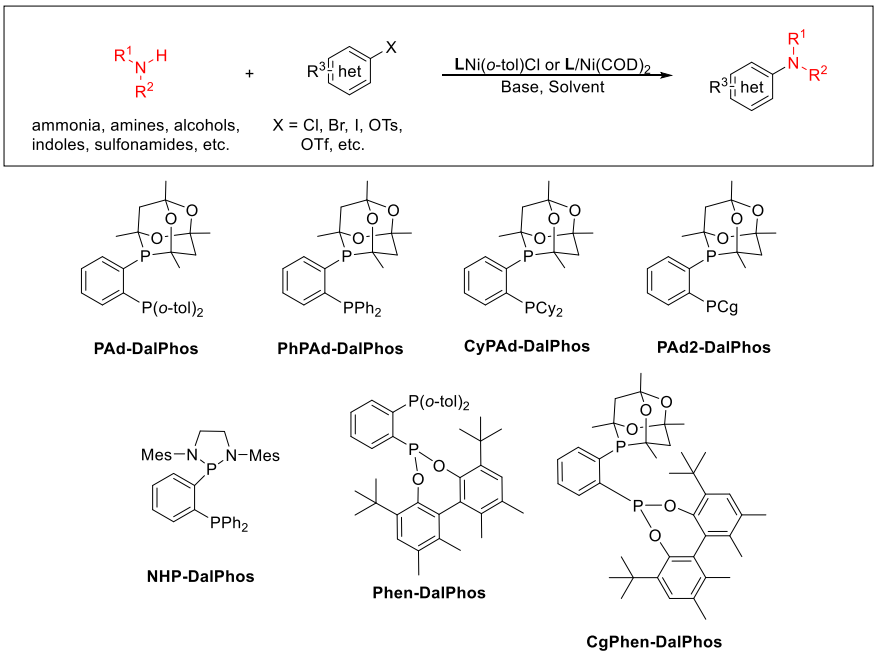

Figure 1.5. A general reaction scheme for ligand-enabled Ni-catalyzed cross-coupling with several **DalPhos** ligands featured.

1.4 Thesis Research Focus

Due to the combined efforts of numerous research groups, the field of Ni-catalyzed cross-coupling has expanded rapidly in the last number of years. Ni now represents a premier choice for the synthetic chemist seeking broad-scope reactivity at sustainable cost and availability. Through both redox-enabled and ligand-enabled methodologies, industries once dominated by Pd catalysis can now expand their operative practices to target previously unattainable substrate pairings.[11] Notwithstanding the level of success in this field, several key challenges remain. As evidenced in the previous discussions, the mechanisms of ligand-enabled Ni-catalyzed cross-couplings remain underexplored. The ability of Ni to readily access oxidation states ranging from Ni^{0}-Ni^{III} via SET can render

the direct study of a catalytic cycle difficult.[9,27] The elucidation of a mechanism could have far-reaching impacts on the future development of Ni-catalysis.

This thesis seeks to address the development of ligand-enabled Ni-catalyzed C-N bond formation in two distinct ways: *i*) by probing the mechanisms of transmetalation and reductive elimination in a presumptive $Ni^{0/II}$ productive catalytic cycle through the experimental study of putative catalytic intermediates; and *ii*) by incorporating the mechanistic lessons learned from the aforementioned study to expand the scope of available nucleophilic coupling partners in Ni-catalysis.

Chapter 2 details a combined experimental and computational study seeking to reveal the mechanistic underpinnings of the synthetically useful Ni-catalyzed cross-coupling of sulfonamides. Synthesis and characterization of (**L**)Ni^{II}(aryl)(NHR) coordination complexes present a unique opportunity to study the behavior of putative catalytic intermediates. Herein the monitoring of such catalytic intermediates stoichiometrically reveals the feasibility of a previously undisclosed base-promoted reductive elimination pathway. Catalytic reaction monitoring and DFT calculations support the identification of the catalyst resting state, and electronic effects on reductive elimination rates are studied.[33]

Chapter 3 focuses on the identification of an effective catalyst system for the first Ni-catalyzed C-N cross-coupling of primary sulfinamides. Precatalysts containing **CyPAd-DalPhos** (**L1**) and **PhPAd-DalPhos** (**L2**) enable the cross-coupling of *tert*-butanesulfinamide (i.e., Ellman's sulfinamide) with (hetero)aryl chlorides and bromides. Subsequent study of putative catalytic intermediates in collaboration with DFT calculations reveals the favorability of a base-promoted reductive elimination pathway mirroring what

was documented in Chapter 2 with Ni-catalyzed cross-coupling of related sulfonamide nucleophiles.

Chapter 2. Identification of a Nitrenoid Reductive Elimination Pathway in Nickel-Catalyzed C-N Cross-Coupling

2.1 Research overview and contribution report

The author wishes to clarify his contributions to the research described in Chapter 2 of this Thesis document. This chapter describes the behavioral study of putative catalytic intermediate complexes of the type (**PhPAd-DalPhos**)Ni(*o*-tol)(NHS(O)$_2$R). The research presented herein identifies a previously unknown base-promoted reductive elimination pathway in nickel cross-coupling catalysis.

My contributions to the study included the synthesis and characterization of the (**PhPAd-DalPhos**)Ni(*o*-tol)(NHS(O)$_2$R) complexes, and studying the reductive elimination behavior from these structures by GC and $^{31}P\{^1H\}$ NMR methods. Samantha L. Dudra and Dr. Erin R. Johnson were responsible for DFT calculations. Ryan T. McGuire and Dr. Mark Stradiotto were responsible for mentoring myself and providing advice over the course of the project.

Reference: Simon, C. M.; Dudra, S. L.; McGuire, R. T.; Ferguson, M. J.; Johnson, E. R.; Stradiotto, M. Identification of a Nitrenoid Reductive Elimination Pathway in Nickel-Catalyzed C-N Cross-Coupling. *ACS Catal.* **2022**, *12* (2), 1475-1480.

2.2 Introduction

Despite the well-established field of (bisphosphine)Ni catalytic protocols, the underlying mechanism of such transformations remains underexplored, particularly in comparison to the level of research surrounding $Pd^{0/II}$ and $Ni^{I/III}$ catalytic cycles.[7,27] Although the coordination of the NH nucleophile and subsequent C-N bond reductive elimination represent key elementary steps that are often invoked as turnover-limiting in (bisphosphine)$Ni^{0/II}$ C-N cross-coupling cycles,[11] such processes have not been well-

studied, primarily due to the challenging syntheses of requisite (bisphosphine)Ni^{II}(aryl)(NR_2) complexes.

Studies directly investigating C-N reductive elimination in nickel catalysis have been limited to putative intermediates of the form (dcype)Ni(aryl)(NR_2).[34] In keeping with the general trend of rate-limiting reductive elimination in nickel chemistry,[9] these studies found promotion of the bond-forming elementary step difficult even at elevated temperatures (≥ 120 °C). While these prior studies offer important findings regarding the behavior of coordinated secondary arylamines, the study of a primary Ni-amido (i.e., Ni-NHR) unit remained an unmet objective.

We previously reported superior Ni-catalyzed protocols using (**PhPAd-DalPhos**)Ni(*o*-tol)Cl and NaO*t*Bu as the optimized precatalyst and base for the C-N cross-coupling of (hetero)aryl halide electrophiles with bulky primary alkylamines[30a] (e.g., *t*BuNH_2) and primary sulfonamides[21] (**Figure 2.1A**). Intrigued by the ability of this catalytic system to enable challenging catalytic transformations of NH nucleophiles spanning more than 20 pK_a units in NH acidity, we initiated a combined experimental and computational study of the transmetalation/C-N reductive elimination processes of catalytic relevance. Herein evidence is provided supporting a bifurcated reductive elimination pathway for the transformations of *t*BuNH_2 or (aryl')SO_2NH_2; whereas direct reductive elimination from the amido complex (**PhPAd-DalPhos**)Ni(aryl)(NH*t*Bu) is favoured, a previously undocumented base-promoted process involving the deprotonation of (**PhPAd-DalPhos**)Ni(aryl)($NHSO_2$(aryl')) to give the anionic imido (herein "nitrenoid") species [(**PhPAd-DalPhos**)Ni(aryl)(NSO_2(aryl'))]$^-$ is identified as the preferred pathway for reductive elimination (**Figure 2.1B**).

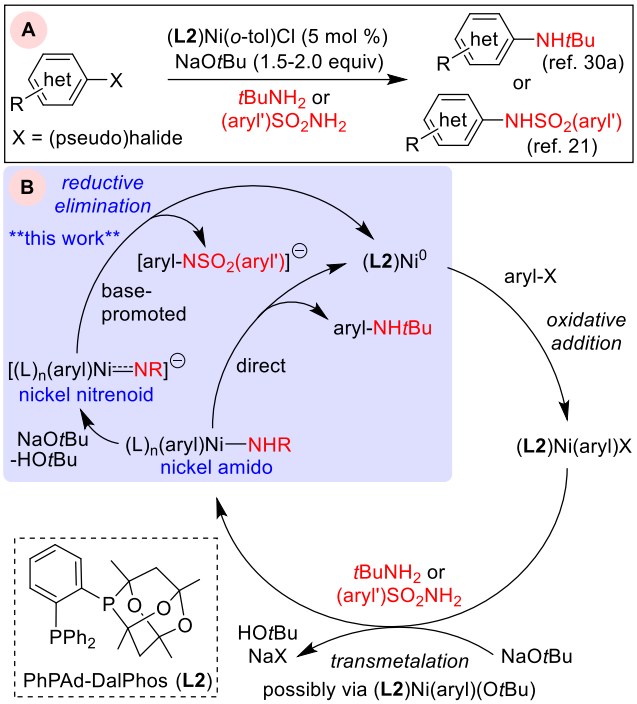

Figure 2.1. A) Catalytic conditions optimized to enable the cross-coupling of bulky primary alkylamines and primary sulfonamides. B) Simplified (**L2**)Ni$^{0/II}$ catalytic cycle depicting direct reductive elimination from a Ni-amido complex and the previously undocumented base-promoted Ni-nitrenoid pathway identified herein.

2.3 Results and Discussion

*2.3.1 Synthesis of new Ni-sulfonamido complexes **C2** and **C3***

In our report regarding the *N*-arylation of primary and secondary sulfonamides, we presented the synthesis and characterization of the primary sulfonamido complex **C1**, which represents the first and only isolable (bisphosphine)Ni(aryl)(NHR) complex reported to date.[21] In this work, we have subsequently prepared *p*-methyl (**C2**) and *m*-cyano (**C3**) variants of **C1** to probe the impact of sulfonamide aryl substitution on the stability of the ensuing complexes (**Figure 2.2**). Conversely, our attempts to prepare and isolate (**PhPAd-DalPhos**)Ni(aryl)(NH*t*Bu) in a similar fashion from *t*BuNH$_2$ afforded a complex mixture of products from which no pure materials could be isolated.

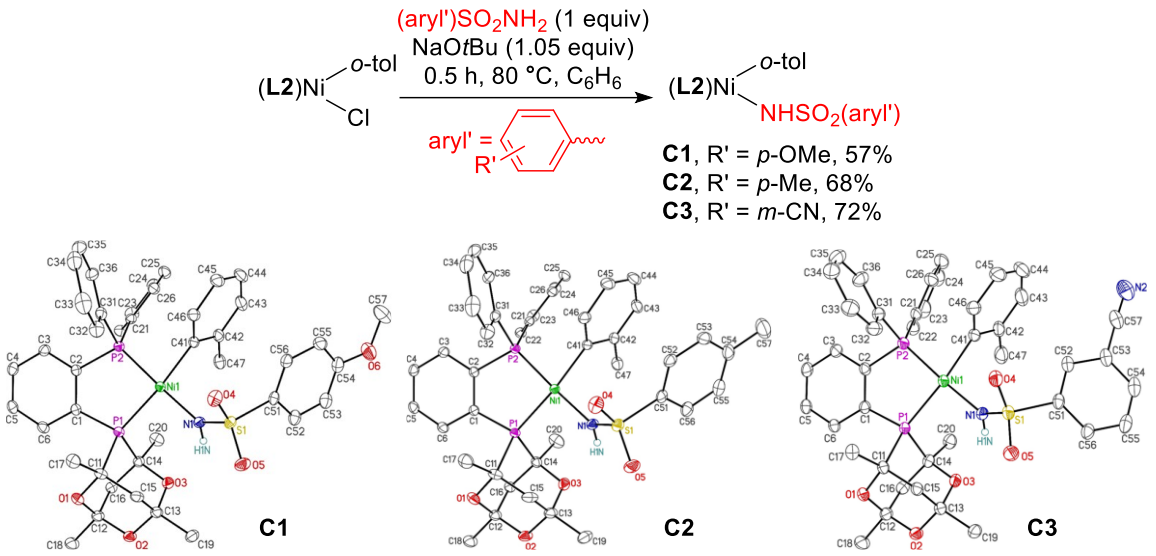

Figure 2.2. General synthetic scheme for the preparation of electronically diverse Ni-sulfonamido complexes featuring the PhPAd-DalPhos ligand (**L2**).

2.3.2 Probing C-N bond-forming reductive elimination

In probing the reductive elimination from **C1-C3**, the appearance of the C-N cross-coupled product (**2.1-2.3**) and 2,2'-dimethylbiphenyl (**2.4**) was monitored. Whereas the reactions herein are reported at 0.5 h, increased formation of **2.1-2.3** was not observed at longer reaction times. In the absence of added NaO*t*Bu, little or no reductive elimination products were observed for **C1-C3** at 25 °C (< 10%). Increasing the temperature to 110 °C results in the detection of both **2.1** and **2.2**, as well as detectable quantities of **2.4**. In the case of **C2**, the formation of **2.2** and **2.4** was accompanied by unidentified side products, whereas for **C3**, a complex mixture of products was formed, but neither **2.3** nor **2.4** was detected in such mixtures (**Figure 2.3A**). The modest formation of **2.1** and **2.2** and the lack of detectable **2.3** in these experiments was initially perplexing, especially given that primary sulfonamide *N*-arylation catalysis proceeds readily at 110 °C.[21]

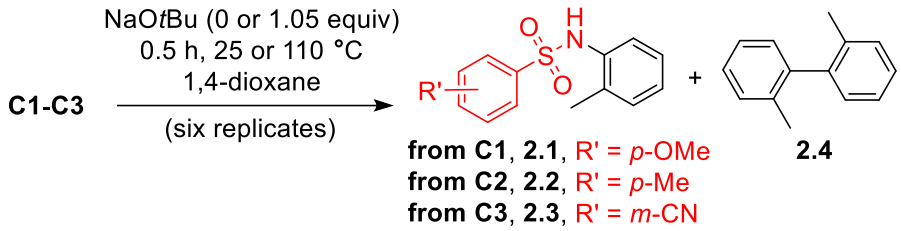

A No added base	25 °C	110 °C
	C1: 8±4% **2.1**, nd **2.4**	**C1**: 21±4% **2.1**, 7±3 **2.4**
	C2: 5±4% **2.2**, nd **2.4**	**C2**: 13±3% **2.2**, <5% **2.4**
	C3: nd **2.3**, nd **2.4**	**C3**: nd **2.3**, nd **2.4**

B NaO*t*Bu (1.05 equiv) added	25 °C	110 °C
	C1: 29±3% **2.1**, <5% **2.4**	**C1**: 48±2% **2.1**, 11±1% **2.4**
	C2: 21±4% **2.2**, <5% **2.4**	**C2**: 44±2% **2.2**, <5% **2.4**
	C3: 28±5 **2.3**, <5% **2.4**	**C3**: 41±4 **2.3**, <5% **2.4**

Figure 2.3. A) Reductive elimination data from **C1-C3** in the absence of added NaO*t*Bu. B) Reductive elimination data from **C1-C3** in the presence of added NaO*t*Bu, clearly demonstrating the dramatic impact of base on reactivity.

Given that NaO*t*Bu (2 equiv) afforded optimal catalytic performance in our primary sulfonamide C-N cross-couplings, with Cs_2CO_3 and K_3PO_4 proving ineffective,[21] we wondered if NaO*t*Bu may facilitate C-N bond reductive elimination in this system. This proved to be the case: with added NaO*t*Bu (1.05 equiv), a distinct increase in the formation of **2.1-2.3** from **C1-C3** was noted at both 25 and 110 °C, and throughout all such experiments, significantly less complex product mixtures were formed (**Figure 2.3B**). Monitoring **C1** (25 °C) or **C3** (80 °C) in the presence of added NaO*t*Bu in 1,4-dioxane using $^{31}P\{^1H\}$ NMR methods did not prove informative, with a loss of signals associated with **C1** or **C3** and the formation of multiple low-intensity signals observed.

2.3.3 Probing the resting state of the active catalyst

In the exploration of the possible role of NaO*t*Bu in forming (**L2**)Ni(*o*-tol)(O*t*Bu) under catalytic conditions, the treatment of (**L2**)Ni(*o*-tol)Cl with NaO*t*Bu (1 equiv)

afforded the incomplete conversion of (**L2**)Ni(*o*-tol)Cl; when using NaO*t*Bu (2 equiv) in benzene, clean conversion was achieved. The $^{31}P\{^{1}H\}$ NMR spectrum of this new product generated *in situ* in benzene, which we propose to be (**L2**)Ni(*o*-tol)(O*t*Bu), features major (40.2 and 8.4 ppm, 1:1 ratio) and minor (42.9 and 5.8 ppm, 1:1 ratio) pairs of signals (~2:1) that can be interpreted as arising from the interplay of the chiral (racemic) cage phosphine and Ni(*o*-tol) groups, whereby hindered Ni-C bond rotation afford the observed diastereomers as noted for **C1-C3** and (**L2**)Ni(*o*-tol)Cl.[21,30b] As with (**L2**)Ni(*o*-tol)(NH*t*Bu), we were not able to isolate (**L2**)Ni(*o*-tol)(O*t*Bu) in pure form given the excess NaO*t*Bu employed and the propensity of this compound to decompose on workup, similar to (**dppf**)Pd(aryl)(O*t*Bu).[35] Nonetheless, in monitoring by $^{31}P\{^{1}H\}$ NMR, the cross-coupling of 2-chlorotoluene with either 4-methoxybenzene sulfonamide (80 °C) or *t*BuNH$_2$ (25 °C) in 1,4-dioxane using NaO*t*Bu (1.5 to 2.0 equiv) and (**L2**)Ni(*o*-tol)Cl (20 mol%), signals consistent with (**L2**)Ni(*o*-tol)(O*t*Bu) were observed throughout the course of these catalytic reactions. These observations point to (**L2**)Ni(*o*-tol)(O*t*Bu) as being the catalyst resting state, in keeping with some Pd-catalyzed C-N cross-couplings.[35,36] Additional experiments established that while (**L2**)Ni(*o*-tol)(O*t*Bu) is immediately and quantitatively transformed into **C1** upon exposure to 4-methoxybenzenesulfonamide (1 equiv) in 1,4-dioxane at 25 °C *in the absence of NaOtBu*, no reaction occurs upon the treatment of **C1** with HO*t*Bu (2.0 equiv) under similar base-free conditions. Given the ease with which **C1** is formed from (**L2**)Ni(*o*-tol)(O*t*Bu) and 4-methoxybenzenesulfonamide in these experiments, the fact that **C1** is not observed as the catalyst resting state where NaO*t*Bu is present raised the question of the true involvement of **C1** as an intermediate from which C-N bond-forming reductive elimination can take place.

With these results in hand, we wondered if deprotonation of the NH group in **C1** might lead to the formation of an anionic Ni-nitrenoid compound [(**L2**)Ni(*o*-tol)(NSO_2(aryl)]$^-$ that could access a lower energy reductive elimination pathway due to the enhanced nitrenoid nucleophilicity[37] versus the amido group in **C1**.[38] To better elucidate the details of the underlying mechanism, we sought out collaboration from Dr. Erin R. Johnson and Samantha L. Dudra to computationally model the free-energy landscape.

2.3.4 Supporting DFT calculations

The results of the DFT calculations provided to us proved to be both informative and supportive of our experimental observations (**Figure 2.4**). Firstly, the calculated resting state of the catalyst matches what was observed experimentally [i.e., (**L2**)Ni(*o*-tol)(O*t*Bu)] in sulfonamide cross-coupling. Secondly, when comparing the sulfonamide cross-coupling landscape to that of the *t*BuNH$_2$ reaction, key differences arise in the transition state energies leading to reductive elimination. In the case of the Ni-sulfonamido intermediate, it is calculated to be 8.0 kcal·mol^{-1} higher in energy than the corresponding deprotonated Ni-nitrenoid complex. Furthermore, accessing the reductive elimination transition state from the Ni-nitrenoid intermediate is far more accessible than from the Ni-amido complex. This is in direct contrast to the calculations provided for the cross-coupling of *t*BuNH$_2$, where the Ni-amido complex is calculated to be 15.6 kcal·mol^{-1} lower in energy than the corresponding deprotonated intermediate. The reductive elimination transition state energies also point to a much more favourable Ni-amido pathway, in keeping with traditionally understood mechanistic pathways.

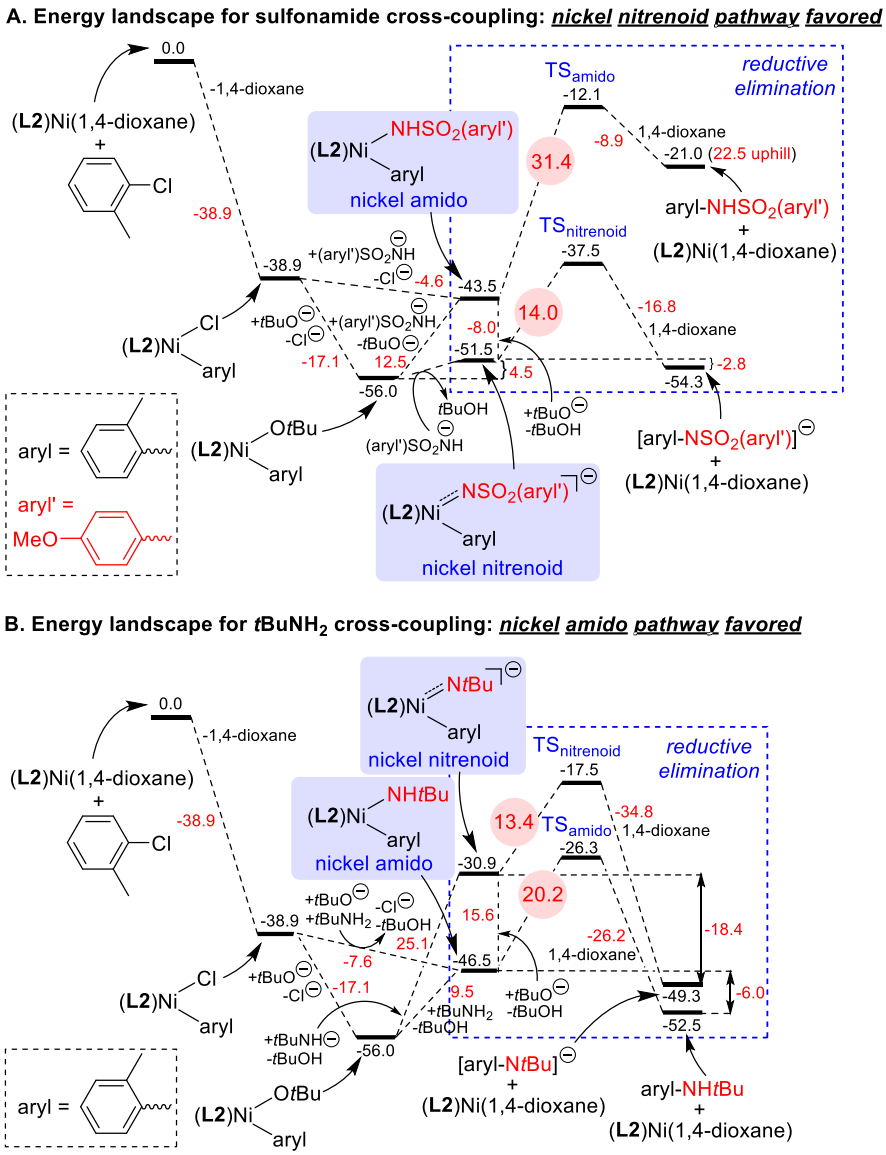

Figure 2.4. A) Computed energy landscape (relative Gibbs free energies in kcal·mol^{-1}) for the elementary steps involved in the C-N cross-coupling of 2-chlorotoluene and A) 4-methoxybenzenesulfonamide, or B) *t*BuNH$_2$, starting from (**L2**)Ni(1,4-dioxane).

2.4 Summary

The data obtained in the course of a collaborative DFT study in combination with experimental observations presented in this chapter establishes the viability of a previously undisclosed base-promoted C-N bond-forming reductive elimination pathway involving anionic Ni-nitrenoid intermediates under conditions relevant to catalysis. The synthesis and

study of electronically diverse Ni-sulfonamido complexes provided a unique opportunity to gather useful information regarding the factors that might influence reductive elimination in such contexts. While the studies performed in this chapter are limited to Ni-sulfonamido complexes, it is not unreasonable to envision similar nitrenoid pathways in other cross-couplings of weakly nucleophilic NH substrates. This aspect is examined in Chapter 3.

2.5 Experimental

2.5.1 General considerations

Unless otherwise noted, all experimental procedures were performed in a nitrogen-filled, inert atmosphere glovebox using oven-dried glassware and purified solvents. For solvents used within the glovebox, the following purification methods were used: pentane was deoxygenated by sparging with nitrogen gas then passed through a double column solvent purification system packed with alumina and copper-Q5 reactant; tetrahydrofuran was dried over Na/benzophenone followed by distillation under an atmosphere of nitrogen gas; deuterated solvents, benzene, *tert*-butanol, and 1,4-dioxane were sparged with nitrogen, and all solvents used within the glovebox were routinely stored over activated 4 Å molecular sieves. (**L2**)Ni(o-tol)Cl (**L2** = **PhPAd-DalPhos**),[30a] **2.1**,[21] and **C1**[21] were prepared according to literature procedures. All other commercial solvents, reagents, and materials were used as received. GC data were obtained on an instrument equipped with an SGE BP-5 column (30 m, 0.25 mm i.d.). Automated flash column chromatography was carried out using a normal-phase SiliCycle SiliaSep 12 g 60 Å column cartridge. All ^{1}H NMR (500.1 and 300 MHz), ^{13}C{^{1}H} NMR (125.8 and 75.4 MHz), and ^{31}P{^{1}H} NMR (202.5 and 121.5 MHz) were recorded at 300 K unless otherwise noted. Spectra were

referenced to residual protio solvent peaks (^{1}H), deuterated solvent peaks (^{13}C{^{1}H}), or external 85% H_3PO_4 (^{31}P{^{1}H}). Splitting patterns are indicated as follows: br, broad; s, singlet; d, doublet; t, triplet; q, quartet; m, multiplet. All coupling constants (*J*) are reported in Hertz (Hz). Mass spectra were obtained using ion trap (ESI) instruments operating in positive mode.

2.5.2 Procedure for the N-arylation of primary sulfonamides with aryl chlorides

Using a published protocol analogous to that used for the preparation of **2.1**,[21] each of **2.2** and **2.3** were prepared in the following manner. Solid (**L2**)Ni(*o*-tol)Cl (5 mol%), NaO*t*Bu (2.0 equiv), aryl chloride (0.48 mmol, 1.0 equiv), primary sulfonamide (0.48 mmol, 1.0 equiv), and THF (0.24 M) were added to a screw-capped vial containing a magnetic stir bar. The vial was sealed with a cap containing a PTFE septum, removed from the glovebox, placed in a temperature-controlled aluminum heating block set at 80 °C, and was allowed to react under the influence of magnetic stirring for 18 h. The resultant mixture was cooled to room temperature and under air was adsorbed onto silica, with subsequent elution through a silica/Celite frit employing ethyl acetate as the eluent (~70 mL). The resulting solution was then dried *in vacuo* to afford a crude solid that was dissolved in a hexanes-ethyl acetate mixture before being loaded onto a Silicycle SiliaSep 12 g 60 Å column cartridge. The product was then purified using a hexanes-ethyl acetate mixture eluent at a predetermined gradient, specified below. The relevant UV-active column fractions were combined and dried *in vacuo* to afford the target product.

2.5.3 Procedure for the monitoring of reductive elimination by GC methods

In a nitrogen-filled glovebox, a stock solution (0.012 M) was prepared by dissolving **C1**, **C2**, or **C3** (0.070 mmol, 1.0 equiv) in 1,4-dioxane (5.8 mL). For

experiments requiring base, NaO*t*Bu (7.1 mg, 0.074 mmol, 1.05 equiv) was added to the stock solution as well. From the resulting solution, 0.8 mL was delivered to six individual screw-capped 1-dram vials, each equipped with a magnetic stir bar. The vials were each sealed with a cap containing a PTFE septum, removed from the glovebox, and stirred magnetically for 0.5 h (within a temperature-controlled aluminum heating block set to 110 °C in the case of heated reactions). The reaction mixtures were then quenched with 3 drops of methanol at room temperature, filtered through a small silica/Celite plug, diluted with ethyl acetate (~5.0 mL), and concentrated *in vacuo* to ~1.0 mL. Phenyldodecane (1.0 equiv) was then added as an internal response-factor calibrated standard versus authentic products, and the resulting solution was then subjected to GC analysis.

2.5.4 Procedure for the monitoring of reductive elimination by NMR methods

In a nitrogen-filled glovebox, a solution of P(mesityl)$_3$ (0.0087 g, 0.0225 mmol, 1.0 equiv) in 1,4-dioxane (0.300 mL) was prepared and transferred to an NMR tube. The NMR tube was then placed in a -33 °C freezer for 0.25 h resulting in a frozen solution. A solution of **C1**, **C2**, or **C3** (0.023 mmol, 1.0 equiv) in 1,4-dioxane (0.325 mL) was prepared and transferred onto the frozen P(mesityl)$_3$ solution in the NMR tube. For experiments requiring base, NaO*t*Bu (2.3 mg, 0.0236 mmol, 1.05 equiv.) was added to the P(mesityl)$_3$ solution. The NMR tube was then sealed with PTFE tape, removed from the glovebox, and placed in an ice bath for transfer. The sample in the NMR tube was then allowed to thaw, shaken to ensure complete mixing, and immediately was inserted into the preheated NMR spectrometer set at 25 °C (for **C1**) or 80 °C (for **C3**) and was allowed to equilibrate. The sample was subsequently monitored by use of $^{31}P\{^{1}H\}$ NMR methods.

2.5.5 Procedure for the monitoring of a catalytic reaction by NMR methods

In a nitrogen-filled glovebox, a 1-dram vial was charged with a magnetic stir bar, 2-chlorotoluene (14.0 μL, 0.12 mmol, 1.0 equiv), 4-methoxybenzenesulfonamide (0.12 mmol, 1.0 equiv) or *t*BuNH$_2$ (0.36 mmol, 3.0 equiv), NaO*t*Bu (4-methoxybenzenesulfonamide: 0.24 mmol, 2.0 equiv; *t*BuNH$_2$: 0.18 mmol, 1.5 equiv), P(mesityl)$_3$ (9.3 mg, 0.024 mmol, 0.2 equiv), and 1,4-dioxane (0.35 mL). The solution was stirred at room temperature until homogeneous, transferred to an NMR tube, and placed in a -33 °C freezer for 0.25 h. A separate 1-dram vial was charged with (**L2**)Ni(*o*-tol)Cl (15.9 mg, 0.024 mmol, 0.2 equiv) and 1,4-dioxane (0.15 mL). This solution was loaded into the NMR tube containing the frozen mixture, sealed with PTFE tape, removed from the glovebox, and quickly placed in an ice bath for transfer. The sample in the NMR tube was then allowed to thaw, shaken to ensure complete mixing, and immediately was inserted into the preheated NMR spectrometer set at 80 ºC (for 4-methoxybenzenesulfonamide) or 25 ºC for (*t*BuNH$_2$), and was allowed to thermally equilibrate for several minutes. The sample was subsequently monitored by use of $^{31}P\{^1H\}$ NMR methods.

*2.5.6 Synthesis and characterization of **C1***

In a nitrogen filled glovebox, a vial containing a magnetic stir bar was charged with (**L2**)NiCl(o-tol) (257.4 mg, 0.389 mmol, 1.0 equiv.), *p*-methoxybenzenesulfonamide(72.8 mg, 0.389 mmol, 1.0 equiv.), NaO*t*Bu (56.0 mg, 0.583 mmol, 1.5 equiv.) and benzene (3.24 mL, 0.12 M). The vial was then sealed with a cap containing a PTFE septum, removed from the glovebox, and placed in a temperature-controlled aluminum heating block set to 80 ˚C and the mixture was stirred at this temperature for 30 minutes. The vial was then removed from heat and brought back into the glovebox prior to work-up. Within the

glovebox, the reaction mixture was filtered over Celite and the resulting benzene filtrate was then concentrated *in vacuo* to a volume of 1-2 mL. Pentane (8-10 mL) was subsequently added to generate a precipitate, which was isolated and then further washed with pentane (2 x 5 mL). The remaining solid was then dried *in vacuo* to afford **C1** in a 57% isolated yield (179.6 mg, 0.222 mmol) as an orange-yellow solid. Please note that **C1** was isolated as a mix of isomers in a relative ratio of 85:15 as estimated on the basis of both ^{1}H and ^{31}P{^{1}H} NMR data. When possible, ^{1}H NMR signals were only assigned and integrated in the case of the major isomer. ^{1}H NMR (500.1 MHz, C_6D_6): δ 8.25-8.21 (m, 2H), 8.08-8.07 (m, 1H), 7.63-7.60 (m, 1H), 7.43 (apparent d, *J* = 9.1 Hz, 2H), 7.08- 7.04 (m, overlapping isomers), 7.00-6.95 (m, overlapping isomers), 6.90-6.87 (m, overlapping isomers), 6.81-6.73 (m, overlapping isomers), 6.62-6.51 (m, overlapping isomers), 6.44 (apparent d, *J* = 8.8 Hz, 2H), 6.27-6.26 (m, 1H), 4.28 (dd, *J* = 14.2, 4.1 Hz, 1H), 3.82-3.81 (m, 1H), 3.17 (s, 3H, OCH_3) 2.16 (s, 3H, CH_3), 2.09 (s, 3H, CH_3), 1.68-1.65 (m, overlapping isomers), 1.46-1.43 (m, overlapping isomers), 1.27-1.26 (m, overlapping isomers). ^{31}P{^{1}H} NMR (202.5 MHz, C_6D_6): δ 53.6 (d, *J* = 3.9 Hz, major isomer), 50.0 (d, *J* = 5.3 Hz, minor isomer), 26.6 (d, *J* = 5.7 Hz, minor isomer), 21.7 (d, *J* = 3.9 Hz, major isomer). Single crystals of **C1**•C_6H_6 suitable for X-ray diffraction analysis was prepared by slow evaporation of pentane into a solution of **C1** in benzene at 25 ˚C. Elemental analysis (crystalline sample): Calculated for $C_{48}H_{51}N_1Ni_1O_6P_2S_1$ (**C1**•C_6H_6): C, 64.73; H, 5.77; N, 1.57. Found: C, 64.56; H, 5.63; N, 1.69.

*2.5.7 Synthesis and characterization of **C2***

In a nitrogen-filled glovebox, a 1-dram vial containing a magnetic stir bar was charged with (**L2**)Ni(*o*-tol)Cl (397.1 mg, 0.60 mmol, 1.0 equiv), *p*-tolylsulfonamide (102.7

mg, 0.60 mmol, 1.0 equiv), NaO*t*Bu (60.5 mg, 0.630 mmol, 1.05 equiv), and benzene (5.0 mL, 0.12 M). The vial was sealed with a cap containing a PTFE septum, removed from the glovebox, placed in a temperature-controlled aluminum heating block set to 80 °C and the mixture was stirred magnetically at this temperature for 0.5 h. After this time, the vial was allowed to cool to room temperature and was brought back into the glovebox prior to work-up. In the glovebox, the reaction mixture was filtered over Celite and the resulting filtrate was then concentrated *in vacuo* to a volume of ~1-2 mL. Pentane (~10 mL) was then added to generate a precipitate, which was isolated and then further washed with pentane (3 x 5 mL). The remaining product was dried *in vacuo* to afford **C2** in a 68% yield (325.0 mg, 0.408 mmol) as a dark orange solid. Elemental analysis: Calculated for $C_{42}H_{45}N_1Ni_1O_5P_2S_1$: C, 63.33; H, 5.69; N, 1.76. Found: C, 63.02; H, 5.74; N, 1.81. Please note that **C2** was isolated as a mixture of isomers (~3:1) as estimated on the basis of $^{31}P\{^1H\}$ NMR data (202.5 MHz, C_6D_6): δ 53.4 (d, J = 4.1 Hz, major isomer), 50.0 (d, J = 5.1 Hz, minor isomer), 26.6 (d, J = 5.1 Hz, minor isomer), 21.9 (d, J = 4.1 Hz, major isomer). The formation of these isomers can be interpreted as arising from the interplay of the chiral (racemic) cage phosphine and Ni(*o*-tol) groups, whereby hindered Ni-C bond rotation affords the observed diastereomers, as noted for **C1**[21] and **C3**. The presence of this isomeric mixture renders the ^1H and $^{13}C\{^1H\}$ NMR spectra of **C2** sufficiently complex so as to preclude definitive assignment; these spectra are provided in **Figures A8** and **A10** for completeness.

*2.5.8 Synthesis and characterization of **C3***

A protocol analogous to that described for **C2** was employed, using 3-cyanobenzenesulfonamide (109.3 mg, 0.60 mmol, 1.0 equiv) in place of *p*-

tolylsulfonamide. The product was dried *in vacuo* to afford **C3** in a 72% isolated yield (348.8 mg, 0.432 mmol) as a yellow solid. Elemental analysis: Calculated for $C_{42}H_{42}N_2Ni_1O_5P_2S_1$: C, 62.47; H, 5.24; N, 3.47. Found: C, 62.33; H, 5.27; N, 3.66. Please note that **C3** was isolated as a mixture of isomers (~3:1) as estimated on the basis of $^{31}P\{^1H\}$ NMR (202.5 MHz, C_6D_6): δ 53.4 (d, J = 4.1 Hz, major isomer), 50.0 (d, J = 6.1 Hz, minor isomer), 27.2 (d, J = 6.1 Hz, minor isomer), 22.7 (d, J = 4.1 Hz, major isomer). The formation of these isomers can be interpreted as arising from the interplay of the chiral (racemic) cage phosphine and Ni(*o*-tol) groups, whereby hindered Ni-C bond rotation affords the observed diastereomers, as noted for **C1**[21] and **C2**. The presence of this isomeric mixture renders the ^1H and $^{13}C\{^1H\}$ NMR spectra of **C3** as being sufficiently complex so as to preclude definitive assignment; these spectra are provided in **Figures A11** and **A13** for completeness.

2.5.9 Characterization data for isolated cross-coupling products

4-tolyl-N-(o-tol)benzenesulfonamide (**2.2**)

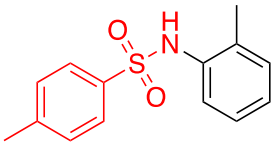

The title compound was synthesized from the corresponding aryl chloride (0.48 mmol) according to ***2.5.2***, conducted at 80 °C in THF using 5 mol% (**PhPAd-DalPhos**)NiCl(*o*-tol) and purified by flash chromatography on silica using an eluent gradient of 0% ethyl acetate in hexanes (4 CV), 0-40% ethyl acetate in hexanes (10 CV), followed by 40% ethyl acetate in hexanes (4 CV), which afforded the title compound in a 72% isolated yield (0.090

g, 0.346 mmol) as an off-white solid. ^{1}H NMR (500.1 MHz, $CDCl_3$): δ 7.60 (d, J = 8.3 Hz, 2H), 7.30 (d, J = 7.9 Hz, 1H), 7.21 (d, J = 8.1 Hz, 2H), 7.13 (m, 1H), 7.08 (m, 2H), 6.25 (br, 1H, NH), 2.38 (s, 3H, CH_3), 2.00 (s, 3H, CH_3). ^{13}C{^{1}H} UDEFT NMR (125.8 MHz, $CDCl_3$): δ 143.8, 136.5, 131.2, 130.7, 129.6, 127.2, 127.0, 126.2, 124.2, 21.5, 17.5. HRMS-ESI (*m/z*): Calc'd for $C_{14}H_{15}NO_2SNa$ $[M+Na]^+$: 284.0716. Found: 284.0711.

3-cyano-N-(o-tolyl)benzenesulfonamide (**2.3**)

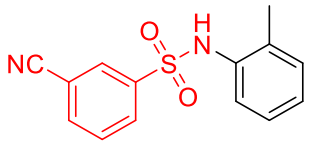

The title compound was synthesized from the corresponding aryl chloride (0.48 mmol) according to ***2.5.2***, conducted at 80 °C in THF using 5 mol% (**PhPAd-DalPhos**)NiCl(*o*-tol), and purified by flash column chromatography on silica using an eluent gradient of 0% ethyl acetate in hexanes (4 CV), 0-30% ethyl acetate in hexanes (12 CV), followed by 30% ethyl acetate in hexanes (4 CV) which afforded the title compound in a 78% isolated yield (0.102 g, 0.374 mmol) as an off-white solid. ^{1}H NMR (500.1 MHz, $CDCl_3$): δ 8.05 (t, J = 1.4 Hz, 1H), 7.97 (m, 1H), 7.87 (m, 1H), 7.62 (t, J = 7.9 Hz, 1H), 7.23-7.16 (m, overlapping Hs, 3H), 6.48 (br, 1H, NH), 2.08 (s, 3H, CH_3). ^{13}C{^{1}H} UDEFT NMR (125.8 MHz, $CDCl_3$): δ 141.4, 136.0, 133.4, 132.1, 131.1 (overlapping ArCs), 130.7, 130.0, 127.3, 125.0, 116.9, 113.7, 17.6. HRMS-ESI (*m/z*): Calc'd for $C_{14}H_{12}N_2O_2SNa$ $[M+Na]^+$: 295.0512. Found: 295.0511.

Chapter 3. Nickel-Catalyzed *N*-arylation of Sulfinamides: A Comparative Study versus Analogous Sulfonamide Cross-Couplings

3.1 Research overview and contribution report

The author wishes to clarify his contributions to the research described in Chapter 3 of this Thesis document. This chapter describes the application of **CyPAd-DalPhos** (herein **L1**) and **PhPAd-DalPhos** (herein **L2**) in the Ni-catalyzed C-N cross-coupling of primary sulfinamides. The transformations presented herein represent the first documented use of Ni catalysis for the *N*-arylation of sulfinamide nucleophiles with (hetero)aryl chlorides and bromides.

My contributions to the study included the optimization of catalytic conditions, developing a substrate scope based on primary sulfinamide *N*-arylation, performing competition studies to gauge selectivity, and the synthesis/subsequent study of putative catalytic intermediates. Dr. Katherine N. Robertson solved the solid-state structures of **C4-C6**. Dr. Patrick. L. DeRoy and Dr. Arun A. Yadav provided conceptual input and project guidance. Dr. Erin R. Johnson was responsible for all DFT calculations presented. Dr. Mark Stradiotto was responsible for mentoring me as well as providing advice and direction throughout this project.

3.2 Introduction

The synthesis of substituted sulfinamides represents an area of considerable interest,[39] given the utility of such compounds including in synthetic chemistry[40] (e.g., as ammonia surrogates[41]), medicinal chemistry[42] (e.g., bioisosteres of carboxylic acids[43]), and in the design of new (chiral) ancillary ligands[44] for use in metal catalysis. However, despite advances in metal-catalyzed C-N cross-coupling methodologies,[7,19b,20] relatively little

progress has been made regarding the development of sulfinamide *N*-arylations employing (hetero)aryl (pseudo)halide electrophiles, with the few examples reported thus far being limited to Pd,[41b,45] Cu,[46] and Cu/Fe[47] catalyst systems (**Figure 3.1A**).

As part of a program in the Stradiotto group targeting the development (P_2)Ni-catalyzed C-N/O cross-couplings (P_2 = bisphosphine)[11] as a means of addressing unmet reactivity challenges, the group recently disclosed the first examples of such reactions employing inexpensive and abundant (hetero)aryl chloride[48] and phenol-derived electrophiles with sulfonamide nucleophiles.[21] In this chemistry, optimal performance was achieved by use of the P_2 ligand **PhPAd-DalPhos** in combination with excess NaO*t*Bu (2 equiv) as base. A subsequent experimental/computational investigation[33] of the reaction mechanism revealed a previously undocumented base-promoted process whereby isolable amido species (P_2)Ni(aryl)(NHS(O)$_2$R'), rather than undergoing direct C-N reductive elimination as is conventionally observed,[34] preferentially undergoes deprotonation to give anionic nitrenoid species [(P_2)Ni(aryl)(NS(O)$_2$R')]$^-$ that engage in facile C-N reductive elimination. This work was discussed in Chapter 2.

Given the dearth of metal-catalyzed C-N cross-couplings of sulfinamides, including the absence of reported base-metal systems capable of enabling transformations of (hetero)aryl chlorides with useful reaction scope, I sought to evaluate if previously developed Ni-catalyzed sulfonamide cross-couplings from the Stradiotto group (**Figure 3.1B**)[21] might be expanded to sulfinamide nucleophiles (**Figure 3.1C**). The results of this work are reported in this chapter, involving catalytic screenings focusing primarily on the use of *tert*-butanesulfinamide (i.e., Ellman's sulfinamide)[41a] as a test nucleophile, as well as coordination chemistry and experimental/computational findings that support the

intermediacy of putative anionic nitrenoid species [(**L**)Ni(*o*-tol)(NS(O)*t*Bu)]$^-$ in such sulfinamide cross-couplings.

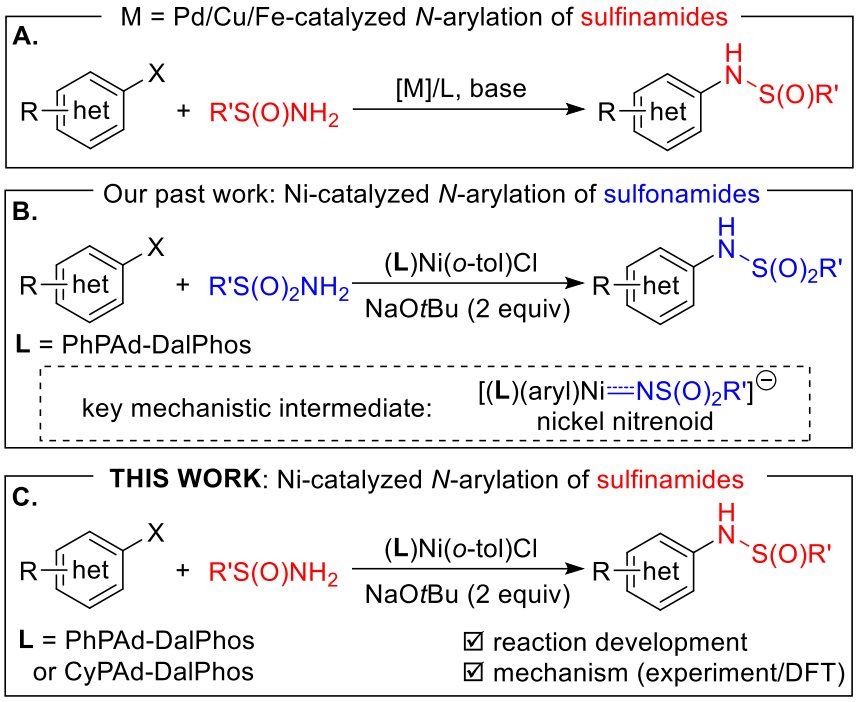

Figure 3.1. A) Known metal-catalyzed C-N cross-couplings of sulfinamides.[41b,45,46b] B) Ni-catalyzed sulfonamide cross-couplings, highlighting a key nickel nitrenoid intermediate.[21] C) Ni-catalyzed C-N cross-couplings of sulfinamides reported in this Chapter.

3.3 Results and discussion

3.3.1 Preliminary ligand / Ni(COD)$_2$ screening

With the intention of identifying possible catalytic conditions for the *N*-arylation of primary sulfinamides with (hetero)aryl chlorides, an initial test ligand screen was performed for the reaction of (R)-*tert*-butanesulfinamide and 4-chlorobenzonitrile in the presence of NaO*t*Bu (2 equiv)[21] and Ni(COD)$_2$ (7.5 mol%). Several DalPhos ligands, as well as other established ligands for Ni-catalyzed C-N cross-couplings were screened (**Figure 3.2**).[29]

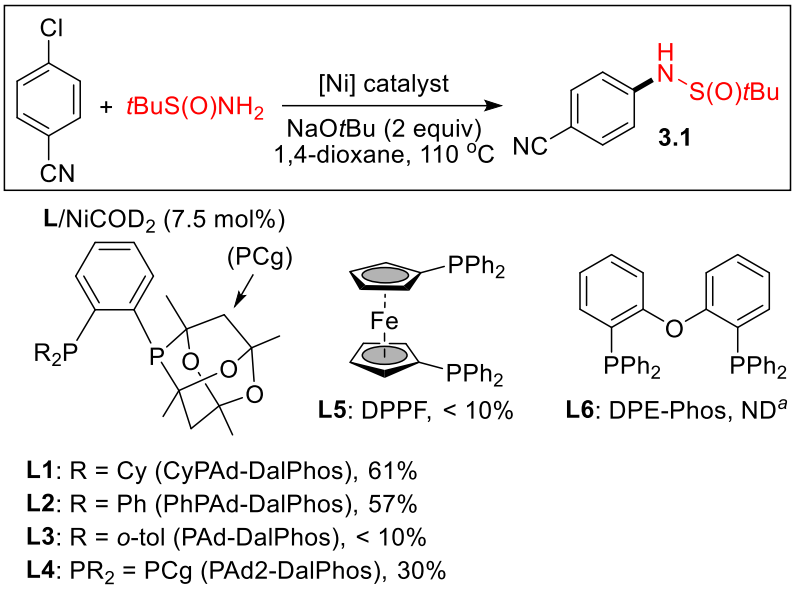

Figure 3.2. Results of Ligand / Ni(COD)$_2$ screens demonstrating the superiority of **CyPAd-DalPhos** and **PhPAd-DalPhos** in facilitating the Ni-catalyzed cross-coupling of *tert*-butanesulfinamide and 4-chlorobenzonitrile in the presence of NaO*t*Bu.

Useful conversions to **3.1** were achieved with both **L1** (61%)[30b] and **L2** (57%),[21,30a] whereas conversion begins to drop off significantly when **PAd2-DalPhos** (30%)[30c] or **PAd-DalPhos** (< 10%)[29] are used. Both **dppf** (< 10%)[49] and **DPEPhos** (ND)[50] proved incompatible under these conditions. With these results, I turned my attention to the synthesis of the (**L1**)Ni(*o*-tol)Cl[30b] precatalyst to further optimize reaction conditions (**Figure 3.3**). Precatalyst implementation immediately improved reactivity for the optimal ligands using the previously identified conditions (**L1** = 85%, **L2** = 82%). Optimization was then further studied by altering the identity and quantity of additive base, and the following trends were observed (entries 3-9): (*i*) reducing the amount of NaO*t*Bu added from 2.0 to 1.5 equiv results in a dramatic drop in overall conversion (85% versus 43%); and (*ii*) alternative bases including Cs_2CO_3, K_3PO_4, Li(HMDS), and the 'dual-base'[51] systems BTPP or DBU with the halide extractor NaTFA each proved inferior to NaO*t*Bu

under analogous conditions. Furthermore, a small drop in conversion was observed when changing solvent from 1,4-dioxane to toluene (85% versus 80%, entries 1 and 10). Changing the solvent and temperature conditions to mirror those from our previous sulfonamide work (entry 11)[21] also proved inferior in this chemistry. Next, the effect of catalyst loading on reaction performance was examined. Increasing the loading to 10 mol% catalyst resulted in only a minor benefit (entries 1 and 12), whereas reduced loadings resulted in a significant drop in conversion (entries 13 and 14). Finally, negligible conversion was noted in the absence of Ni catalyst.

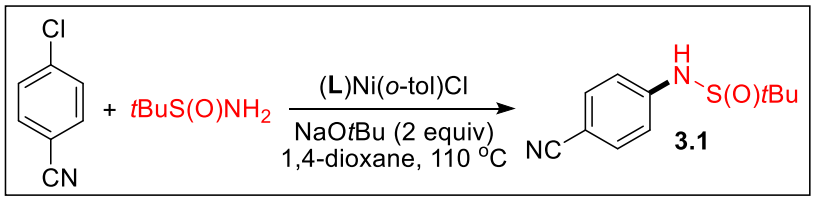

(**L**)Ni(*o*-tol)Cl (7.5 mol%), **L** = CyPAd-DalPhos

Entry	Deviation from Standard Conditions	Yield **3a** (%)
1	None	85
2	**L** = PhPAd-DalPhos	82
3	NaO*t*Bu (1.5 equiv)	43
4	Cs_2CO_3 (2.0 equiv)	60
5	Cs_2CO_3 (1.5 equiv)	22
6	BTPP/NaTFA (2.0 equiv)	< 5
7	DBU/NaTFA (2.0 equiv)	< 5
8	K_3PO_4 (2.0 equiv)	ND
9	Li(HMDS) (2.0 equiv)	ND
10	Toluene, 110 °C	80
11	THF, 80 °C	38
12	10 mol% (**L**)NiCl(*o*-tol)	88
13	5 mol% (**L**)NiCl(*o*-tol)	68
14	2.5 mol% (**L**)NiCl(*o*-tol)	28
15	0 mol% (**L**)NiCl(*o*-tol)	< 5

Figure 3.3. Optimization screening for the Ni-catalyzed cross-coupling of 4-chlorobenzonitrile with (R)-*tert*-butanesulfinamide (i.e., Ellman's sulfinamide) to give **3.1**.

3.3.2 Primary sulfinamide N-arylation scope

Having identified the optimal catalytic conditions for the ligand-enabled Ni-catalyzed *N*-arylation of sulfinamides, the scope of reactivity in the electrophile was

examined, using primarily *tert*-butanesulfinamide as a coupling partner (**Figure 3.3**). Due to the competitive conversions provided by **L1** and **L2** in the optimization screening, each electrophile pairing was screened against both precatalysts for comparative purposes. In this chemistry it was found that the performance ranking of **L1** versus **L2** depended on the electrophile involved; as such, isolated yields are provided for reactions using each. Electron-rich and electron-poor (hetero)aryl chloride and bromide electrophiles featuring *ortho-, meta-, or para-* substitution proved to be suitable in this chemistry, as were some representative heteroaryl electrophiles based on pyridine, quinaldine, benzothiophene, and benzo[*d*]isothiazole core structures. The successful cross-coupling of *para*-tolylsulfinamide with 1-chloronaphthalene also demonstrates that the reactions reported herein are not restricted to *tert*-butanesulfinamide. As is evident in **Figure 3.4**, the scope of the reactivity, while reasonably broad, fails to offer isolated yields > 80%, and in several cases < 50% isolated yield is obtained. In this context, HPLC analyses of the crude reaction mixtures confirm that while the mass balance corresponds primarily to unreacted electrophile, multiple side-products were detected in many cases.

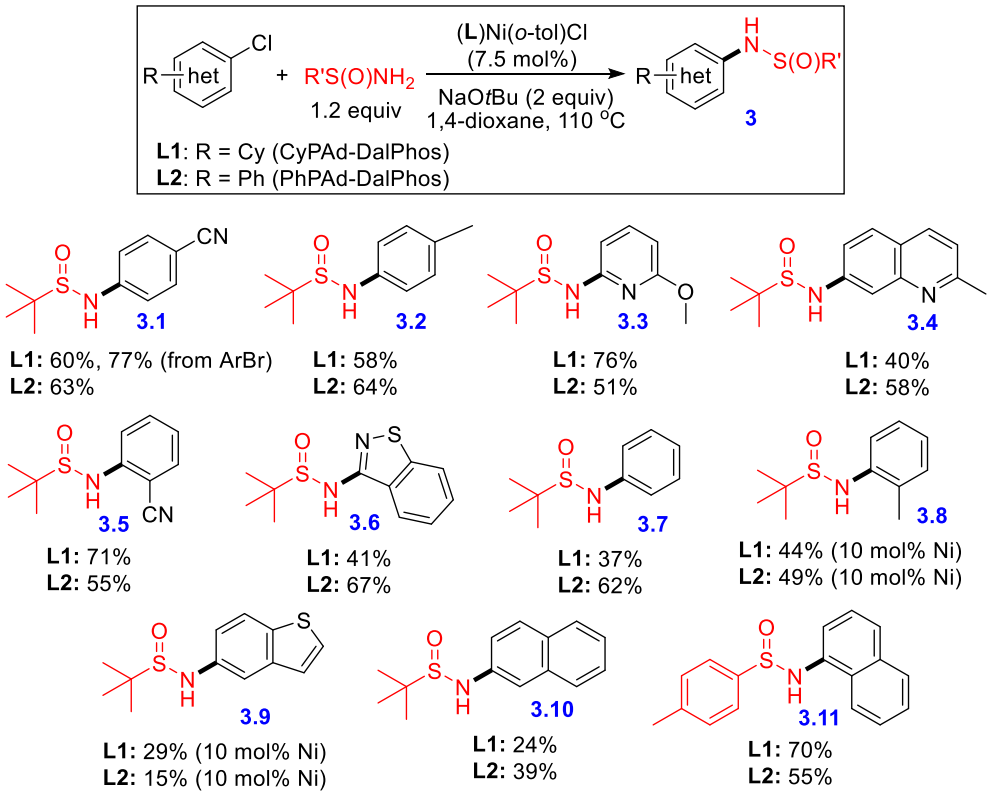

Figure 3.4. Substrate scope for the cross-coupling of primary sulfinamides with (hetero)aryl halides enabled by (**L1**)Ni(*o*-tol)Cl and (**L2**)Ni(*o*-tol)Cl. Reactions were conducted at 0.48 mmol scale in (hetero)aryl halide, and isolated yields are reported.

3.3.3 Sulfinamide versus sulfonamide competition study

The efficacy of the (**PhPAd**)Ni(*o*-tol)Cl catalyst system in enabling C-N cross-coupling of both sulfonamides[21] and sulfinamides prompted interest in conducting competition experiments to ascertain the relative reactivity ranking of such substrates. In competitions employing tBuS(O)$_X$NH$_2$ (X = 1 or 2) with 7-chloroquinaldine, the sulfinamide product (**3.4**) was not detected, despite its successful formation under the conditions in **Figure 3.4**. While the analogous sulfonamide product was observed, thereby confirming sulfonamide over sulfinamide preference in this system, the overall conversion to sulfonamide product (33% HPLC yield) was much lower than that obtained in the absence of sulfonamide competitor (> 95% GC yield[21]) (**Figure 3.5**). The reduced yield of

sulfonamide product in this context might arise from the suboptimal nucleophile:base ratio (2.4:2 rather than 1.2:2), or due to sulfinamide inhibition of the catalyst in a manner that diminishes turnover of the sulfonamide reactant.

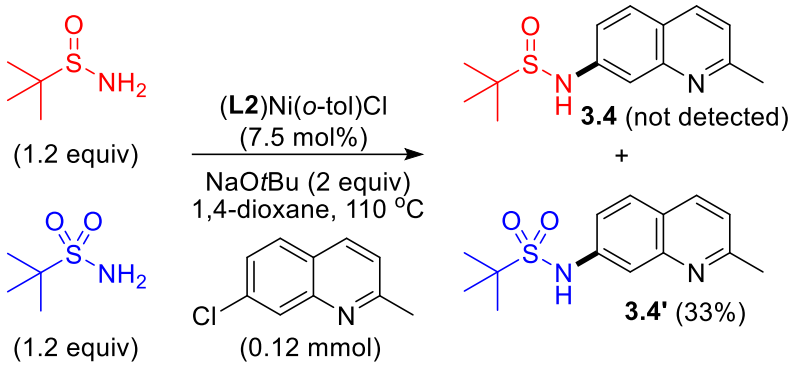

Figure 3.5. General scheme of the competition reaction between *tert*-butanesulfinamide and *tert*-butanesulfonamide with 7-chloroquinaldine, leading to **3.4** or **3.4'** respectively. Yields are determined by HPLC response-factor calibrated data using mesitylene as an internal standard.

3.3.4 Probing C-N bond-forming reductive elimination

Encouraged our previous successes in probing the reductive elimination behaviour of **L**Ni^{II}(aryl)(NHR) intermediates (see Chapter 2 of this Thesis),[33] we became interested in the possibility of isolating **L**Ni^{II}(*o*-tol)(NHS(O)*t*Bu) complexes. Treatment of the corresponding (**L**)Ni(*o*-tol)Cl precatalysts with (R)-*t*BuS(O)NH$_2$ in the presence of NaO*t*Bu (1.05 equiv) at 80 °C enabled the formation, and subsequent high yielding isolation, of the diamagnetic sulfinamido complexes **C4** and **C5** (**Figure 3.6**). The crystallographic characterization of these complexes confirmed their identity as rare examples of isolable primary Ni-amido species (i.e., Ni-NHR), featuring in each case an approximate square-planar geometry. Interestingly, the crystallization of the (**CyPAd**)Ni(*o*-tol)(NHS(O)*t*Bu) complex featured the co-crystallization of a dimerized [(**CyPAd**)Ni(*o*-tol)]$_2$ complex containing bridging Cl and O atoms. Though this structure

did not prove valuable in our subsequent studies, its structure and refinement details are included in **Appendix 4**.

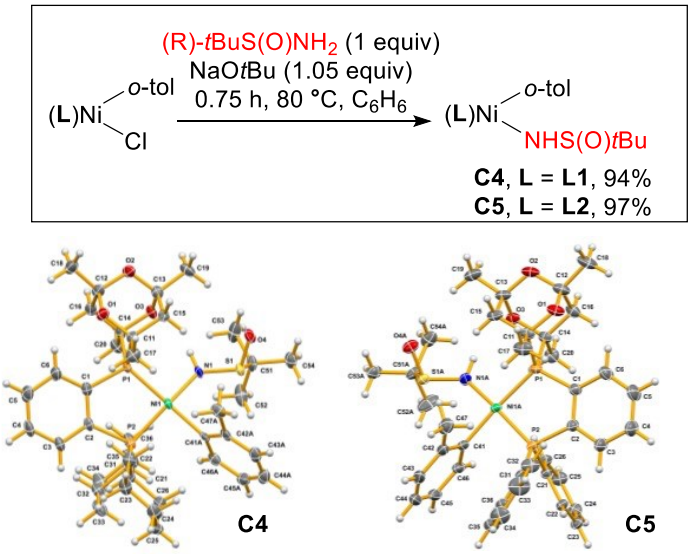

Figure 3.6. General synthetic method for the synthesis of Ni-sulfinamido complexes **C4** and **C5**, with solved solid state structures.

In monitoring C-N bond-forming reductive elimination involving **C4** and **C5** leading to **3.8** under catalytically relevant conditions by use of HPLC methods (**Figure 3.7**), relatively low levels of conversion were observed in the absence of NaO*t*Bu. However, in line with our previous study of Ni-sulfonamido species (Chapter 2),[33] substantial quantities of **3.8** were generated rapidly on heating of **C4** and **C5** in the presence of NaO*t*Bu, as would be present under catalytic conditions. These observations are consistent with our findings that NaO*t*Bu (2 equiv) is required for optimal catalytic turnover. DFT calculations carried out by Dr. Erin R. Johnson also support deprotonation of Ni-sulfinamido species to yield nitrenoid intermediates, from which C-N bond-forming reductive elimination is favourable. While not demonstrated to a statistically significant degree, the data obtained may suggest that such reductive eliminations are facilitated by

the less electron-rich **PhPAd-DalPhos** (**L2**) ligand versus **CyPAd-DalPhos** (**L1**), which is in line with well-understood trends of Ni-catalysis (see Chapter 1 of this Thesis).[11]

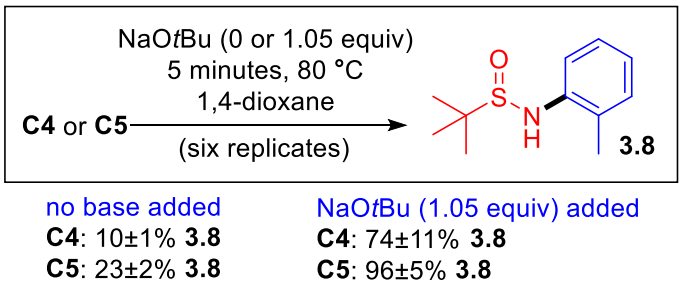

Figure 3.7. Data obtained for the formation of **3.8** from the corresponding Ni-sulfinamido complexes **C4** and **C5**.

3.3.5 Scope limitations in Ni-catalyzed N-arylation of sulfinamides

As noted in Section 3.3.2, the Ni-catalyzed *N*-arylation of sulfinamides often featured poor conversion to product and unidentified side products. Included in this section is a description of (hetero)aryl electrophile substrates that were not suitable in this catalytic system (**Figure 3.8**). (Hetero)aryl chlorides including pyridine, thiophene, and quinoline moieties reacted cleanly with *tert*-butanesulfinamide, but featured poor activity overall, as did the deactivated 4-chloroanisole electrophile. 4-chlorobenzotrifluoride, although activated, also produced poor results in this chemistry. Naphthyl derivatives 1-chloronaphthalene and 6-chloroquinoline also featured minimal conversion to product. The scope of electrophiles leading to complex mixtures is broad. Substrates bearing di-*ortho* and *ortho-meta*- substitutions, pyridines, quinoxalines, benzophenones, imidazole, pyrazole, pyrimidine, and extended biaryl structures all yielded intractable mixtures from which no pure material could be isolated from.

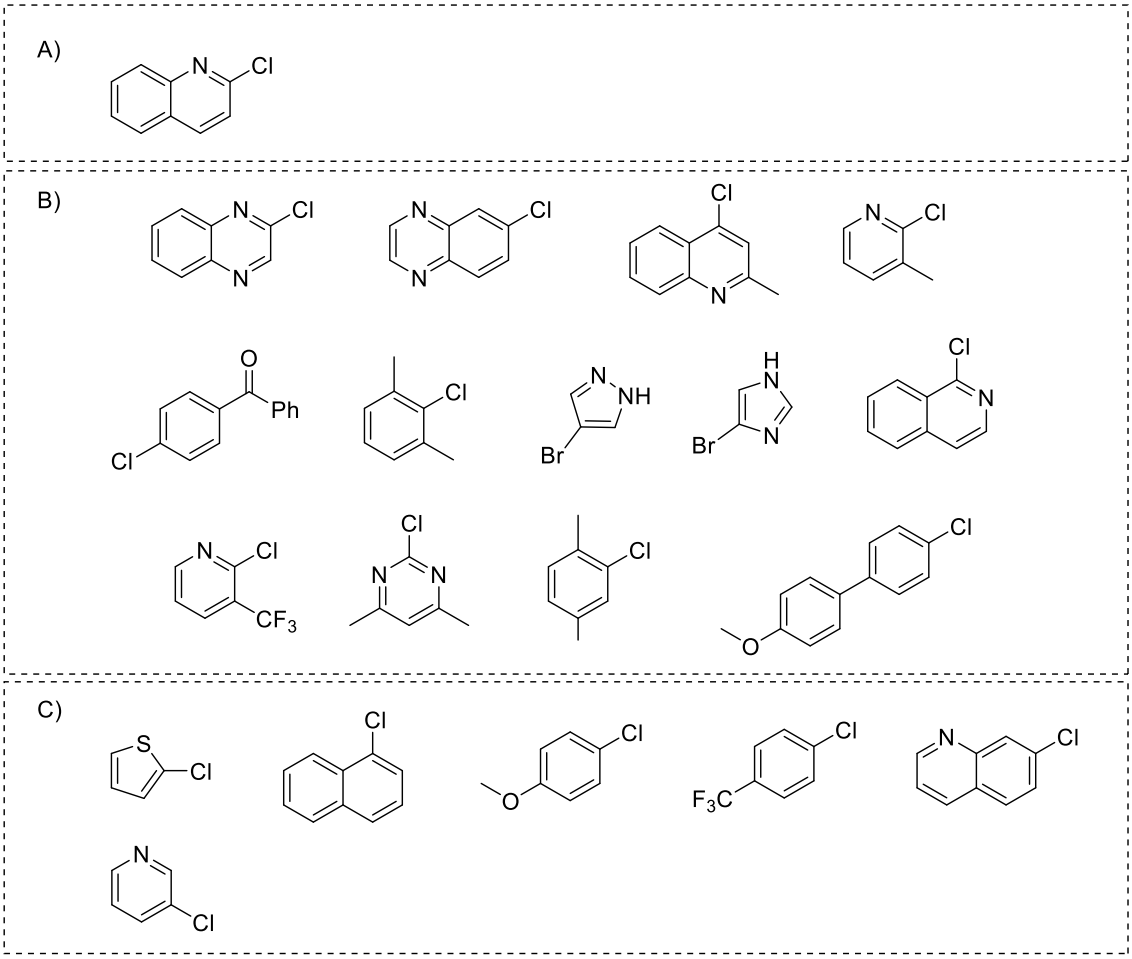

Figure 3.8. (Hetero)aryl halide electrophiles determined to be incompatible in this catalytic system. A) Reaction proceeds in the absence of Ni-catalyst. B) the (hetero)aryl halide is consumed and a complex mixture of products is formed. C) low conversion of (hetero)aryl halide.

3.4 Summary

This chapter details the first Ni-catalyzed *N*-arylation of primary sulfinamides with (hetero)aryl chlorides and bromides enabled by **CyPAd-DalPhos** and **PhPAd-DalPhos** ancillary ligands. This offers a base-metal alternative to previously reported Pd-catalyzed *N*-arylations, and expands the scope of available electrophiles over Fe/Cu co-catalyzed systems. Isolable **L**Ni(*o*-tol)(NHR) sulfinamido complexes enabled the experimental study of reductive elimination mechanisms in catalytically relevant conditions. DFT calculations

support the observation of a deprotonated Ni-nitrenoid complex from which facile reductive elimination can take place (**Figure 3.9**).

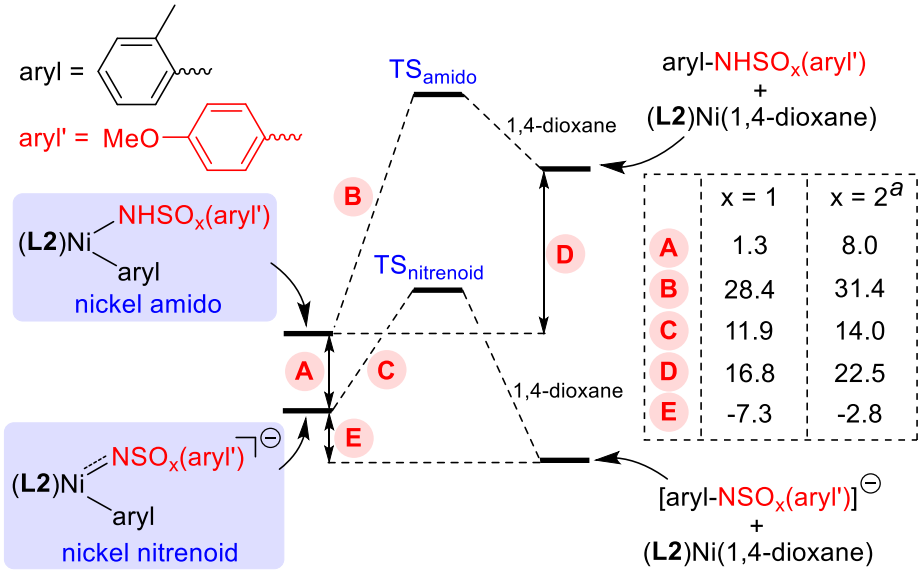

Figure 3.9. Computed energy landscape (relative Gibbs free-energies in kcal·mol^{-1}) for model reductive eliminations from nickel amido and nickel nitrenoid intermediates of relevance to the **L2**/Ni-catalyzed C-N cross-coupling of 2-chlorotoluene and 4-methoxybenzene sulfinamide or 4-methoxybenzenesulfonamide.

3.5 Experimental

3.5.1 General considerations

Unless otherwise noted, all experimental procedures were carried out in a nitrogen-filled, inert atmosphere glovebox using oven-dried glassware and purified solvents. Workup for organic products was conducted on the benchtop in air. For solvents used within the glovebox, the following purification methods were used: benzene was deoxygenated by sparging with nitrogen gas then passed through a double column solvent purification system packed with alumina and copper-Q5 reactant; deuterated solvents, pentane, and 1,4-dioxane were sparged with nitrogen gas, and all solvents used within the glovebox were routinely stored over activated 4 Å molecular sieves (**L**)Ni(*o*-tol)Cl (**L1** =

CyPAd-DalPhos,[30b] **L2** = PhPAd-DalPhos[30a]) and **3.4'**[21] were prepared according to literature procedures. All other commercial solvents, reagents, and materials were used as received. HPLC data were obtained on an instrument equipped with an Agilent InfinityLab Poroshell 120 EC-C18 reverse-phase column (3.0 x 150 mm, 2.7 Micron, 1000 bar). Automated flash column chromatography was carried out using a normal-phase SiliCycle Silia*Sep* 12g 60 Å column cartridge. All ^{1}H NMR (500 and 300 MHz), ^{13}C{^{1}H} NMR (125.8 and 75.4 MHz), and ^{31}P{^{1}H} NMR (202.5 and 121.5 MHz) were recorded at 300 K unless otherwise noted. Spectra were referenced to residual protio solvent peaks (^{1}H), deuterated solvent peaks (^{13}C{^{1}H}), or external 85% H_3PO_4 (^{31}P{^{1}H}). Splitting patterns are indicated as follows: br, broad; s, singlet; d, doublet; t, triplet; q, quartet; m, multiplet. All coupling constants (*J*) are reported in Hertz (Hz). Mass spectra were obtained using ion trap (ESI) instruments operating in positive mode.

3.5.2 Procedure for the N-arylation of sulfinamides with (hetero)aryl halides

Unless otherwise indicated in the text, solid (**L1**)Ni(*o*-tol)Cl or (**L2**)Ni(*o*-tol)Cl (7.5 mol%), NaO*t*Bu (2.0 equiv), (hetero)aryl halide (0.12 or 0.48 mmol, 1.0 equiv), sulfinamide (1.2 equiv), and 1,4-dioxane (0.24 M (hetero)aryl halide) were added to a screw-capped vial. In the case of ligand/Ni(COD)$_2$ screens, reactions were carried out on 0.12 mmol scale in (hetero)aryl chloride, and the Ni(COD)$_2$ was delivered from a stock solution in 1,4-dioxane so that the final concentration of (hetero)aryl chloride remained at 0.24 M. The vial was then charged with a magnetic stir bar, sealed with a cap containing a PTFE septum, removed from the glovebox, and placed in a temperature-controlled aluminum heating block set at the specified temperature, where it was allowed to react under the influence of magnetic stirring for 18 h (unoptimized).

3.5.3 Procedure for competition experiments

In a nitrogen-filled glovebox (**L2**)Ni(*o*-tol)Cl (7.5 mol%), NaO*t*Bu (2.0 equiv), 7-chloroquinaldine (0.12 mmol, 1.0 equiv), nucleophilic NH coupling partners (1.2 equiv each) and 1,4-dioxane (0.5 mL) were added to a 1 dram screw capped vial containing a magnetic stir bar. The vial was sealed with a cap containing a PTFE septum, removed from the glovebox, and placed on a temperature-controlled aluminum heating block set at the specified temperature. The mixture was allowed to react under the influence of magnetic stirring for 18 h (unoptimized). The vial was then removed from the heating block, allowed to cool to room temperature, and quenched with 2 drops of methanol. Mesitylene (1.0 equiv) was added as internal standard, and an aliquot of the mixture was filtered through a short Celite/silica plug, diluted with acetonitrile (~1.0 mL), and subjected to HPLC analysis.

3.5.4 Procedure for the monitoring of reductive elimination by HPLC methods

In a nitrogen-filled glovebox, a stock solution (0.036 M) was prepared by dissolving **C4** (119.7 mg, 0.1575 mmol, 1.0 equiv) or **C5** (117.6 mg, 0.1575 mmol, 1.0 equiv) in 1,4-dioxane (4.375 mL). For experiments requiring base, NaO*t*Bu (16.1 mg, 0.1652 mmol, 1.05 equiv) was added to the stock solution. From the resulting stock solution, 0.625 mL was delivered to six individual 1 dram screw-capped vials, each charged with a magnetic stir bar. The vials were sealed with a cap containing a PTFE septum, removed from the glovebox, and placed in a temperature-controlled aluminum heating block set to 80 °C. The vials were removed from the heating source (longer than 5 minute heating duration did not result in increased conversion). Upon cooling to room temperature, each reaction was quenched with 3 drops of methanol, filtered through a small

silica/Celite plug, eluting with ethyl acetate (~5 mL). Solvent was removed *in vacuo*, and solutions were taken up in 1 mL of acetonitrile. Mesitylene (1.0 equiv) was added as internal standard for response-factor calibration against authentic products, and the resulting mixture was syringe filtered (0.45 μM) into an HPLC vial for analysis.

*3.5.5 Ni-sulfinamido complexes **C4** and **C5**: Synthesis and characterization*

In a nitrogen-filled glovebox, a 1-dram screw-capped vial was charged with a magnetic stir bar, (**L1**)Ni(*o*-tol)Cl (30.3 mg, 0.045 mmol, 1.0 equiv) or (**L2**)Ni(*o*-tol)Cl (29.8 mg, 0.045 mmol, 1.0 equiv), (*R*)-*tert*-butanesulfinamide (5.5 mg, 0.045 mmol, 1.0 equiv), NaO*t*Bu (4.5 mg, 0.0473 mmol, 1.05 equiv), and benzene (1.0 mL). The vial was sealed with a cap containing a PTFE septum, removed from the glovebox, placed in a temperature-controlled aluminum heating block set to 80 °C, and was allowed to react under the influence of magnetic stirring for 0.75 h. Upon cooling to room temperature, the vial containing the reaction mixture was brought back into the glovebox prior to work-up and filtered over Celite, eluting with benzene (~5 mL). The resulting solution was concentrated *in vacuo* to a volume of ~1-2 mL. Pentane (~10 mL) was added to generate a precipitate, which was then isolated and further washed with pentane (3 x 5 mL). The isolated product was dried *in vacuo* to afford **C4** (from (**L1**)Ni(*o*-tol)Cl) in a 94% yield (31.9 mg, 0.043 mmol) as a dark orange-brown solid, or **C5** (from (**L2**)Ni(*o*-tol)Cl) in a 97% yield (32.6 mg, 0.043 mmol) as a dark orange solid. Elemental analysis (**C4**): Calculated for $C_{39}H_{59}N_1Ni_1O_4P_2S_1$: C, 61.75; H, 7.84; N, 1.85. Found: C, 61.43; H, 7.92; N, 1.83. Elemental analysis (**C5**): Calculated for $C_{39}H_{47}N_1Ni_1O_4P_2S_1$: C, 62.75; H, 6.35; N, 1.88. Found: C, 62.59; H, 6.22; N, 1.91. Each of **C4** and **C5** was isolated as a mixture of isomers, on the basis of $^{31}P\{^1H\}$ NMR data (202.5 MHz, C_6D_6,): **C4** (major isomer): δ

55.31 (d, J = 10.7 Hz), 28.34 (d, J = 10.8 Hz); **C5** (major isomer): δ 52.86 (d, J = 7.8 Hz), 31.66 (d, J = 7.9 Hz). The formation of these isomers can be interpreted as arising from the interplay of the chiral (enantioenriched) sulfinamido moiety, the chiral (racemic) cage phosphine, and the Ni(*o*-tol) groups, whereby hindered Ni-C bond rotation affords diastereomers as is observed crystallographically. We also cannot rule out the existence of *cis*/*trans* isomers, as is observed for (**L1**)Ni(*o*-tol)Cl).[30b] The presence of this isomeric mixture renders the ^{1}H, ^{13}C{^{1}H}, and ^{31}P{^{1}H} NMR spectra sufficiently complex so as to preclude definitive assignment; these spectra are provided in **Figures A40** and **A41** (for **C4**), and **Figures A43** and **A44** (for **C5**) for completeness.

3.5.6 Procedure for the preparation of HPLC samples

Following ***3.5.2-3.5.4*** (0.12 mmol scale in (hetero)aryl halide for ***3.5.2***), at room temperature in air the reaction mixture was quenched with 2 drops of methanol, diluted using ethyl acetate, and passed through a Kimwipe filter containing Celite and silica gel, with the eluent collected in an HPLC vial. The solvent within the HPLC vial was removed under reduced pressure, and the resulting crude solid was taken up in ~1 mL of HPLC-grade acetonitrile and water. This mixture was then filtered through a 0.45 μM syringe filter into a new HPLC vial, capped, and subjected to HPLC analysis.

3.5.7 Purification of N-aryl sulfinamide products via flash column chromatography

Following ***3.5.2*** (0.48 mmol scale), at room-temperature in air the resultant mixture was adsorbed onto silica and eluted through a silica/Celite frit using ethyl acetate as eluent (~20-80 mL). Water (40 mL) was then added, and the solution was extracted with additional ethyl acetate (2 x 30 mL). The combined organic fractions were washed with brine (2 x 30 mL) and dried over sodium sulfate. The resultant solution was concentrated

in vacuo, affording a crude residue which was dissolved in either dichloromethane, or a hexanes/ethyl acetate mixture before being loaded onto either a silica-based flash column or a normal-phase SiliCycle Silia*Sep* 12g 60 Å column cartridge. The product was then purified chromatographically using either a dichloromethane/methanol mixture, or a hexanes/ethyl acetate mixture in each case. The relevant UV-active fractions were combined and dried *in vacuo* to afford the target product.

3.5.8 Characterization data for isolated cross-coupling products

N-(4-cyanophenyl)-2-methylpropane-2-sulfinamide **(3.1)**

The title compound was synthesized from the corresponding aryl chloride (0.48 mmol) according to ***3.5.2***, conducted at 110 °C in 1,4-dioxane using 7.5 mol% (**L2**)Ni(*o*-tol)Cl and purified according to ***3.5.7***. Purified by automated flash column chromatography using an eluent gradient of 10% EtOAc in hexanes (6 CV), 10-60% EtOAc in hexanes (14 CV), followed by 60% EtOAc in hexanes (6 CV), which afforded the title compound in a 63% isolated yield (67.2 mg, 0.302 mmol) as an off-white solid. ^{1}H NMR (500.1 MHz, $CDCl_3$): δ 7.54 (d, J = 8.8 Hz, 2H), 7.04 (d, J = 8.8 Hz, 2H), 5.99 (br, 1H, NH), 1.34 (s, 9H). $^{13}C\{^{1}H\}$ UDEFT NMR (125.8 MHz, $CDCl_3$): 146.48, 133.68, 118.84, 117.14, 105.43, 57.16, 22.27. HRMS-ESI (*m/z*): Calc'd for $C_{11}H_{14}N_2OSNa$ $[M+Na]^+$: 245.0719. Found: 245.0718.

2-methyl-N-(p-tolyl)propane-2-sulfinamide **(3.2)**

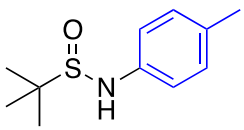

The title compound was synthesized from the corresponding aryl chloride (0.48 mmol) according to ***3.5.2***, conducted at 110 °C in 1,4-dioxane using 7.5 mol% (**L2**)Ni(*o*-tol)Cl and purified according to ***3.5.7***. Purified by automated flash column chromatography using an eluent gradient of 0% DCM (6 CV), 0-6% MeOH in DCM (14 CV), followed by 6% MeOH in DCM (6 CV), affording the title compound in a 64% isolated yield (64.9 mg, 0.307 mmol) as a white solid. ^{1}H NMR (500.1 MHz, $CDCl_3$): δ 7.08 (d, J = 8.25 Hz, 2H), 6.91 (d, J = 8.35 Hz, 2H), 5.17 (br, 1H, NH), 2.29 (s, 3H), 1.32 (s, 9H). ^{13}C{^{1}H} UDEFT NMR (125.8 MHz, $CDCl_3$): δ 139.30, 132.80, 129.93, 118.99, 56.32, 22.44, 20.63. HRMS-ESI (*m/z*): Calc'd for $C_{11}H_{17}NOSNa$ $[M+Na]^+$: 234.0923. Found: 234.0922.

N-(6-methoxypyridin-2-yl)-2-methylpropane-2-sulfinamide (**3.3**)

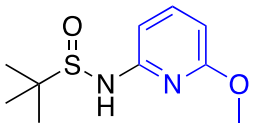

The title compound was synthesized from the corresponding aryl chloride (0.48 mmol) according to ***3.5.2***, conducted at 110 °C in 1,4-dioxane using 7.5 mol% (**L1**)Ni(*o*-tol)Cl and purified according to ***3.5.7***. Purified by automated flash column chromatography using an eluent gradient of 0% DCM (4 CV), 0-6% MeOH in DCM (12 CV), followed by 6% MeOH in DCM (4 CV), which afforded the title compound in a 76% isolated yield (83.3 mg, 0.365 mmol) as a white solid. ^{1}H NMR (500.1 MHz, $CDCl_3$): δ 7.43 (t, J = 7.8 Hz, 1H), 6.45 (d, J = 7.7 Hz, 1H), 6.30 (d, J = 8.05 Hz, 1H), 6.11 (br, 1H, NH), 3.86 (s, 3H), 1.33 (s, 9H). ^{13}C{^{1}H} UDEFT NMR (125.8 MHz, $CDCl_3$): δ 163.43, 153.31, 140.50, 103.23, 101.15, 56.35, 53.49, 22.39. HRMS-ESI (*m/z*): Calc'd for $C_{10}H_{16}N_2O_2SNa$ $[M+Na]^+$: 251.0825. Found: 251.0828.

2-methyl-N-(2-methylquinolin-7-yl)propane-2-sulfinamide (**3.4**)

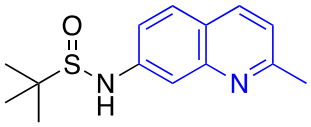

The title compound was synthesized from the corresponding aryl chloride (0.48 mmol) according to ***3.5.2***, conducted at 110 °C in 1,4-dioxane using 7.5 mol% (**L2**)Ni(*o*-tol)Cl and purified according to ***3.5.7***. Purified by automated flash column chromatography using an eluent gradient of 0% DCM (6 CV), 0-6% MeOH in DCM (16 CV), followed by 6% MeOH in DCM (4 CV), affording the title compound in a 58% yield (73.04 mg, 0.278 mmol) as an off-white solid. ^{1}H NMR (500.1 MHz, $CDCl_3$): δ 7.91 (d, J = 8.35, 1H), 7.62 (d, J = 8.70, 1H), 7.56 (m, 1H), 7.19 (m, 1H), 7.14 (d, J = 8.3, 1H), 5.84 (br, 1H, NH), 2.71 (s, 3H, CH_3), 1.36 (s, 9H). ^{13}C{^{1}H} UDEFT NMR (125.8 MHz, $CDCl_3$): δ 159.39, 147.77, 144.11, 136.67, 128.81, 122.58, 120.26, 118.63, 112.92, 56.98, 22.39, 22.10. HRMS-ESI (*m/z*): Calc'd for $C_{14}H_{19}N_2OS$ $[M+H]^+$: 263.1213. Found: 263.1207.

N-(2-cyanophenyl)-2-methylpropane-2-sulfinamide (**3.5**)

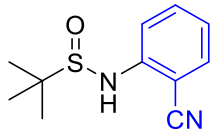

The title compound was synthesized from the corresponding aryl chloride (0.48 mmol) according to ***3.5.2***, conducted at 110 °C in 1,4-dioxane using 7.5 mol% (**L1**)Ni(*o*-tol)Cl and purified according to ***3.5.7***. Purified by flash column chromatography using an eluent gradient of 70% EtOAc in hexanes, affording the title compound in a 71% yield (75.8 mg, 0.341 mmol) as a white solid. ^{1}H NMR (500.1 MHz, $CDCl_3$): δ 7.53 (apparent t, J = 7.9 Hz, 2H), 7.38 (d, J = 8.25 Hz, 1H), 7.06 (apparent td, J = 7.60, 0.80 Hz, 1H), 6.07 (br, 1H,

NH), 1.38 (s, 9H). $^{13}C\{^{1}H\}$ UDEFT NMR (125.8 MHz, $CDCl_3$): δ 145.03, 134.30, 132.86, 122.60, 117.11, 116.35, 101.62, 57.50, 22.36. HRMS-ESI (*m/z*): Calc'd for $C_{11}H_{14}N_2OSNa$ $[M+Na]^+$: 245.0719. Found: 245.0723.

N-(benzo[d]isothiazol-3-yl)-2-methylpropane-2-sulfinamide (**3.6**)

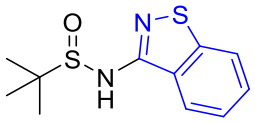

The title compound was synthesized from the corresponding aryl chloride (0.48 mmol) according to ***3.5.2***, conducted at 110 °C in 1,4-dioxane using 7.5 mol% (**L2**)Ni(*o*-tol)Cl and purified according to ***3.5.7***. Purified by automated flash column chromatography using an eluent gradient of 0% EtOAc in hexanes (4 CV), 0-40% EtOAc in hexanes (16 CV), 40% EtOAc in hexanes (4 CV), affording the title compound in a 67% isolated yield (81.8 mg, 0.322 mmol) as an off-white solid. ^{1}H NMR (500.1 MHz, $CDCl_3$): δ 7.96 (d, J = 8.2 Hz, 1H), 7.76 (d, J = 8.20 Hz, 1H), 7.50 (apparent td, J = 8.05, 0.80 Hz, 1H), 7.40 (apparent td, J = 7.95, 0.70 Hz, 1H), 7.11 (br, 1H, NH), 1.41 (s, 9H). $^{13}C\{^{1}H\}$ UDEFT NMR (125.8 MHz, $CDCl_3$): δ 154.70, 152.49, 128.36, 126.35, 124.59, 122.30, 120.19, 57.32, 22.42. HRMS-ESI (*m/z*): Calc'd for $C_{11}H_{14}N_2OS_2Na$ $[M+Na]^+$: 277.0440. Found: 277.0440.

2-methyl-N-phenylpropane-2-sulfinamide (**3.7**)

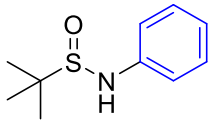

The title compound was synthesized from the corresponding aryl chloride (0.48 mmol) according to ***3.5.2***, conducted at 110 °C in 1,4-dioxane using 7.5 mol% (**L2**)Ni(*o*-tol)Cl

and purified according to ***3.5.7***. Purified by automated flash column chromatography using an eluent gradient of 0% EtOAc in hexanes (4 CV), 0-60% EtOAc in hexanes (14 CV), 60% EtOAc in hexanes (6 CV), affording the title compound in a 62% isolated yield (58.2 mg, 0.298 mmol) as a pale yellow solid. ^{1}H NMR (500.1 MHz, $CDCl_3$): δ 7.24 (apparent td, J = 9.8, 2.45 Hz, 2H), 7.00 (m, overlapping ArHs, 3H), 5.68 (d, J = 13.9 Hz, 1H, NH), 1.32 (s, 9H). ^{13}C{^{1}H} UDEFT NMR (125.8 MHz, $CDCl_3$): 142.17, 129.35, 122.81, 118.25, 56.48, 22.45. HRMS-ESI (*m/z*): Calc'd for $C_{10}H_{15}NOSNa$ $[M+Na]^+$: 220.0767. Found: 220.0767.

2-methyl-N-(o-tolyl)propane-2-sulfinamide (**3.8**)

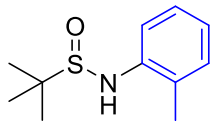

The title compound was synthesized from the corresponding aryl chloride (0.48 mmol) according to ***3.5.2***, conducted at 110 °C in 1,4-dioxane using 7.5 mol% (**L2**)Ni(*o*-tol)Cl and purified according to ***3.5.7***. Purified by automated flash column chromatography using an eluent gradient of 0% EtOAc in hexanes (4 CV), 0-60% EtOAc in hexanes (12 CV), 60% EtOAc in hexanes (4 CV), affording the title compound in a 49% isolated yield (49.7 mg, 0.235 mmol) as an off-white solid. ^{1}H NMR (500.1 MHz, $CDCl_3$): δ 7.16 (m, overlapping ArHs, 3H), 6.97 (m, 1H), 5.19 (br, 1H, NH), 2.27 (s, 3H, CH_3), 1.35 (s, 9H). ^{13}C{^{1}H} UDEFT NMR (125.8 MHz, $CDCl_3$): δ 139.99, 130.84, 127.55, 127.14, 123.48, 119.23, 56.54, 22.50, 17.70. HRMS-ESI (*m/z*): Calc'd for $C_{11}H_{17}NOSNa$ $[M+Na]^+$: 234.0923. Found: 234.0923.

N-(benzo[b]thiophen-5-yl)-2-methylpropane-2-sulfinamide (**3.9**)

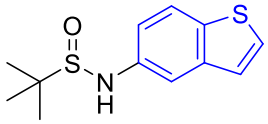

The title compound was synthesized from the corresponding aryl chloride (0.48 mmol) according to ***3.5.2***, conducted at 110 °C in 1,4-dioxane using 10 mol% (**L1**)Ni(*o*-tol)Cl and purified according to ***3.5.7***. Purified by automated flash column chromatography using an eluent gradient of 0% EtOAc in hexanes (6 CV), 0-60% EtOAc in hexanes (14 CV), 60% EtOAc in hexanes (6 CV), affording the title compound in a 29% isolated yield (35.3 mg, 0.139 mmol) as an off-white solid. ^{1}H NMR (500.1 MHz, $CDCl_3$): δ 7.73 (d, J = 8.55, 1H), 7.47 (s, 1H), 7.44 (d, J = 5.40 Hz, 1H), 7.21 (d, J = 5.35 Hz, 1H), 7.05 (apparent dd, J = 8.50, 1.50 Hz, 1H), 5.57 (br, 1H, NH), 1.36 (s, 9H). ^{13}C{^{1}H} UDEFT NMR (125.8 MHz, $CDCl_3$): 140.53, 139.02, 134.75, 127.86, 123.49, 123.17, 117.28, 113.02, 56.56, 22.51. HRMS-ESI (*m/z*): Calc'd for $C_{12}H_{15}NOS_2Na$ $[M+Na]^+$: 276.0487. Found: 276.0491.

2-methyl-N-(napthalen-2-yl)propane-2-sulfinamide (**3.10**)

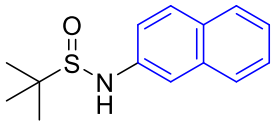

The title compound was synthesized from the corresponding aryl chloride (0.48 mmol) according to ***3.5.2***, conducted at 110 °C in 1,4-dioxane using 7.5 mol% (**L2**)Ni(*o*-tol)Cl and purified according to ***3.5.7***. Purified by automated flash column chromatography using an eluent gradient of 0% EtOAc in hexanes (4 CV), 0-50% EtOAc in hexanes (10 CV), 50% EtOAc in hexanes (6 CV), affording the title compound in a 39% isolated yield (46.3 mg, 0.187 mmol) as a purple solid. ^{1}H NMR (500.1 MHz, $CDCl_3$): δ 7.75 (d, J = 8.55, 2H),

7.69 (d, J = 8.20, 1H), 7.42 (m, overlapping ArHs, 2H), 7.35 (t, J = 7.55, 1H), 7.20 (apparent dd, J = 8.75, 2.1 Hz, 1H), 5.61 (br, 1H, NH), 1.38 (s, 9H). $^{13}C\{^{1}H\}$ UDEFT NMR (125.8 MHz, $CDCl_3$): δ 139.60, 134.10, 130.09, 129.47, 127.69, 126.82, 126.71, 124.44, 119.32, 114.01, 56.64, 22.48. HRMS-ESI (*m/z*): Calc'd for $C_{14}H_{17}NOSNa$ $[M+Na]^+$: 270.0923. Found: 270.0921.

4-methyl-N-(naphthalen-1-yl)benzenesulfinamide (**3.11**)

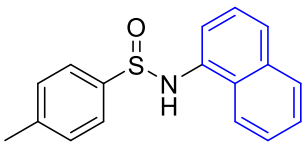

The title compound was synthesized from the corresponding aryl chloride (0.48 mmol) according to ***3.5.2***, conducted at 110 °C in 1,4-dioxane using 7.5 mol% (**L1**)Ni(*o*-tol)Cl and purified according to ***3.5.7***. Purified by automated flash column chromatography using an eluent gradient of 0% EtOAc in hexanes (4 CV), 0-60% EtOAc in hexanes (14 CV), 60% EtOAc in hexanes (6CV), affording the title compound in a 70% isolated yield (94.5 mg, 0.336 mmol) as an off-white solid. ^{1}H NMR (500.1 MHz, $CDCl_3$): δ 7.99 (apparent t, J = 5.30 Hz, 1H), 7.84 (apparent t, J = 5.05 Hz, 1H), 7.73 (apparent dd, J = 8.15, 1.95 Hz, 2H), 7.63 (d, J = 8.20 Hz, 1H), 7.52 (d, J = 7.35 Hz, 1H), 7.48 (apparent t, J = 4.7 Hz, 2H), 7.37 (apparent td, J = 7.85, 2.1 Hz, 1H), 7.29 (apparent t, J = 7.9 Hz, 2H), 6.73 (d, J = 10.70 Hz, 1H, NH), 2.41 (s, 3H, CH_3).$^{13}C\{^{1}H\}$ UDEFT NMR (125.8 MHz, $CDCl_3$): δ 142.13, 141.97, 136.06, 134.35, 129.83, 128.56, 127.65, 126.27, 126.23, 125.77, 125.46, 125.32, 121.38, 118.29, 21.41. HRMS-ESI (*m/z*): Calc'd for $C_{17}H_{16}NOS$ $[M+H]^+$: 282.0947. Found: 282.0947.

Chapter 4. Research Conclusions and Future Work

4.1 Chapter 2

The superior ability of the **(PhPAd-DalPhos)**Ni(*o*-tol)Cl / NaO*t*Bu catalyst system to enable the C-N cross-coupling of both bulky primary alkylamines ($pK_a > 40$)[52] and primary aryl sulfonamides ($pK_a \sim 16$)[53] prompted a study of the mechanistic underpinnings governing these challenging reactions. Combined experimental and computational study of transmetalation and reductive elimination processes revealed the favourability of a previously undisclosed reductive elimination pathway promoted by the deprotonation of a putative Ni-NHR amido intermediate, leading to an anionic Ni-nitrenoid species.

The synthesis and characterization of the electronically diverse (**L2**)Ni(*o*-tol)(NHS(O)$_2$R) complexes **C1-C3** presented a unique opportunity for the study of putative Ni^{II} catalytic intermediates. Whereas previous studies of this type were limited to secondary arylamine coordination complexes of the form (**dcype**)Ni(aryl)(NR$_2$),[34] the presence of the NH unit in the primary Ni-amido structure introduced the possibility of a more complex turnover step. Indeed, under catalytically relevant conditions, it was determined that the presence of NaO*t*Bu promoted C-N bond-forming reductive elimination from **C1-C3**. Unfortunately, the corresponding (**L2**)Ni(*o*-tol)(NH*t*Bu) species could not be reliably synthesized, and therefore could not be probed experimentally.

The catalyst resting state was determined through the $^{31}P\{^1H\}$ NMR monitoring of catalytic reactions between 2-chlorotoluene and 4-methoxybenzene sulfonamide or *t*BuNH$_2$, in which signals consistent with the transient (**L2**)Ni(*o*-tol)(O*t*Bu) species could be observed. This observation was supported by DFT calculations, which placed the Ni-alkoxide species as the lowest energy species in the free-energy landscape. Subsequent experimental and computational study of transmetalation supported the prospect of a

deprotonated Ni-nitrenoid species providing an alternative pathway to reductive elimination for the case of the weakly nucleophilic sulfonamides. DFT calculations suggested the opposite trend for the case of primary alkylamines, which is consistent with the experimental requirement of only 1.5 equivalents of added NaO*t*Bu.

The details revealed by the study of the Ni-catalyzed sulfonamide *N*-arylation represent an interesting alternative mechanism that could potentially be exploited in similar Ni-catalyzed cross-couplings. Given the early indications that this process may be active for the case of weakly nucleophilic substrates featuring amide functionalities, it is not unreasonable to propose the possible activity of this pathway in related mechanisms such as the Ni-catalyzed *N*-arylation of primary amides. Stradiotto and co-workers have previously demonstrated the ability of Ni to enable these transformations using **PAd-DalPhos** / K_3PO_4 (1.5 equiv)[54] and **CyPAd-DalPhos** / DBU + NaTFA (2.0 equiv)[55], and while the scope of these reactions combined is quite impressive, the mechanism remains underexplored (**Figure 4.1**).

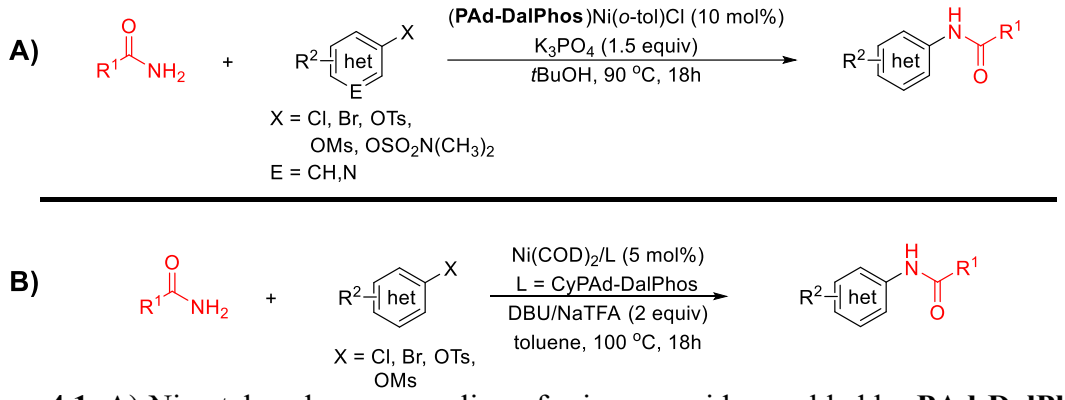

Figure 4.1. A) Ni-catalyzed cross-coupling of primary amides enabled by **PAd-DalPhos** and K_3PO_4.[54] B) Ni-catalyzed cross-coupling of primary amides enabled by **CyPAd-DalPhos** and soluble organic 'dual-base' DBU/NaTFA. Both mechanisms are presently underexplored.[55]

.

Applying similar concepts from this Chapter, the catalytic pathway of primary amide cross-coupling could perhaps be elucidated via the synthesis of corresponding Ni-NHR complexes. Pending the success of these syntheses, the effects of base and/or elevated temperatures could be probed to gain insights regarding the elementary steps that make these reactions feasible. Subsequent DFT calculations could provide useful a useful comparative landscape for the energetics of various Ni-nucleophile systems.

4.2 Chapter 3

The development of the first reported Ni-catalyzed *N*-arylation of primary sulfinamides is reported, incorporating tailored ancillary ligands **CyPAd-DalPhos** and **PhPAd-DalPhos**. A reasonably diverse scope of (hetero)aryl chlorides were accommodated in this system, albeit in moderate isolated yields. In comparison to our previously reported sulfonamide *N*-arylation system,[21] resultant sulfinamide reaction mixtures were often significantly more complex, leading to difficulties in the isolation of pure material. The comparative abilities of **CyPAd-DalPhos** and **PhPAd-DalPhos** were assessed, and the degree of success appears to depend solely on the electrophile chosen. The ability of (**PhPAd-DalPhos**)Ni(*o*-tol)Cl to enable the catalytic *N*-arylation of both sulfonamides and sulfinamides prompted us to investigate the selectivity between the two nucleophiles. It was determined that the catalyst system is entirely selective for the sulfonamide *N*-aryl product, though conversion is significantly hindered in the presence of the sulfinamide nucleophile.

Given the apparent necessity of employing two equivalents of NaO*t*Bu in this catalytic system, I became interested in the possible activity of a Ni-nitrenoid reductive elimination pathway. Synthesis and isolation of the requisite Ni-sulfinamido complexes

proved both possible and highly replicable for each of the optimal ligands. Monitoring the C-N bond-forming reductive elimination of both complexes by HPLC analysis revealed a similar trend to what was seen in Chapter 2 of this Thesis (i.e., reductive elimination is significantly improved by the addition of base),[33] providing further evidence for the activity of a deprotonated Ni-nitrenoid intermediate. This was supported by collaborative DFT calculations, which maintained the tendency of the anionic intermediate to undergo reductive elimination more readily.

The success of the (**PhPAd-DalPhos**)Ni(*o*-tol)Cl precatalyst in both the sulfonamide and sulfinamide systems prompts the question of whether or not further weakly-nucleophilic compounds can be activated by this catalyst or a related **DalPhos** ligand. One moiety that stands out in particular is the *NH*-sulfoximine, receiving a large degree of interest from synthetic and medicinal chemists alike due to its promising physicochemical properties (**Figure 4.2**).[56] Several methods targeting the *N*-arylation of these compounds exist, dating back to a Pd-catalyzed BHA reaction introduced by Carsten Bolm and Jens P. Hildebrand in 2000.[57] Since then, several base-metal catalyzed systems have been developed in the quest for more sustainable chemistry. A Cu-catalyzed method was developed by Bolm and Jörg Sedelmeier,[58] and several Ni-redox methods have been introduced in recent years.[59] However, the ligand-enabled Ni-catalyzed *N*-arylation of sulfoximines represents an unmet challenge in cross-coupling chemistry. The characteristic ability of **DalPhos** ligands to access difficult (hetero)aryl electrophiles (i.e., chlorides and phenol derivatives) could dramatically increase the quantity of available functionalization to the sulfoximine core if it can be accommodated in our catalytic systems.

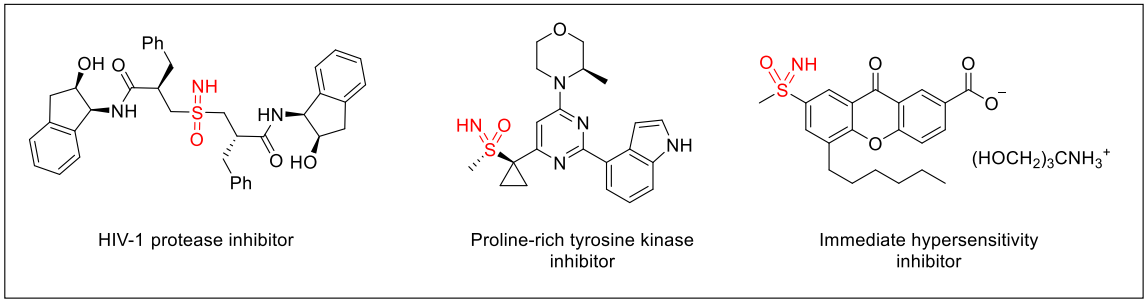

Figure 4.2. Examples of promising bioactive moieties containing a synthetically-useful free sulfoximine-*NH*.[56a]

5. References

1. Magano, J. and Dunetz, J. R. Large-Scale Applications of Transition Metal-Catalyzed Couplings for the Synthesis of Pharmaceuticals. *Chem. Rev.* **2011**, 111, *3*, 2177-2250.

2. Lundgren, R. J. and Stradiotto, M. in *Ligand Design in Metal Chemistry*, John Wiley & Sonds, Ltd, 2016, pp. 1-14.

3. Ruiz-Castillo, P. and Buchwald, S. L. Applications of Palladium-Catalyzed C-N Cross-Coupling Reactions. *Chem. Rev.* **2016**, 116, *9*, 12564-12649.

4. Roughley, S. D. and Jordan, A. M. The Medicinal Chemist's Toolbox: An Analysis of Reactions Used in the Pursuit of Drug Candidates. *J. Med. Chem.* **2011**, 54, *10*, 3451-3479.

5. Terrier, F., *Modern Nucleophilic Aromatic Substitution*. Wiley-VCH: Weinheim, 2013.

6. Badgujar, D. M.; Talawar, M. B.; Mahulikar, P. P. Review on Greener and Safer Synthesis of Nitro Compounds. *Propellants Explos. Pyrotech.* **2015**, 41, *1*, 24-34.

7. Dorel, R.; Grugel, C. P.; Haydl, A. M. The Buchwald-Hartwig Amination After 25 Years. *Angew. Chem. Int. Ed.* **2019**, 58, *48*, 17118-17129.

8. Surry, D. S.; Buchwald, S. L. Biaryl Phosphine Ligands in Palladium-Catalyzed Amination. *Angew. Chem. Int. Ed.* **2008**, 47, *34*, 6338-6361.

9. Ananikov, V. P. Nickel: The "Spirited Horse" of Transition Metal Catalysis. *ACS Catal*. **2015**, 5, *3*, 1964-1971.

10. Ahmad, K.; Khan, B. A.; Akram, B.; Khan, J.; Mahmood, R. and Roy, S. K. Theoretical Investigations on Copper Catalyzed C-N Cross-Coupling between Aryl Chlorides and Amines. *Comput. Theoret. Chem.* **2018**, 1134, 1-7.

11. Lavoie, C. M. and Stradiotto, M. Bisphosphines: A Prominent Ancillary Ligand Class for Application in Nickel-Catalyzed C-N Cross-Coupling. *ACS Catal*. **2018**, 8, *8*, 7228-7250.

12. Guram, A. S., Rennels, R. A.; Buchwald, S. L. A Simple Catalytic Method for the Conversion of Aryl Bromides to Arylamines. *Angew. Chem. Int. Ed.* **1995**, 34, *12*, 1348-1350.

13. Louie, J. and Hartwig, J. F. Palladium-Catalyzed Synthesis of Arylamines from Aryl Halides: Mechanistic Studies Lead to Coupling in the Absence of Tin Reagents. *Tetrahedron Lett.* **1995**, 36, *12*, 3609-3612.

14. Ingoglia, B. T.; Wagen, C. C.; Buchwald, S. L. Biaryl monophosphine ligands in palladium-catalyzed C-N coupling: An updated User's guide. *Tetrahedron*, **2019**, 75, *32*, 4199-4211.

15. (a) Alsabeh, P. G.; Stradiotto, M. Addressing Challenges in Palladium-Catalyzed Cross-Couplings of Aryl Mesylates: Monoarylation of Ketones and Primary Alkyl Amines *Angew. Chem. Int. Ed.* 2013, *52*, 7242-7246. (b) Fors, B. P.; Watson, D. A.; Biscoe, M. R.; Buchwald, S. L. A Highly Active Catalyst for Pd-Catalyzed Amination Reactions: Cross-Coupling Reactions Using Aryl Mesylates and the Highly Selective Monoarylation of Primary Amines Using Aryl Chlorides. *J. Am. Chem. Soc.* 2008, *130*, 13552-13554.

16. Sun, X.; Tu, X.; Dai, C.; Zhang, X.; Zeng, Q. Palladium-Catalyzed Cross Coupling of Sulfinamides and Aryl Halides. *J. Org. Chem.* **2012**, 77, *9*, 4454-4459.

17. Hartwig, J. F. Evolution of a Fourth Generation Catalyst for the Amination and Thioetherification of Aryl Halides. *Acc. Chem. Res.* **2008**, 41, *11*, 1534-1544.

18. (a) Lundgren, R. J.; Peters, B. D.; Alsabeh, P. G.; Stradiotto, M. A P,N-Ligand for Palladium- Catalyzed Ammonia Arylation: Coupling of Deactivated Aryl Chlorides, Chemoselective Arylations, and Room Temperature Reactions. *Angew. Chem. Int. Ed.* **2010**, 49, *24*, 4701-4074. (b) Tardiff, B. J.; Stradiotto, M. Buchwald-Hartwig Amination of (Hetero)aryl Chlorides by Employing Mor-DalPhos under Aqueous and Solvent-Free Conditions. *Chem. Eur. J.* **2012**, 21, 3972-3977.

19. (a) Zhang, Y.; Yang, X.; Yao, Q.; Ma, D. CuI/DMPAO-Catalzyed *N*-Arylation of Secondary Amines. *Org. Lett.* **2012**, 14, *12*, 3056-3059. (b) Chen, J. Q.; Li, J. H.; Dong, Z. B. A Review on the Latest Progress of Chan-Lam Coupling Reaction. *Adv. Synth. Catal.* **2020**, 362, *16*, 3311-3331.

20. Marin, M.; Rama, R. J.; Nicasio, C. Ni-Catalyzed Amination Reactions: An Overview. *Chem. Rec.* **2016**, 16, *4*, 1819-1832.

21. McGuire, R. T., Simon, C. M.; Yadav, A. A.; Ferguson, M. J.; Stradiotto, M. Nickel-Catalyzed Cross-Coupling of Sulfonamides with (Hetero)aryl Chlorides. *Angew. Chem. Int. Ed.* **2020**, 59, *23*, 8952-8956.

22. (a) Lavoie, C. M.; McDonald, R.; Johnson, E. R.; Stradiotto, M. Bisphosphine-Ligated Nickel Pre-catalysts in C(sp^2)-N Cross Couplings of Aryl Chlorides: a Comparison of Nickel(I) and Nickel(II). *Adv. Synth. Catal.* **2017**, 359, *17*, 2972-2980. (b) Kampmann, S. S.; Skelton, B. W.; Wild, D. A.; Koutsantonis, G. A.; Stewart, S. G. An Air-Stable Nickel(0) Phosphite precatalyst for Primary Alkylamine C-N Cross-Coupling Reactions. *Eur. J. Org. Chem.* **2015**, 2015, *27*, 5995-6004.

23. Kawamata, Y.; Vantourout, J. C.; Hickey, D. P.; Bai, P.; Chen, L.; Hou, Q.; Qiao, W.; Barman, K.; Edwards, M. A.; Garrido-Castro, A. F.; deGruyter, J. N.; Nakamura, H.; Knouse, K.; Qin, C.; Clay, K. J.; Bao, D.; Starr, J. T. Garcia-Irizarry, C.; Sach, N.; White, H. S.; Neurock, M.; Minteer, S. D.; Baran, P. S. Electrochemically Driven, Ni-Catalyzed Aryl Amination: Scope, Mechanism, and Applications. *J. Am. Chem. Soc.* **2019**, 141, *15*, 6392-6402.

24. Chan, A. Y.; Perry, I. B.; Bissonnette, N. B.; Buksh, B. F.; Edwards, G. A.; Frye, L. I.; Garry, O. L.; Lavagnino, M. N.; Li, B. X.; Liang, Y.; Mao, E.; Millet, A.; Oakley, J. V.; Reed, N. L.; Sakai, H. A.; Seath, C. P.; MacMillan, D. W. C. Metallaphodoredox: The Merger of Photoredox and Transition Metal Catalysis. *Chem. Rev.* **2022**, 122, *2*, 1485-1542.

25. Corcoran, E. B.; Pirnot, M. T.; Lin, S.; Dreher, S. D.; DiRocco, D. A.; Davies, I. W.; Buchwald, S. L.; MacMillan, D. W. C. Aryl amination using ligand-free Ni(II) salts and photoredox catalysis. *Science* **2016**, 353, 279-283.

26. (a) Kim, T.; McCarver, S. J.; Lee, C.; MacMillan, D. W. C. Sulfonamidation of Aryl and Heteroaryl Halides through Photosensitized Nickel Catalysis. *Angew. Chem. Int. Ed.* **2018**, 57, *13*, 3488-3492. (b) Wimmer, A. and König, B. *N*-Arylation of *NH*-Sulfoximines vis Dual Nickel Photocatalysis. *Org. Lett.* **2019**, 21, *8*, 2740-2744.

27. Zhu, C.; Yue, H.; Jia, J.; Rueping, M. Nickel Catalyzed C-Heteroatom Cross-Coupling Reactions under Mild Conditions via Facilitated Reductive Elimination. *Angew. Chem. Int. Ed.* **2020**, 60, *33*, 17810-17831.

28. Lim, C. H.; Kudisch, M.; Liu, B.; Miyake, G. M. C-N Cross-Coupling via Photoexcitation of Nickel-Amine Complexes. *J. Am. Chem. Soc.* **2018**, 140, *24*, 7667-7673.

29. Lavoie, C. M.; MacQueen, P. M.; Rotta-Loria, N. L.; Sawatzky, R. S.; Borzenko, A.; Chisholm, A. J.; Hargreaves, B. K. V.; McDonald, R.; Ferguson, M. J.; Stradiotto, M. Challenging nickel-catalysed amine arylations enabled by tailored ancillary ligand design. *Nat. Commun.* **2016**, 11073.

30. (a) Tassone, J. P.; England, E. V.; MacQueen, P. M.; Ferguson, M. J. Stradiotto, M. PhPAd-DalPhos: Ligand-Enabled, Nickel-Catalyzed Cross-Coupling of (Hetero)aryl Electrophiles with Bulky Primary Alkylamines. *Angew. Chem. Int. Ed.* **2019**, 58, *8*, 2485-2489. (b) Tassone, J. P.; MacQueen, P. M.; Lavoie, C. M.; Ferguson, M. J.; McDonald, R.; Stradiotto, M. Nickel-Catalyzed *N*-Arylation of Cyclopropylamine and Related Ammonium Salts with (Hetero)aryl (Pseudo)halides at Room Temperature. *ACS Catal.* **2017**, 7, *9*, 6048-6059. (c) Clark, J. S. K.; Ferguson, M. J.; McDonald, R.; Stradiotto, M. Pad2-DalPhos Enables the Nickel-Catalyzed C-N Cross-Coupling of Primary Heteroarylamines and (Hetero)aryl Chlorides. *Angew. Chem. Int. Ed.* **2019**, 58, *19*, 6391-6395. (d)

McGuire, R. T.; Yadav, A. A.; Stradiotto, M. Nickel-Catalyzed N-Arylation of Fluoroalkylamines. *Angew. Chem, Int. Ed.* **2020**, 60, *8*, 4080-4084.

31. (a) Gatien, A. V.; Lavoie, C. M.; Bennett, R. N.; Ferguson, M. J.; McDonald, R.; Johnson, E. R.; Speed, A. W. H.; Stradiotto, M. Application of Diazaphospholidine/Diazaphospholene-Based Bisphosphines in Room-Temperature Nickel-Catalyzed C(sp^2)-N Cross-Couplings of Primary Alkylamines with (Hetero)aryl Chlorides and Bromides. *ACS Catal.* **2018**, 8,*6*, 5328-5339. (b) McGuire, R. T.; Paffile, J. F. J.; Zhou, Y.; Stradiotto, M. Nickel-Catalyzed C-N Cross-Coupling of Ammonia, (Hetero)anilines, and Indoles with Activated (Hetero)aryl Chlorides Enabled by Ligand Design. *ACS Catal.* **2019**, 9, *10*, 9292-9297.

32. Morrison, K. M.; McGuire, R. T.; Ferguson, M. J.; Stradiotto, M. CgPhen-DalPhos Enables the Nickel-Catalyzed *O*-Arylation of Tertiary Alcohols with (Hetero)aryl Electrophiles. *ACS Catal.* **2021**, 11, *17*, 10878-10884.
33. Simon, C. M.; Dudra, S. L.; McGuire, R. T.; Ferguson, M. J.; Johnson, E. R., Stradiotto, M. identification of a Nitrenoid Reductive Elimination Pathway in Nickel-Catalyzed C-N Cross-Coupling. *ACS Catal.* **2022**, 12, *2*, 1475-1480.

34. (a) Morioka, T.; Nakatani, S.; Sakamoto, Y.; Kodama, T.; Ogoshi, S.; Chatani, N.; Tobisu, M., Nickel-Catalyzed Decarbonylation of N-Acylated N-Heteroarenes. *Chem. Sci.* **2019**, *10*, 6666-6671; (b) Malapit, C. A.; Borrell, M.; Milbauer, M. W.; Brigham, C. E.; Sanford, M. S., Nickel-Catalyzed Decarbonylative Amination of Carboxylic Acid Esters. *J. Am. Chem. Soc.* **2020**, *142*, 5918-5923; (c) Bismuto, A.; Delcaillau, T.; Muller, P.; Morandi, B., Nickel-Catalyzed Amination of Aryl Thioethers: A Combined Synthetic and Mechanistic Study. *ACS Catal.* **2020**, *10*, 4630-4639.

35. Mann, G.; Hartwig, J. F., Palladium Alkoxides: Potential Intermediacy in Catalytic Amination, Reductive Elimination of Ethers, and Catalytic Etheration. Comments on Alcohol Elimination from Ir(III). *J. Am. Chem. Soc.* **1996**, *118*, 13109-13110.

36. Brusoe, A. T.; Hartwig, J. F., Palladium-Catalyzed Arylation of Fluoroalkylamines. *J. Am. Chem. Soc.* **2015**, *137*, 8460-8468.

37. (a) Ray, K.; Heims, F.; Pfaff, F. F., Terminal Oxo and Imido Transition-Metal Complexes of Groups 9-11. *Eur. J. Inorg. Chem.* **2013**, 3784-3807; (b) Grunwald, A.; Anjana, S. S.; Munz, D., Terminal Imido Complexes of the Groups 9-11: Electronic Structure and Developments in the Last Decade. *Eur. J. Inorg. Chem.* **2021**, 4147-4166.

38. The strongly nucleophilic character of an isolable four-coordinate Pd sulfonimido complex has been documented: Grunwald, A.; Orth, N.; Scheurer, A.; Heinemann, F. W.; Pothig, A.; Munz, D., An Isolable Terminal Imido Complex of Palladium and Catalytic Implications. *Angew. Chem. Int. Ed.* **2018**, *57*, 16228-16232.

39. Qingle, Z.; Zhang, Q.; Xi, J.; Ze, H., Syntheses and Transformations of Sulfinamides. *Synthesis* **2021**, *53*, 2570-2582.

40. (a) Lo, P. K. T.; Oliver, G. A.; Willis, M. C., Sulfinamide Synthesis Using Organometallic Reagents, DABSO, and Amines. *J. Org. Chem.* **2020**, *85*, 5753-5760; (b) Hervieu, C.; Kirillova, M. S.; Suarez, T.; Muller, M.; Merino, E.; Nevado, C., Asymmetric, visible light-mediated radical sulfinyl-Smiles rearrangement to access all-carbon quaternary stereocentres. *Nat. Chem.* **2021**, *13*, 327-334; (c) Sephton, T.; Large, J. M.; Butterworth, S.; Greaney, M. F., Diarylamine Synthesis via Desulfinylative Smiles Rearrangement. *Org. Lett.* **2022**, *24*, 1132-1135.

41. (a) Liu, G.; Cogan, D. A.; Ellman, J. A., Catalytic Asymmetric Synthesis of tert-Butanesulfinamide. Application to the Asymmetric Synthesis of Amines. *J. Am. Chem. Soc.* **1997**, *119*, 9913-9914; (b) Prakash, A.; Dibakar, M.; Selvakumar, K.; Ruckmani, K.; Sivakumar, M., Efficient indoles and anilines syntheses employing tert-butyl sulfinamide as ammonia surrogate. *Tetrahedron Lett.* **2011**, *52*, 5625-5628.

42. Scott, K. A.; Njardarson, J. T., Analysis of US FDA-Approved Drugs Containing Sulfur Atoms. *Top. Curr. Chem.* **2018**, *376*.

43. Ballatore, C.; Huryn, D. M.; Smith, A. B., Carboxylic Acid (Bio)Isosteres in Drug Design. *ChemMedChem* **2013**, *8*, 385-395.

44. Du, G.; Binda, P.; Abbina, S., Modular Synthesis of Chiral β-Diketiminato-Type Ligands Containing 2-Oxazoline Moiety via Palladium-Catalyzed Amination. *Synthesis* **2011**, *2011*, 2609-2618.

45. Sun, X.; Tu, X.; Dai, C.; Zhang, X.; Zhang, B.; Zeng, Q., Palladium-catalyzed C-N cross coupling of sulfinamides and aryl halides. *J. Org. Chem.* **2012**, *77*, 4454-9.

46. (a) Baffoe, J.; Hoe, M. Y.; Toure, B. B., Copper-Mediated N-Heteroarylation of Primary Sulfonamides: Synthesis of Mono-N-heteroaryl Sulfonamides. *Org. Lett.* **2010**, *12*, 1532-1535; (b) Liu, Y.; Wang, Z.; Guo, B.; Cai, Q., Asymmetric synthesis of N-aryl sulfinamides: copper(I)-catalyzed coupling of sulfinamides with aryl iodides via kinetic resolution. *Tetrahedron Lett.* **2016**, *57*, 2379-2381.

47. Qin, S.; Luo, Y.; Sun, Y.; Tian, L.; Jiang, S.; yan, J.; Yang, G., Iron/copper co-catalyzed highly selective arylation of sulfinamides with aryl iodides (*Note*: Corrigendum exists for this article). *Tetrahedron Lett.* **2019**, *60*, 151167.

48. Grushin, V. V.; Alper, H., Transformations of chloroarenes, catalyzed by transition-metal complexes. *Chem. Rev.* **1994**, *94*, 1047-1062.

49. (a) Park, N. H.; Teverovskiy, G.; Buchwald, S. L., Development of an air-stable nickel precatalyst for the amination of aryl chlorides, sulfamates, mesylates, and triflates. *Org. Lett.* **2014**, *16*, 220-223; (b) Clark, J. S. K.; Voth, C. N.; Ferguson, M.

J.; Stradiotto, M., Evaluating 1,1′-Bis(phosphino)ferrocene Ancillary Ligand Variants in the Nickel-Catalyzed C–N Cross-Coupling of (Hetero)aryl Chlorides. *Organometallics* **2017**, *36*, 679-686.

50. Sawatzky, R. S.; Ferguson, M. J.; Stradiotto, M., Thieme Chemistry Journals Awardees - Where Are They Now? Efficient Cross-Coupling of Secondary Amines/Azoles and Activated (Hetero)Aryl Chlorides Using an Air-Stable DPEPhos/Nickel Pre-Catalyst. *Synlett* **2017**, *28*, 1586-1591.

51. (a) Beutner, G. L.; Coombs, J. R.; Green, R. A.; Inankur, B.; Lin, D.; Qiu, J.; Roberts, F.; Simmons, E. M.; Wisniewski, S. R., Palladium-Catalyzed Amidation and Amination of (Hetero)aryl Chlorides under Homogeneous Conditions Enabled by a Soluble DBU/NaTFA Dual-Base System. *Org. Process Res. Dev.* **2019**, *23*, 1529-1537; (b) MacMillan, J. W. M.; McGuire, R. T.; Stradiotto, M., Organic Base Enabled Nickel-Catalyzed Mono-alpha-Arylation of Feedstock Solvents. *Chem. Eur. J.* **2022**, *28*, e202200764.

52. Bordwell, F. G.; Fried, H. E.; Hughes, D. L.; Lynch, T. Y.; Satish, A. V.; Whang, Y. E., Acidities of Carboxamides, Hydroxamic Acids, Carbohydrazides, Benzenesulfonamides, and Benzenesulfonohydrazides in DMSO Solution. *J. Org. Chem.* **1990**, *55*, 3330-3336.

53. Olmstead, W. N.; Margolin, Z.; Bordwell, F. G., Acidities of Water and Simple Alcohols in Dimethylsulfoxide Solution. *J. Org. Chem.* **1980**, *45*, 3295-3299.

54. Lavoie, C. M.; MacQueen, P. M.; Stradiotto, M. Nickel-Catalyzed N-Arylation of Primary Amides and Lactams with Activated (Hetero)aryl Electrophiles. *Chem. Eur. J.* **2016**, 22, *52*, 18752-18755.

55. Lundrigan, T.; Tassone, J. P.; Stradiotto, M. Nickel-Catalyzed *N*-Arylation of (Hetero)aryl Electrophiles by Using a DBU/NaTFA Dual-Base System. *Synlett*, **2021**, 32, *16*, 1665-1669.

56. (a) Frings, M.; Bolm, C.; Blum, A.; Gnamm, C. Sulfoximine's from a Medicinal Chemist's Perspective: Physicochemical and in vitro Parameters Relevant for Drug Discovery. *Eur. J. Med. Chem.*, **2017**, 126, *27*, 225-245. (b) Mäder, P. and Kattner, L. Sulfoximines as Rising Stars in Modern Drug Discovery? Current Status and Perspective on an Emerging Functional Group in Medicinal Chemistry. *J. Med. Chem.* **2020**, 63, *23*, 14243-14275.

57. Bolm, C. and Hildebrand, J. P. Palladium-Catalyzed *N*-Arylation of Sulfoximines with Aryl Bromides and Aryl Iodides. *J. Org. Chem.* **2000**, 65, *1*, 169-175.

58. Bolm, C. and Sedelmeier, J. Efficient Copper-Catalyzed N-Arylation of Sulfoximines with Aryl Iodides and Aryl Bromides. *J. Org. Chem.* **2005**, 70, *17*, 6904-6906.

59. (a) Wimmer, A. and König, B. *N*-Arylation of *NH*-Sulfoximines via Dual Nickel Photocatalysis. *Org. Lett.* **2019**, 21, *8*, 2740-2744. (b) Liu, D.; Liu, Z. R.; Ma, C.; Jiao, K. J.; Sun, B.; Wei, L.; Lefranc, J.; Herbert, S.; Mei, T. S. Nickel-Catalyzed *N*-Arylatio of *NH*-Sulfoximines with Aryl Halides via Paired Electrolysis. *Angew. Chem. Int. Ed.* **2021**, 60, *17*, 9444-9449.

Appendix 1: Chapter 2 NMR Data

Figure A1. ^{1}H NMR Spectrum of **2.2** (500.1 MHz, $CDCl_3$)

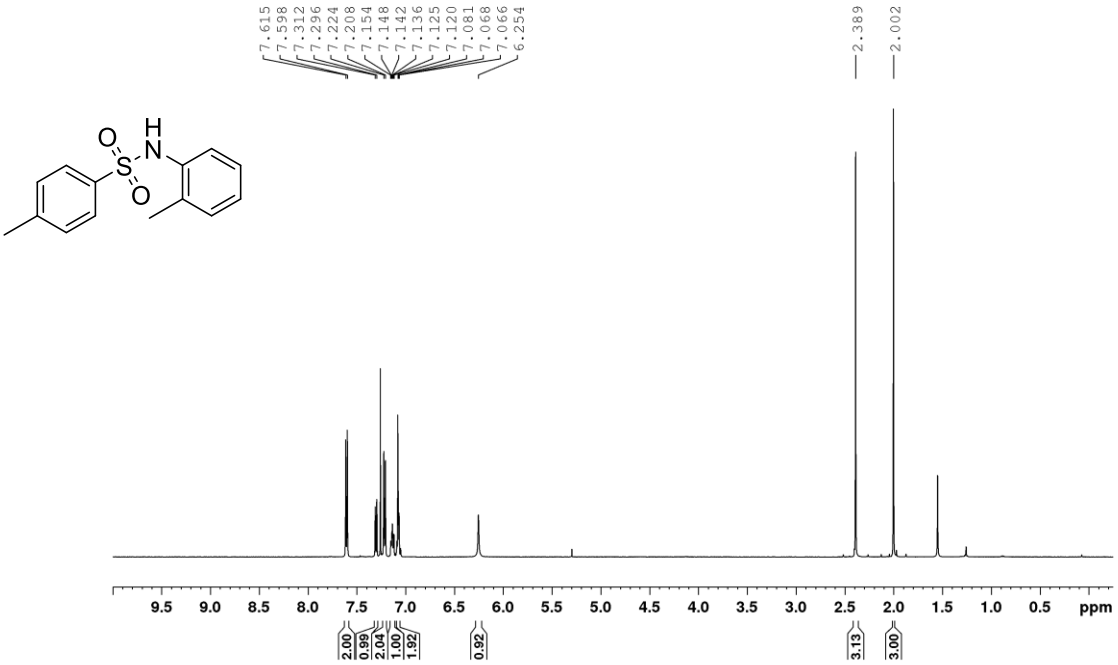

Figure A2. $^{13}C\{^{1}H\}$ UDEFT NMR Spectrum of **2.2** (125.8 MHz, $CDCl_3$)

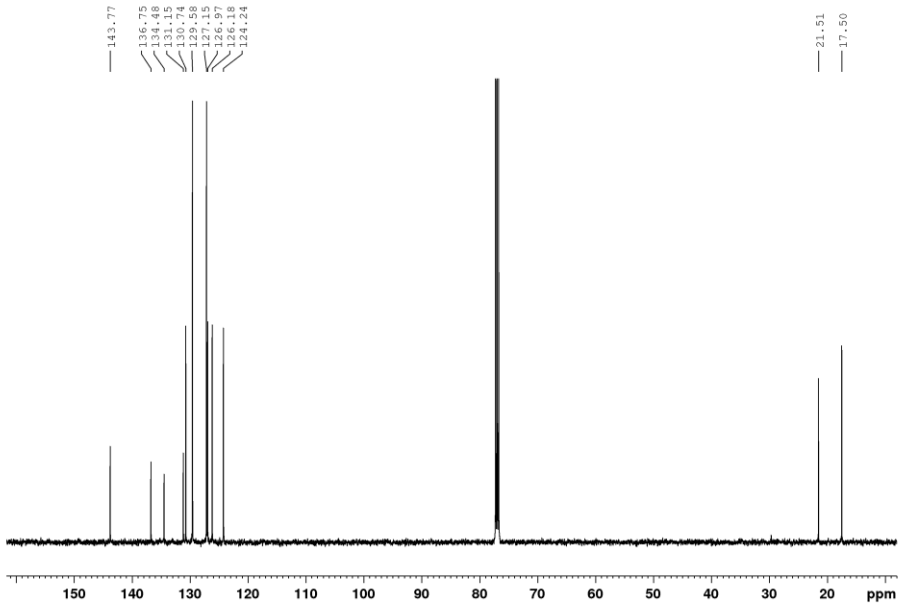

Figure A3. ^{1}H NMR Spectrum of **2.3** (500.1 MHz, $CDCl_3$)

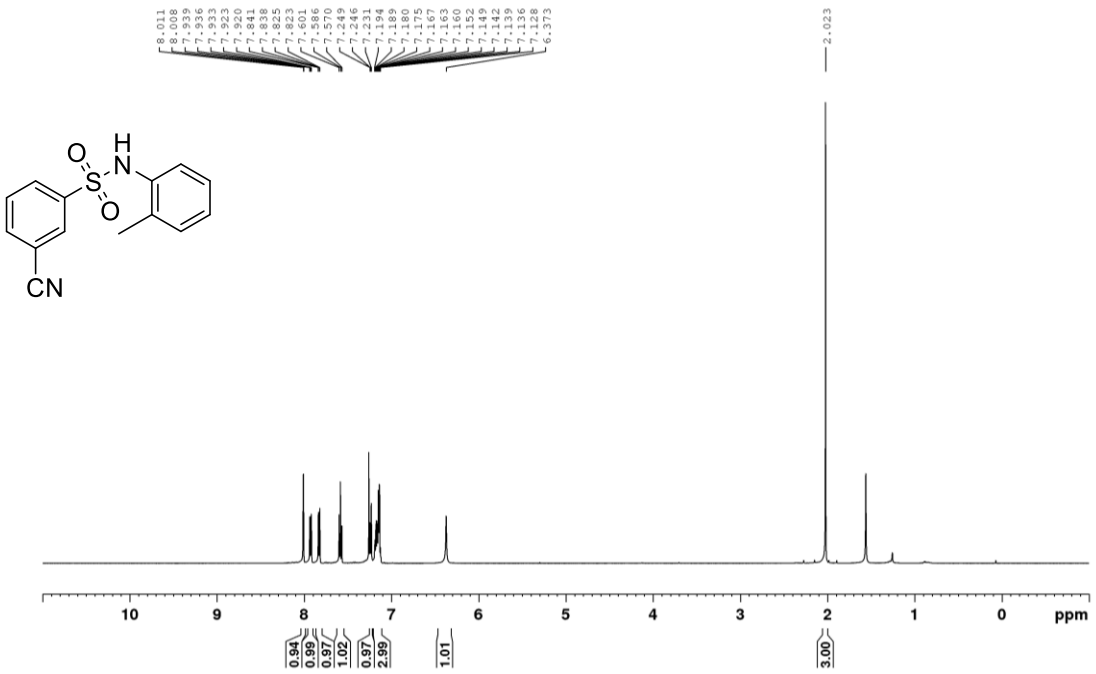

Figure A4. $^{13}C\{^{1}H\}$ UDEFT NMR Spectrum of **2.3** (125.8 MHz, $CDCl_3$)

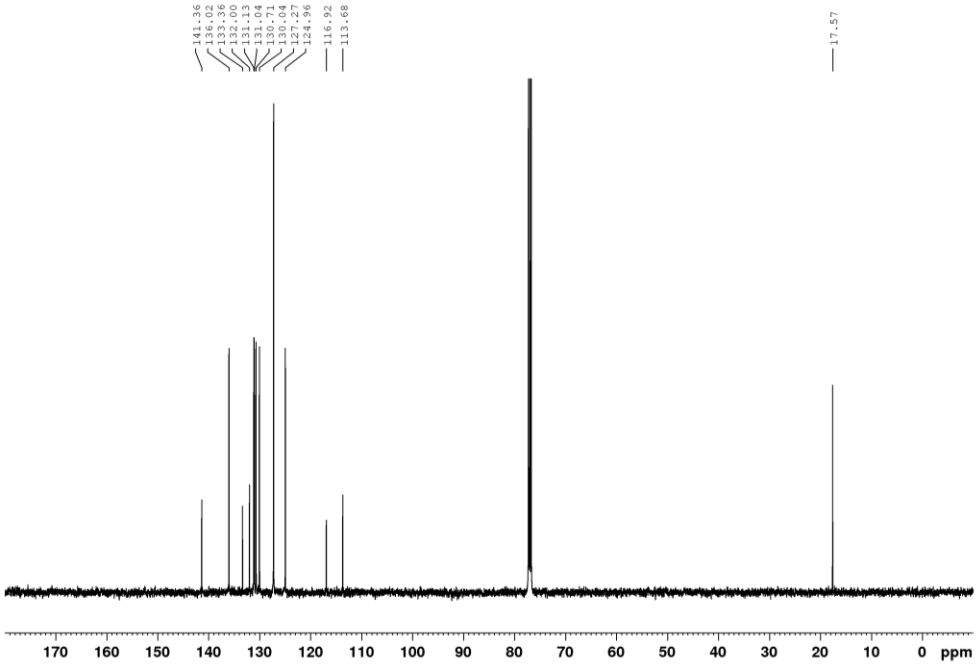

Figure A5. ^{1}H NMR Spectrum of **C1** (500.1 MHz, C_6D_6)

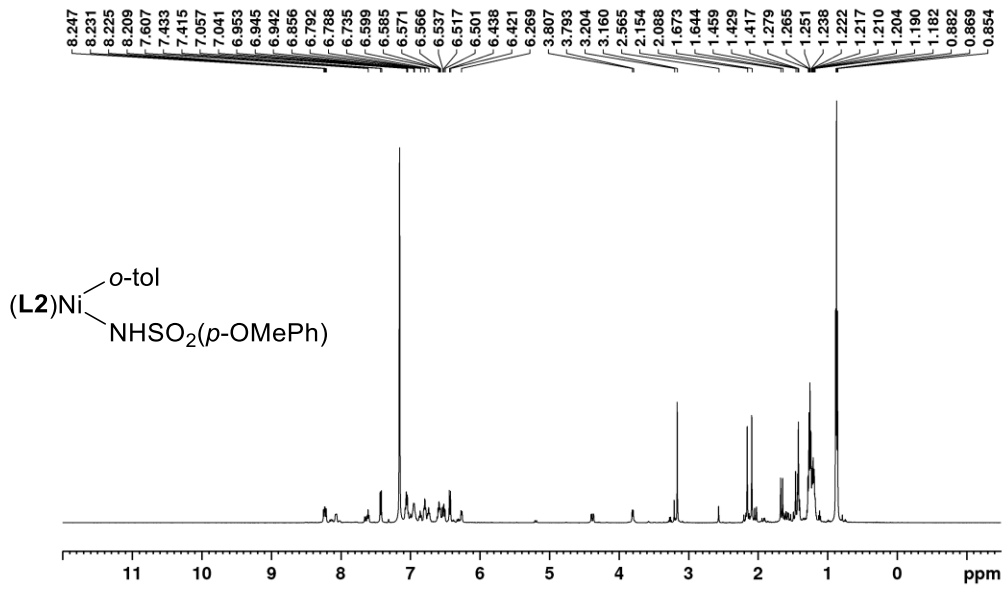

Figure A6. $^{31}P\{^{1}H\}$ NMR Spectrum of **C1** (202.5 MHz, C_6D_6)

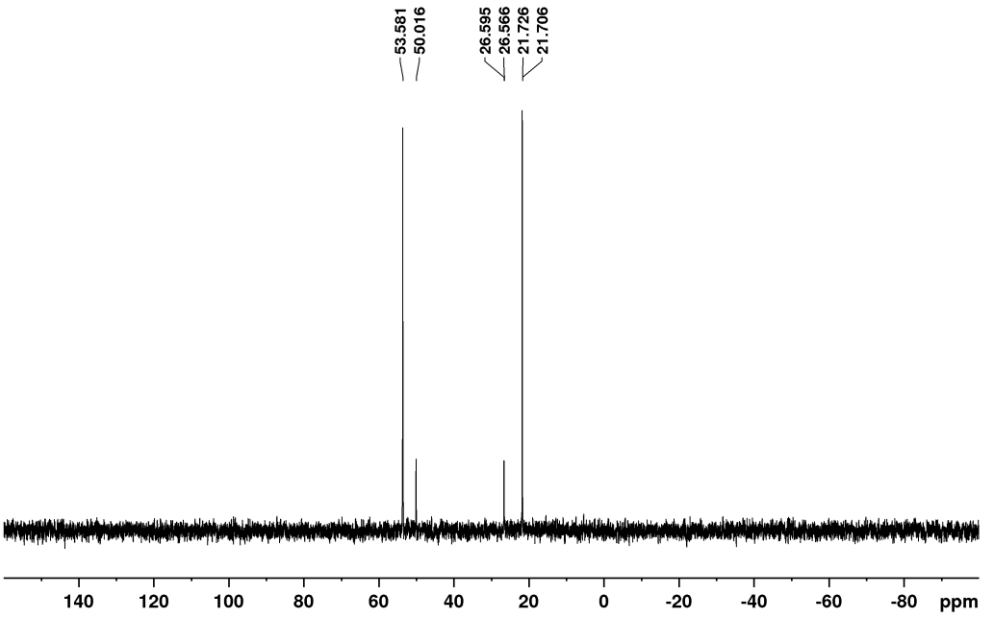

Figure A7. $^{13}C\{^{1}H\}$ NMR Spectrum of **C2** (125.8 MHz, C_6D_6)

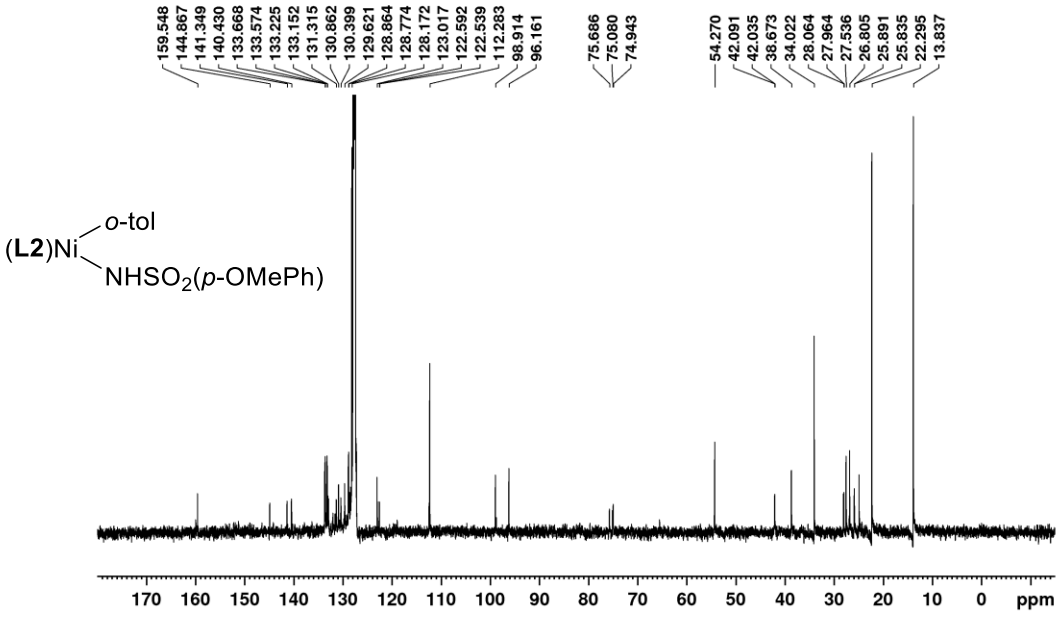

Figure A8. ^{1}H NMR Spectrum of **C2** (500.1 MHz, C_6D_6)

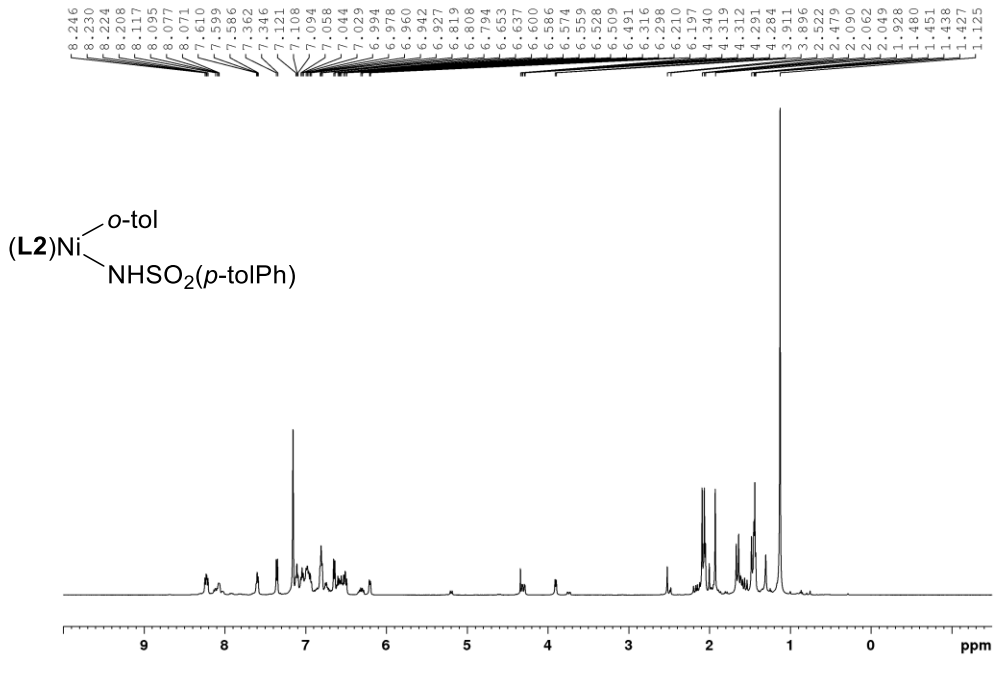

Figure A9. $^{31}P\{^{1}H\}$ NMR Spectrum of **C2** (202.5 MHz, C_6D_6)

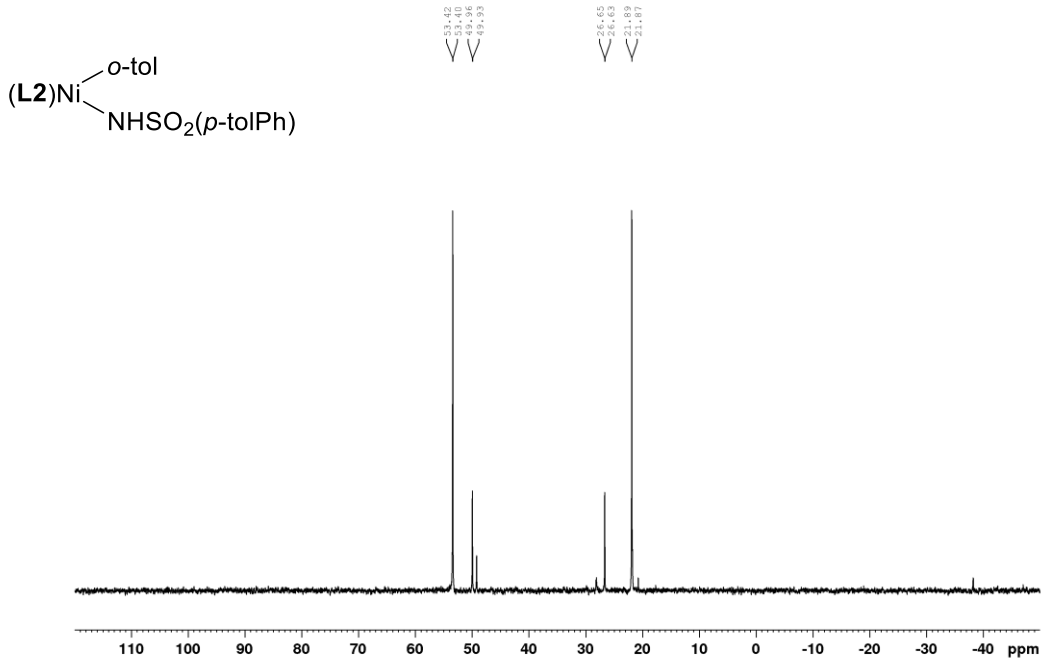

Figure A10. $^{13}C\{^{1}H\}$ NMR Spectrum of **C2** (125.8 MHz, C_6D_6)

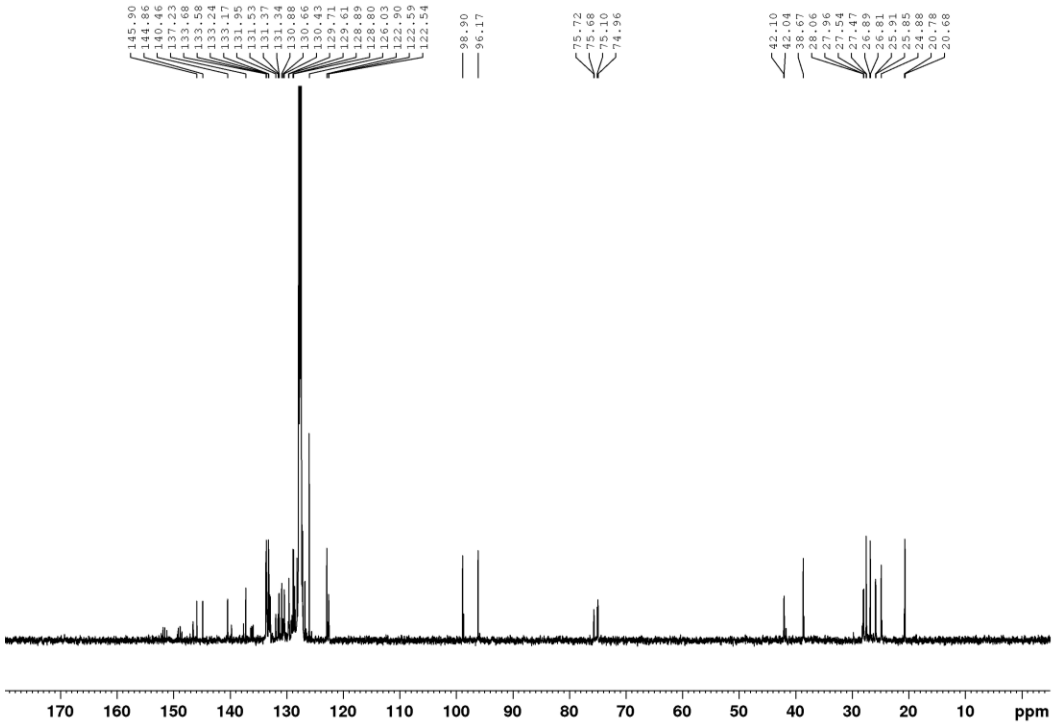

Figure A11. ^{1}H NMR Spectrum of **C3** (500.1 MHz, C_6D_6)

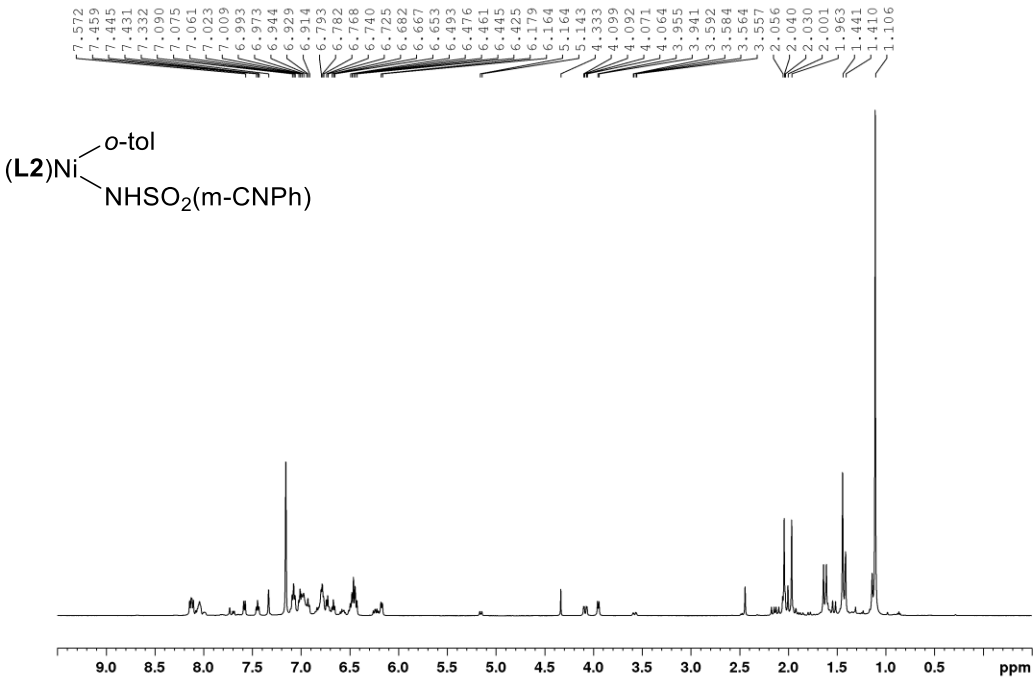

Figure A12. $^{31}P\{^{1}H\}$ NMR Spectrum of **C3** (202.5 MHz, C_6D_6)

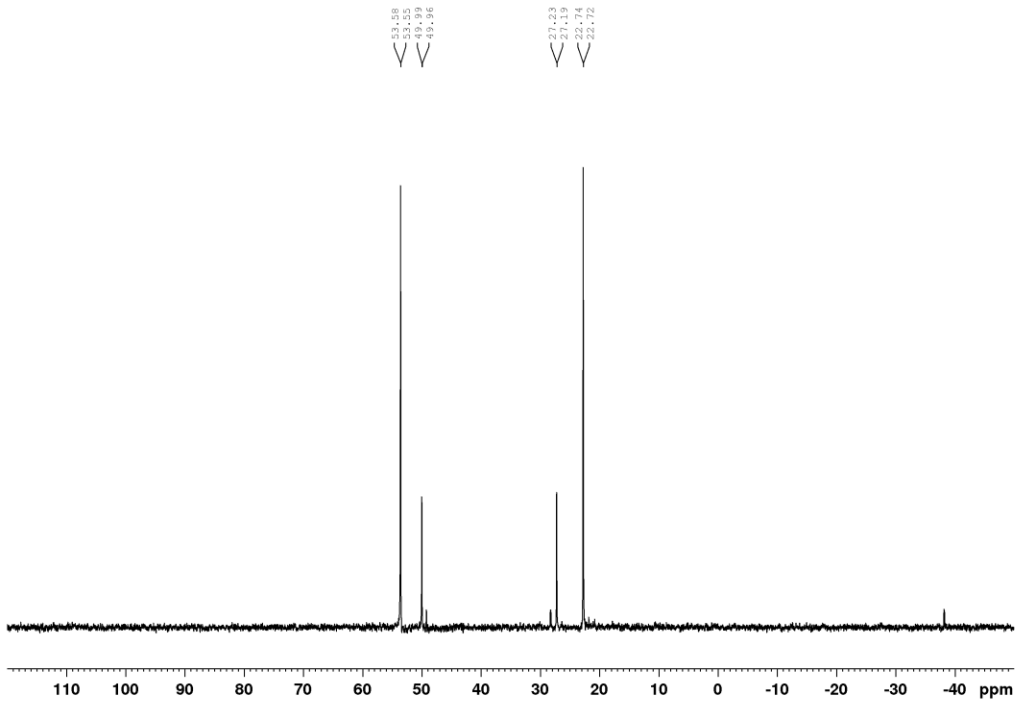

Figure A13. $^{13}C\{^{1}H\}$ NMR Spectrum of **C3** (125.8 MHz, C_6D_6)

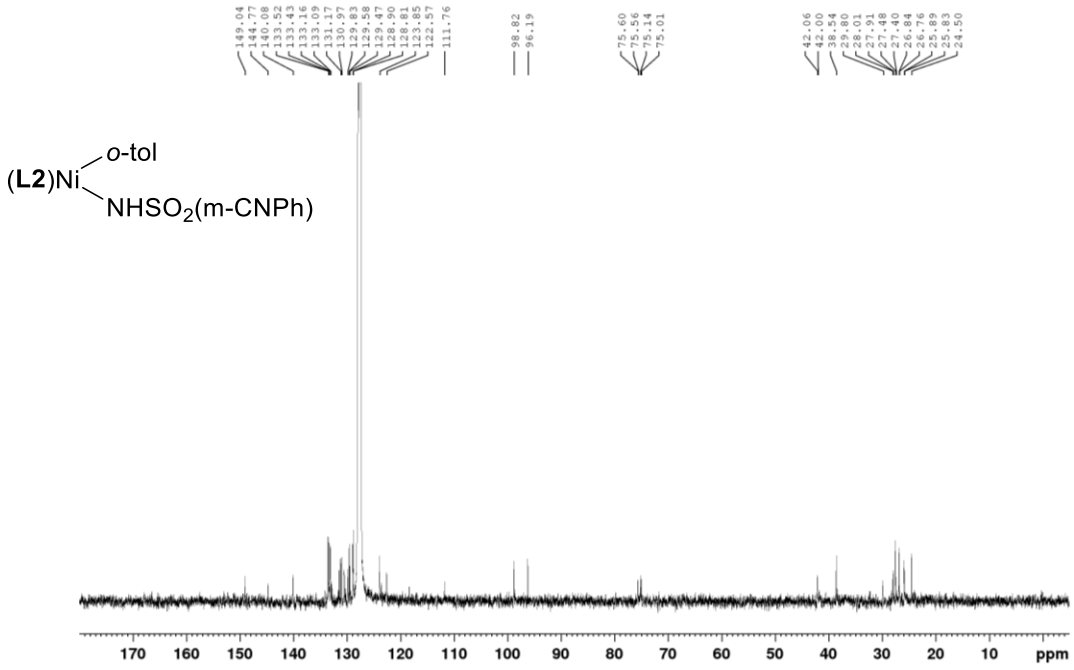

Figure A14. $^{31}P\{^{1}H\}$ NMR of (**L1**)Ni(*o*-tol)(O*t*Bu) formed in-situ upon treatment of (**L1**)Ni(*o*-tol)Cl with NaO*t*Bu (two equiv) (202.5 MHz, C_6D_6)

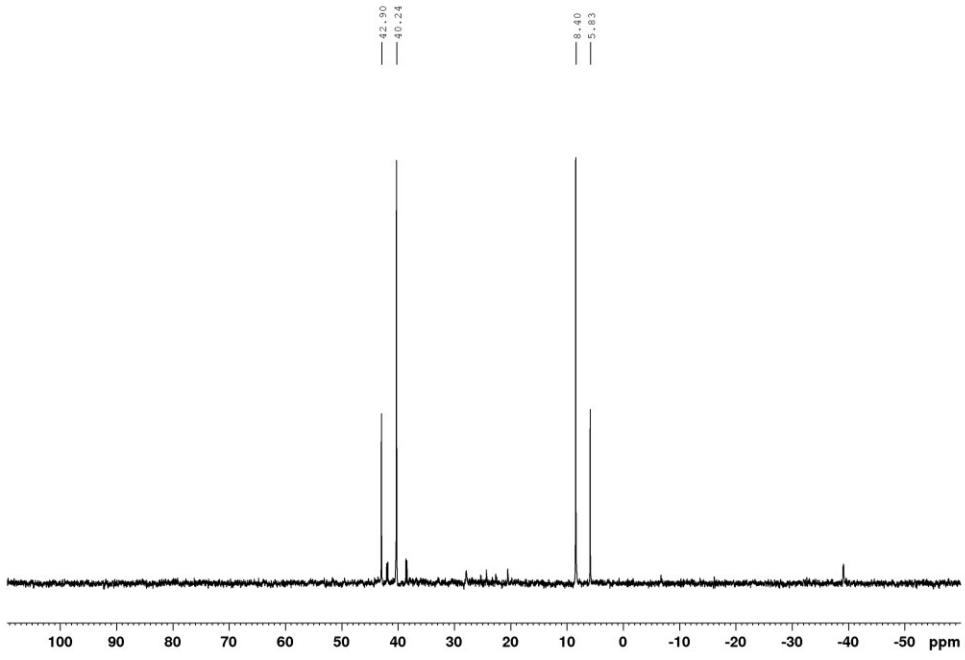

Figure A15a. $^{31}P\{^{1}H\}$ NMR of the catalytic reaction between 2-chlorotoluene and 4-methoxybenzenesulfonamide following 1 hour at 80 °C (121.5 MHz, 1,4-dioxane, with $P(mesityl)_3$ internal standard).

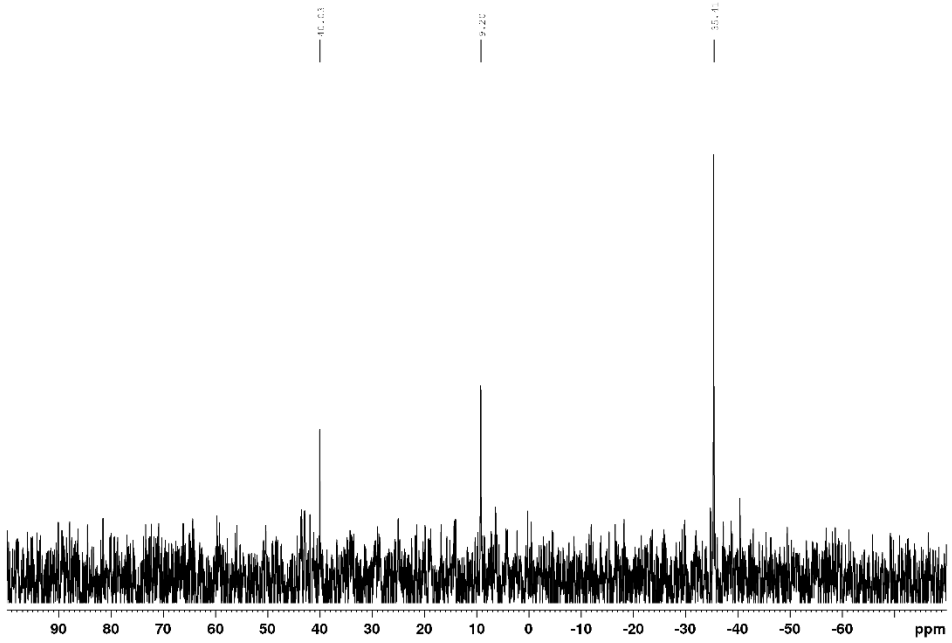

Figure A15b. $^{31}P\{^{1}H\}$ NMR of the catalytic reaction between 2-chlorotoluene and $tBuNH_2$ following 1 hour at 25 °C (121.5 MHz, 1,4-dioxane, with $P(mesityl)_3$ internal standard).

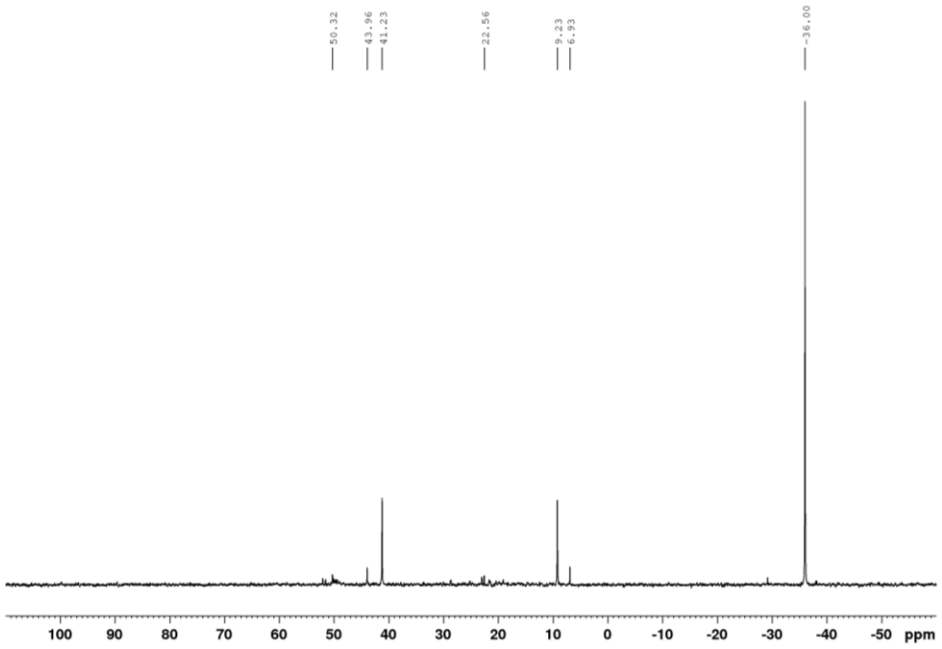

Figure A16. $^{31}P\{^{1}H\}$ NMR spectrum upon treatment of (**L1**)Ni(*o*-tol)(O*t*Bu) (formed in-situ) with 4-methoxybenzenesulfonamide (one equiv) to give **C1** (202.5 MHz, 1,4-dioxane; P(mesityl)$_3$ internal standard)

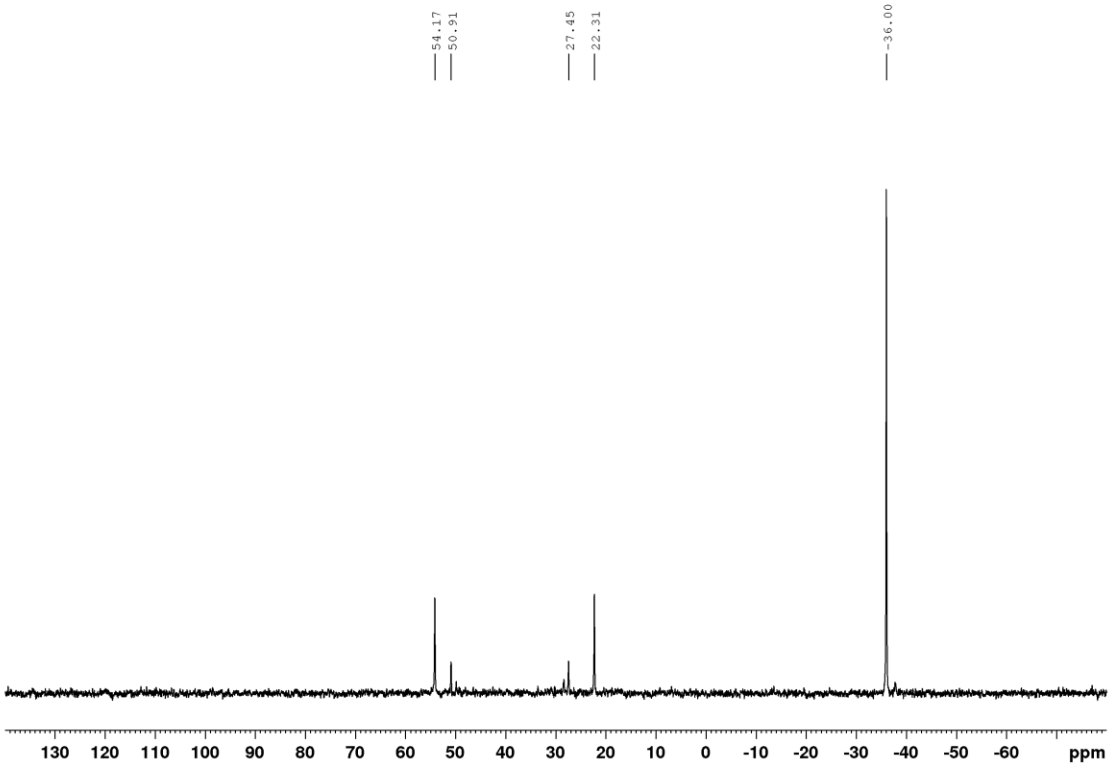

Appendix 2: Chapter 2 X-Ray Data

Crystallographic solution and refinement details. Crystallographic data were obtained at 173(2) K on a Bruker D8/APEX II CCD diffractometer equipped with a CCD area detector, using Cu Kα (1.54178) (microfocus source) radiation and employing samples that were mounted in inert oil and transferred to a cold gas stream on the diffractometer. Data reduction, correction for Lorentz polarization, and absorption correction (Gaussian integration; face-indexed) were each performed. Structure solution by using intrinsic phasing was carried out, followed by least-squares refinement on F 2 . All non-hydrogen atoms were refined with anisotropic displacement parameters, while all hydrogen atoms were added at calculated positions and refined by use of a riding model employing isotropic displacement parameters based on the isotropic displacement parameter of the attached atom.

Crystallographic solution and refinement details for **C1·C_6H$_6$** (CCDC 1979953)

Table A1. Crystallographic Experimental Details

A. Crystal Data	
formula	$C_{48}H_{51}NNiO_6P_2S$
formula weight	890.60
crystal dimensions (mm)	0.23 x 0.17 x 0.06
crystal system	triclinic
space group	$P\bar{1}$ (No. 2)
unit cell parameters[a]	
a (Å)	10.8076(4)
b (Å)	11.9702(4)
c (Å)	18.4921(7)
α (deg)	81.4622(6)
β (deg)	77.1368(6)
γ (deg)	71.8254(6)
V (Å^3)	2207.84(14)
Z	2
ρ_{calcd} (g cm^{-3})	1.340
μ (mm^{-1})	0.609
B. Data Collection and Refinement Conditions	
diffractometer	Bruker D8/APEX II CCD[b]
radiation (λ [Å])	graphite-monochromated Mo Kα (0.71073)
temperature (°C)	–100
scan type	ω scans (0.3°) (20 s exposures)
data collection 2θ limit (deg)	55.22
total data collected	20408 ($-14 \le h \le 14$, $-15 \le k \le 15$, $-24 \le l \le 24$)

independent reflections	10226 (R_{int} = 0.0185)
number of observed reflections (*NO*)	8580 [$F_o^2 \geq 2\sigma(F_o^2)$]
structure solution method	intrinsic phasing (*SHELXT-2014*[c])
refinement method	full-matrix least-squares on F^2 (*SHELXL–2017*[d])
absorption correction method	Gaussian integration (face-indexed)
range of transmission factors	0.9891–0.8935
data/restraints/parameters	10226 / 0 / 542
goodness-of-fit (*S*)[e] [all data]	1.042
final *R* indices[f]	
R_1 [$F_o^2 \geq 2\sigma(F_o^2)$]	0.0372
wR_2 [all data]	0.1003
largest difference peak and hole	0.781 and –0.346 e Å^{-3}

[a]Obtained from least-squares refinement of 9866 reflections with 4.42° < 2θ < 55.06°.

[b]Programs for diffractometer operation, data collection, data reduction and absorption correction were those supplied by Bruker.

[c]Sheldrick, G. M. *Acta Crystallogr.* **2015**, *A71*, 3–8. (*SHELXT-2014*)

[d]Sheldrick, G. M. *Acta Crystallogr.* **2015**, *C71*, 3–8. (*SHELXL-2017*)

[e]$S = [\Sigma w(F_o^2 - F_c^2)^2/(n-p)]^{1/2}$ (n = number of data; p = number of parameters varied; $w = [\sigma^2(F_o^2) + (0.0476P)^2 + 1.2969P]^{-1}$ where $P = [\mathrm{Max}(F_o^2, 0) + 2F_c^2]/3$).

[f]$R1 = \Sigma||F_o| - |F_c||/\Sigma|F_o|$; $wR_2 = [\Sigma w(F_o^2 - F_c^2)^2/\Sigma w(F_o^4)]^{1/2}$.

Crystallographic solution and refinement details for **C2·C$_6$H$_6$** (CCDC 2115353)

Table A2. Crystallographic Experimental Details

A. Crystal Data	
formula	$C_{48}H_{51}NNiO_5P_2S$
formula weight	874.60
crystal dimensions (mm)	0.16 x 0.15 x 0.14
crystal system	triclinic
space group	$P\bar{1}$ (No. 2)
unit cell parameters[a]	
a (Å)	10.7191(3)
b (Å)	12.0090(4)
c (Å)	18.2064(6)
α (deg)	82.6614(12)
β (deg)	76.5673(11)
γ (deg)	71.5732(10)
V (Å^3)	2158.90(12)
Z	2
ρ_{calcd} (g cm^{-3})	1.345
μ (mm^{-1})	2.180
B. Data Collection and Refinement Conditions	
diffractometer	Bruker D8/APEX II CCD[b]
radiation (λ [Å])	Cu Kα (1.54178) (microfocus source)
temperature (°C)	–100
scan type	ω and ϕ scans (1.0°) (5 s exposures)
data collection 2θ limit (deg)	140.48
total data collected	93908 (-13 ≤ h ≤ 13, -14 ≤ k ≤ 14, -21 ≤ l ≤ 22)
independent reflections	7920 (R_{int} = 0.0254)
number of observed reflections (*NO*)	7677 [$F_o^2 \geq 2\sigma(F_o^2)$]
structure solution method	intrinsic phasing (*SHELXT-2014*[c])
refinement method	full-matrix least-squares on F^2 (*SHELXL–2018*[d])
absorption correction method	Gaussian integration (face-indexed)
range of transmission factors	0.8611–0.7304
data/restraints/parameters	7920 / 0 / 529
goodness-of-fit (*S*)[e] [all data]	1.027
final R indices[f]	
R_1 [$F_o^2 \geq 2\sigma(F_o^2)$]	0.0363
wR_2 [all data]	0.0929
largest difference peak and hole	1.048 and –0.389 e Å^{-3}

[a]Obtained from least-squares refinement of 9643 reflections with $7.78° < 2\theta < 140.42°$.

[b]Programs for diffractometer operation, data collection, data reduction and absorption correction were those supplied by Bruker.

[c]Sheldrick, G. M. *Acta Crystallogr.* **2015**, *A71*, 3–8. (*SHELXT-2014*)

[d]Sheldrick, G. M. *Acta Crystallogr.* **2015**, *C71*, 3–8. (*SHELXL-2018/3*)

[e]$S = [\Sigma w(F_o^2 - F_c^2)^2/(n - p)]^{1/2}$ (n = number of data; p = number of parameters varied; $w = [\sigma^2(F_o^2) + (0.0420P)^2 + 2.0232P]^{-1}$ where $P = [\mathrm{Max}(F_o^2, 0) + 2F_c^2]/3$).

[f]$R1 = \Sigma||F_o| - |F_c||/\Sigma|F_o|$; $wR2 = [\Sigma w(F_o^2 - F_c^2)^2/\Sigma w(F_o^4)]^{1/2}$.

Crystallographic solution and refinement details for **C3** (CCDC 2115352)

Table A3. Crystallographic Experimental Details

A. Crystal Data	
formula	$C_{42}H_{42}N_2NiO_5P_2S$
formula weight	807.48
crystal dimensions (mm)	0.13 x 0.08 x 0.05
crystal system	monoclinic
space group	$P2_1/n$ (an alternate setting of $P2_1/c$ [No. 14])
unit cell parameters[a]	
a (Å)	11.9758(4)
b (Å)	27.1961(9)
c (Å)	12.6870(4)
β (deg)	107.865(2)
V (Å^3)	3932.9(2)
Z	4
ρ_{calcd} (g cm^{-3})	1.364
μ (mm^{-1})	2.355
B. Data Collection and Refinement Conditions	
diffractometer	Bruker D8/APEX II CCD[b]
radiation (λ [Å])	Cu Kα (1.54178) (microfocus source)
temperature (°C)	–100
scan type	ω and ϕ scans (1.0°) (5 s exposures)
data collection 2θ limit (deg)	140.47
total data collected	56247 (-14 ≤ h ≤ 14, -33 ≤ k ≤ 33, -15 ≤ l ≤ 15)
independent reflections	7487 (R_{int} = 0.0720)
number of observed reflections (*NO*)	6023 [$F_o^2 \geq 2\sigma(F_o^2)$]
structure solution method	intrinsic phasing (*SHELXT-2014*[c])
refinement method	full-matrix least-squares on F^2 (*SHELXL–2018*[d])
absorption correction method	Gaussian integration (face-indexed)
range of transmission factors	0.9425–0.8121
data/restraints/parameters	7487 / 0 / 488
extinction coefficient (x)[e]	0.00062(7)
goodness-of-fit (S)[f] [all data]	1.032
final R indices[g]	
R_1 [$F_o^2 \geq 2\sigma(F_o^2)$]	0.0420
wR_2 [all data]	0.1169
largest difference peak and hole	0.345 and –0.361 e Å^{-3}

[a]Obtained from least-squares refinement of 5819 reflections with $6.50° < 2\theta < 139.98°$.

[b]Programs for diffractometer operation, data collection, data reduction and absorption correction were those supplied by Bruker

[c]Sheldrick, G. M. *Acta Crystallogr.* **2015**, *A71*, 3–8. (*SHELXT-2014*)

[d]Sheldrick, G. M. *Acta Crystallogr.* **2015**, *C71*, 3–8. (*SHELXL-2018/3*)

[e]$F_c^* = kF_c[1 + x\{0.001F_c^2\lambda^3/\sin(2\theta)\}]^{-1/4}$ where k is the overall scale factor.

[f]$S = [\Sigma w(F_o^2 - F_c^2)^2/(n - p)]^{1/2}$ (n = number of data; p = number of parameters varied; $w = [\sigma^2(F_o^2) + (0.0595P)^2 + 0.9847P]^{-1}$ where $P = [\text{Max}(F_o^2, 0) + 2F_c^2]/3$).

[g]$R_1 = \Sigma||F_o| - |F_c||/\Sigma|F_o|$; $wR_2 = [\Sigma w(F_o^2 - F_c^2)^2/\Sigma w(F_o^4)]^{1/2}$.

Appendix 3: Chapter 3 NMR Data

Figure A17. ^{1}H NMR Spectrum of **3a** (500.1 MHz, $CDCl_3$)

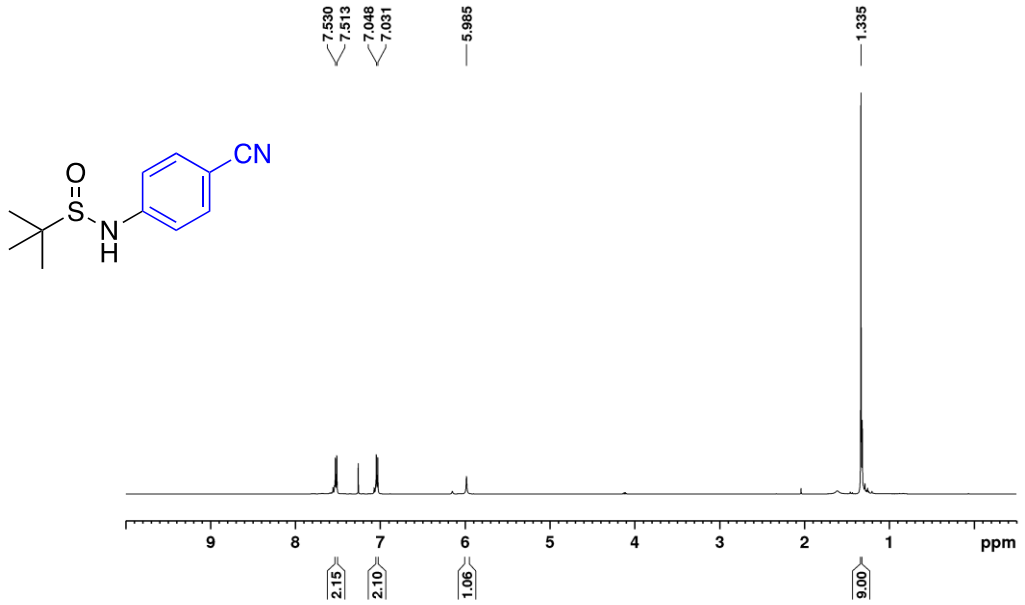

Figure A18. $^{13}C\{^{1}H\}$ UDEFT NMR Spectrum of **3a** (125.8 MHz, $CDCl_3$)

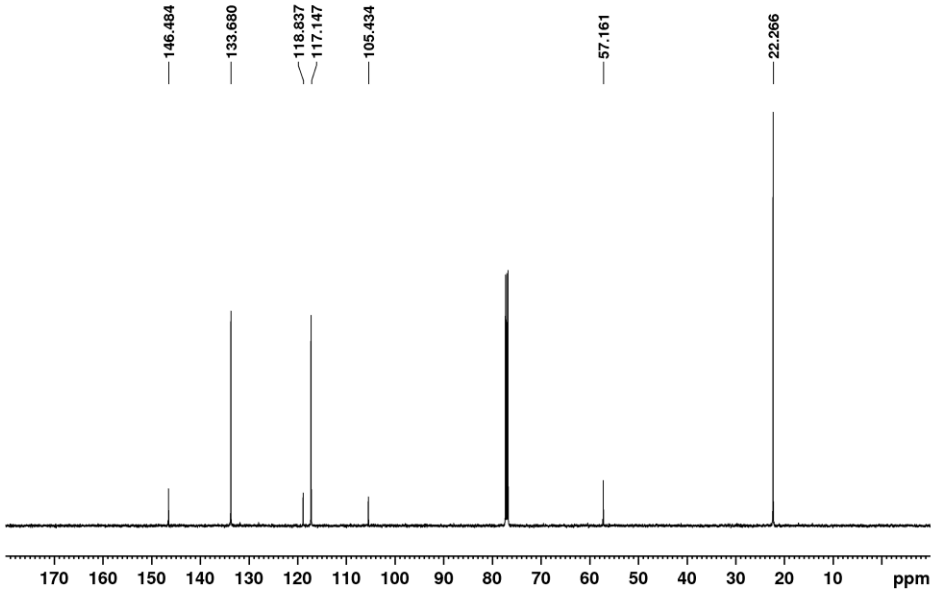

Figure A19. ^{1}H NMR Spectrum of **3b** (500.1 MHz, $CDCl_3$)

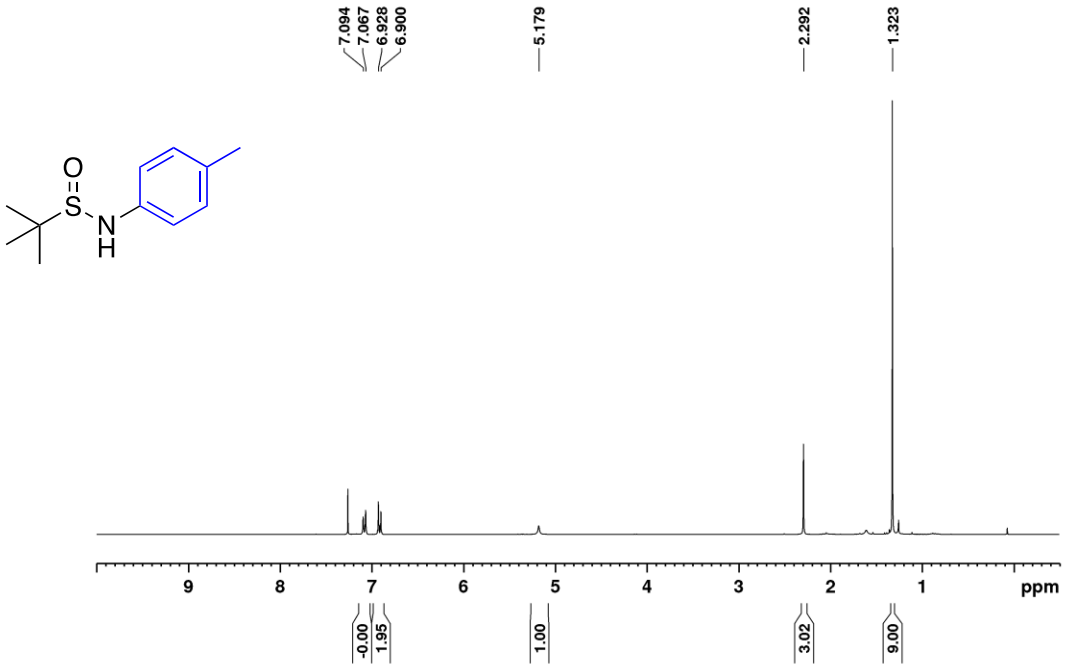

Figure A20. $^{13}C\{^{1}H\}$ UDEFT NMR Spectrum of **3b** (125.8 MHz, $CDCl_3$)

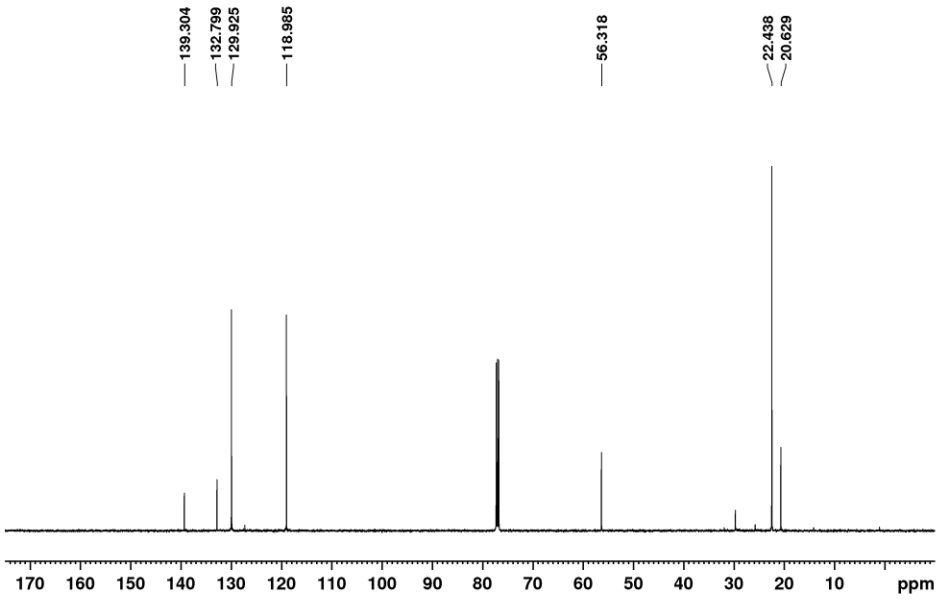

Figure A21. ^{1}H NMR Spectrum of **3c** (500.1 MHz, $CDCl_3$)

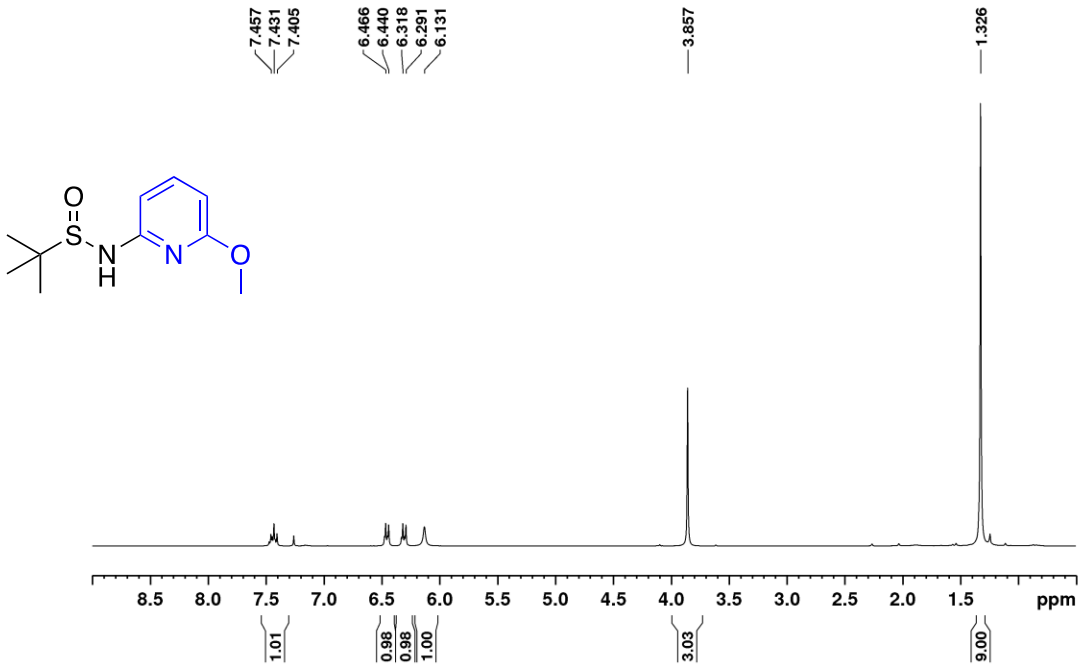

Figure A22. $^{13}C\{^{1}H\}$ UDEFT NMR Spectrum of **3c** (125.8 MHz, $CDCl_3$)

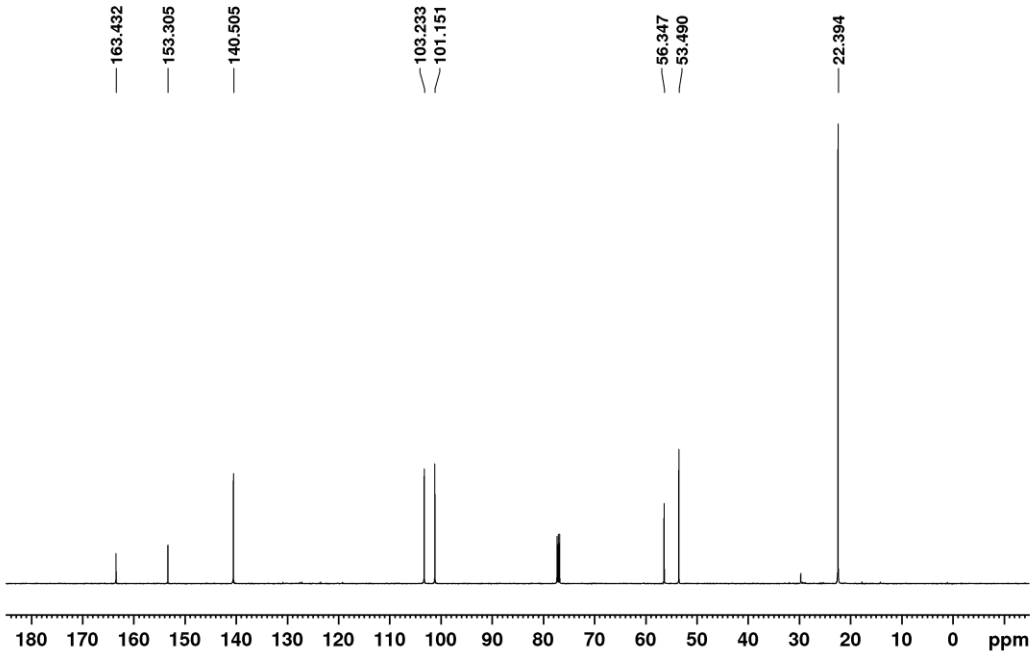

Figure A23. ^{1}H NMR Spectrum of **3d** (500.1 MHz, $CDCl_3$)

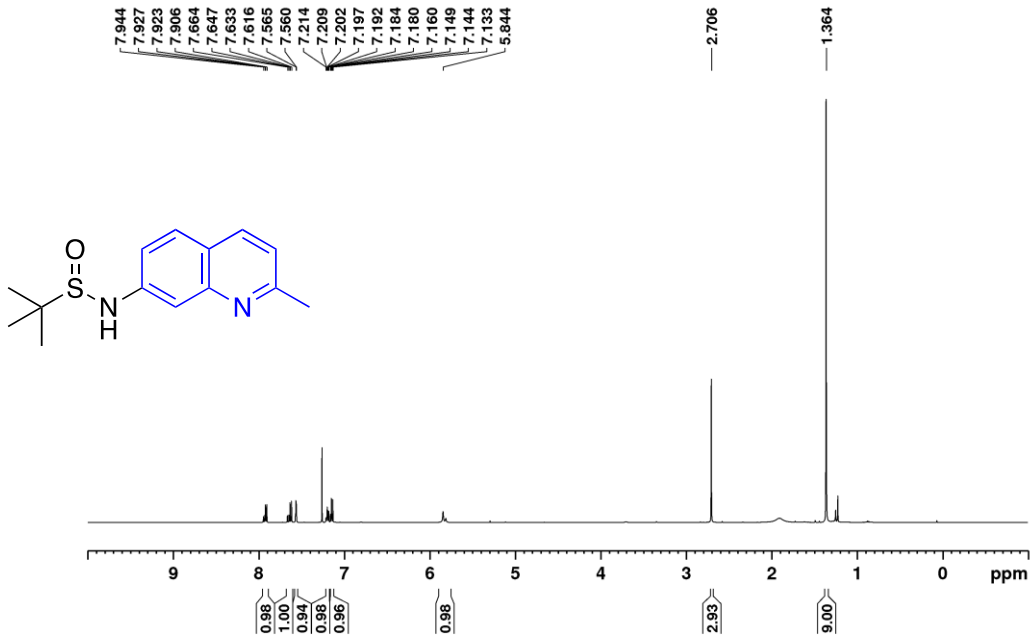

Figure A24. $^{13}C\{^{1}H\}$ UDEFT NMR Spectrum of **3d** (125.8 MHz, $CDCl_3$)

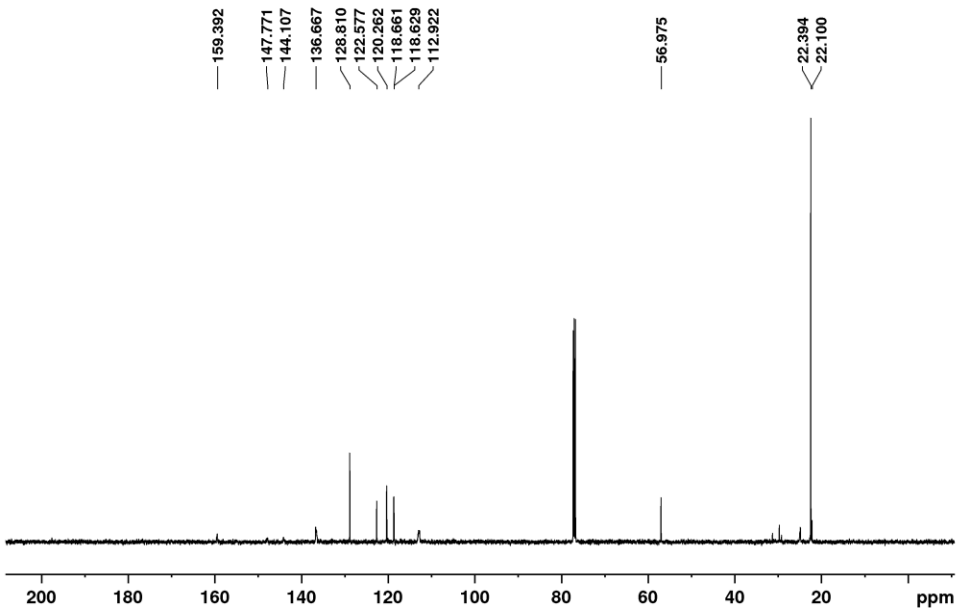

Figure A25. ^{1}H NMR Spectrum of **3e** (500.1 MHz, $CDCl_3$)

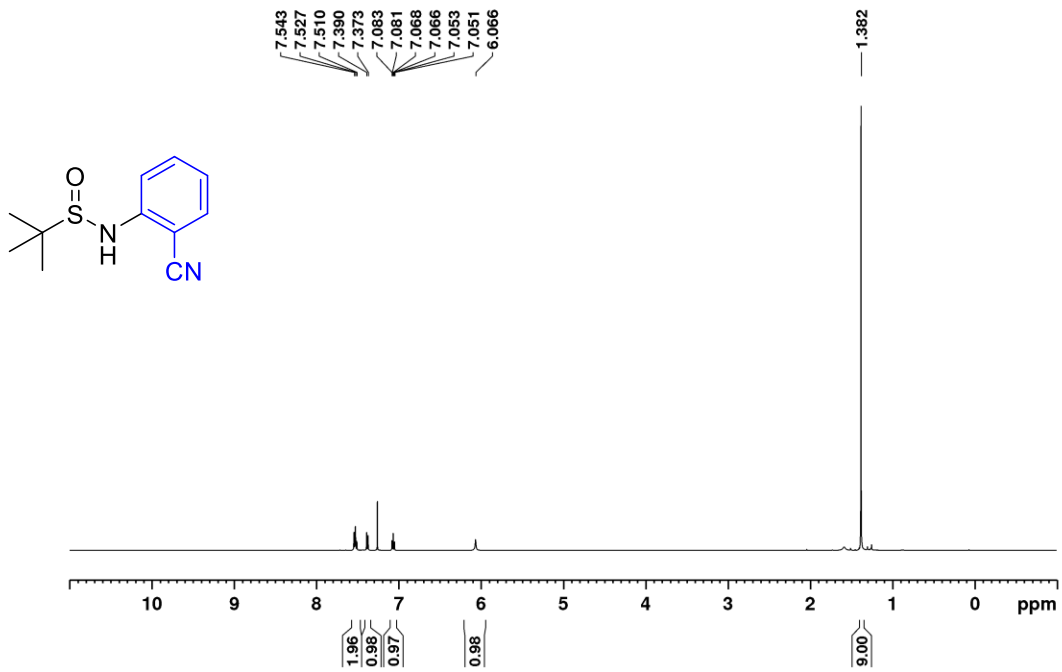

Figure A26. $^{13}C\{^{1}H\}$ UDEFT NMR Spectrum of **3e** (125.8 MHz, $CDCl_3$)

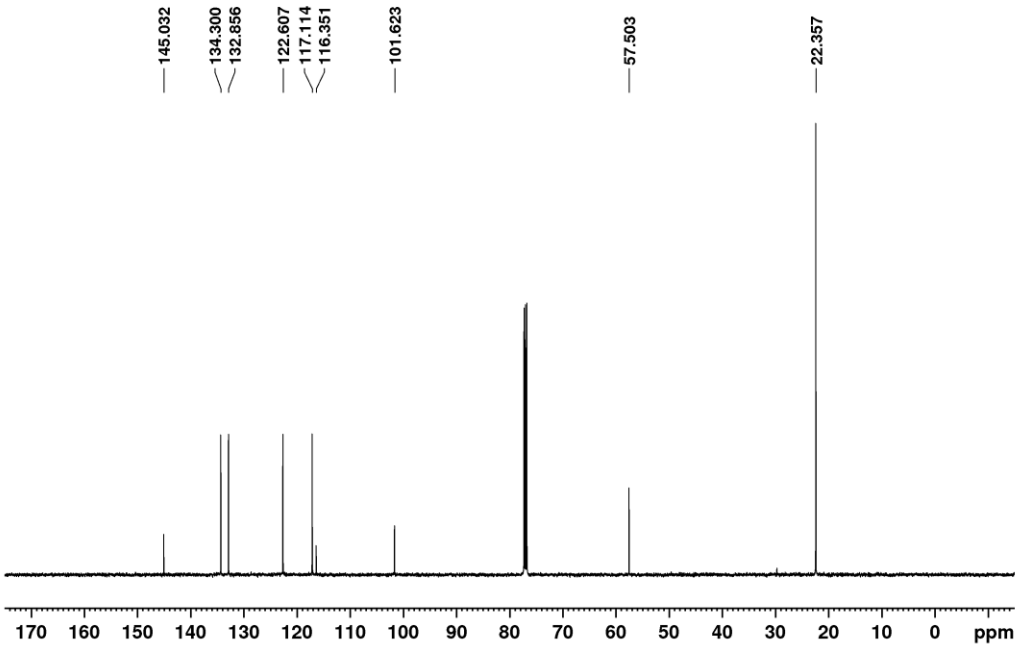

Figure A27. ^{1}H NMR Spectrum of **3f** (500.1 MHz, $CDCl_3$)

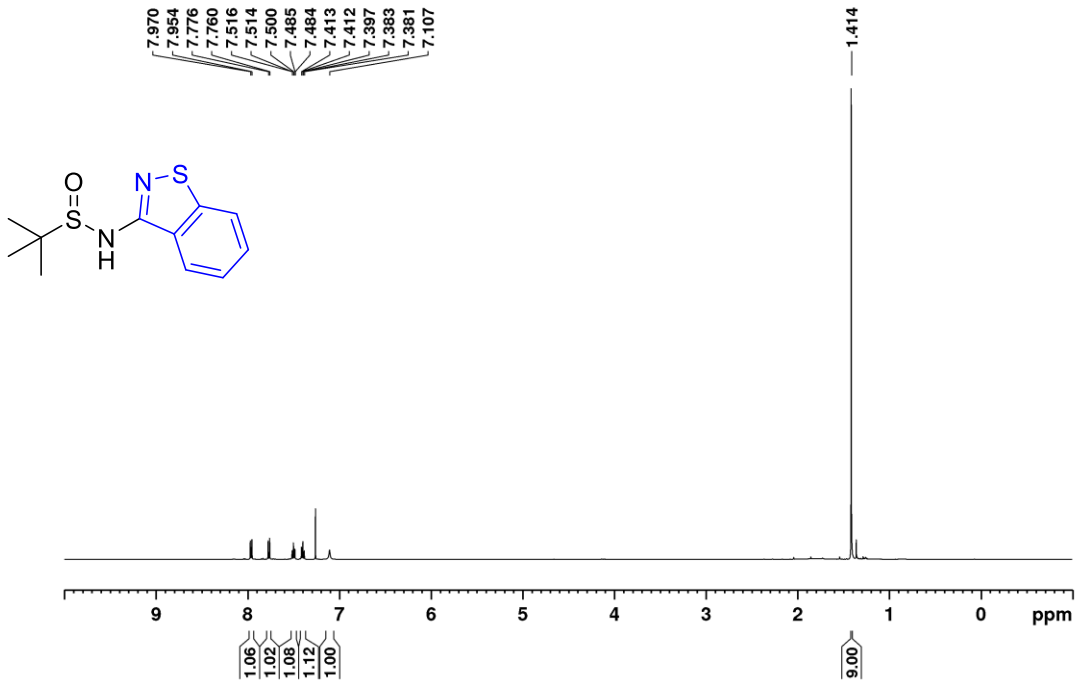

Figure A28. $^{13}C\{^{1}H\}$ UDEFT NMR Spectrum of **3f** (125.8 MHz, $CDCl_3$)

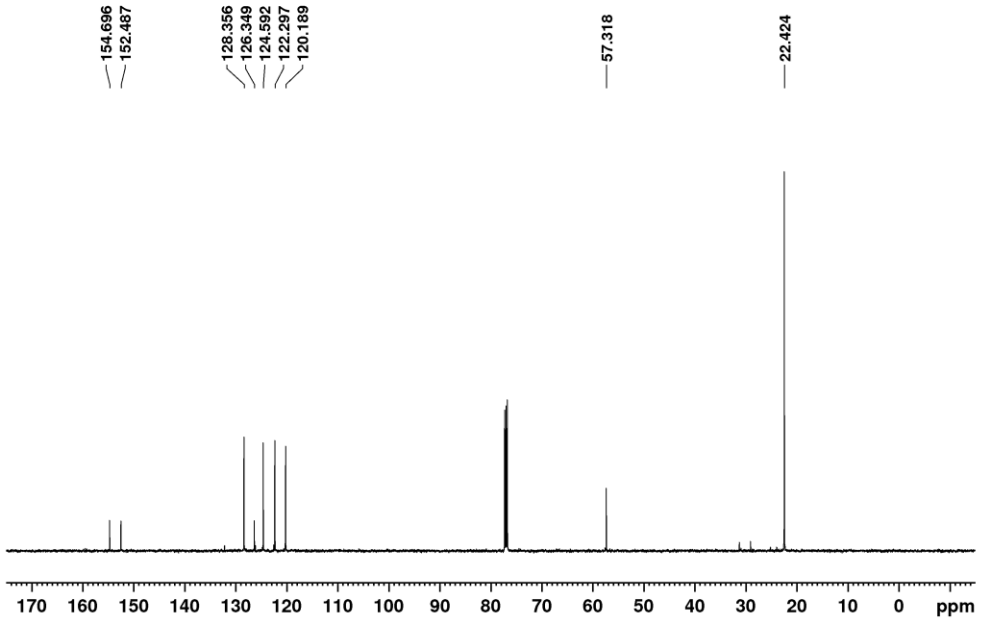

Figure A29. ^{1}H NMR Spectrum of **3g** (500.1 MHz, $CDCl_3$)

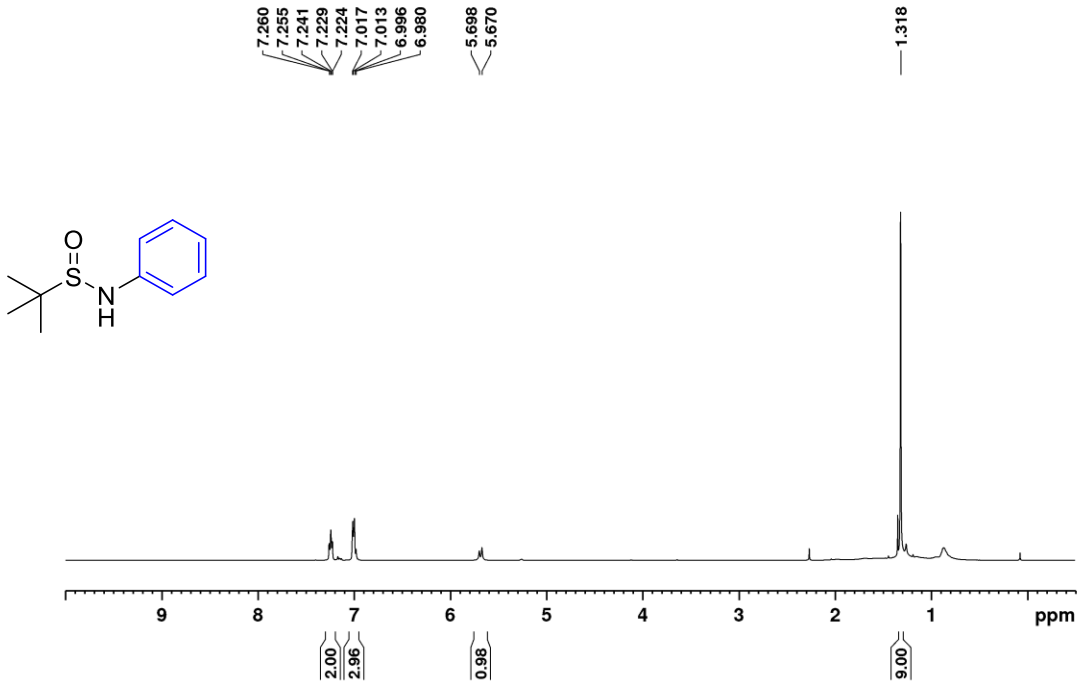

Figure A30. $^{13}C\{^{1}H\}$ UDEFT NMR Spectrum of **3g** (125.8 MHz, $CDCl_3$)

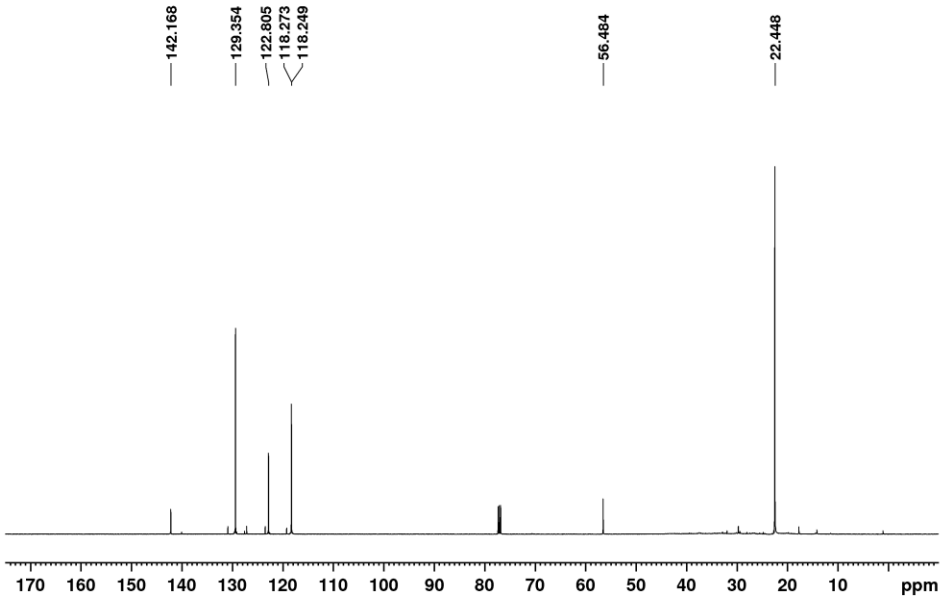

Figure A31. ^{1}H NMR Spectrum of **3h** (500.1 MHz, $CDCl_3$)

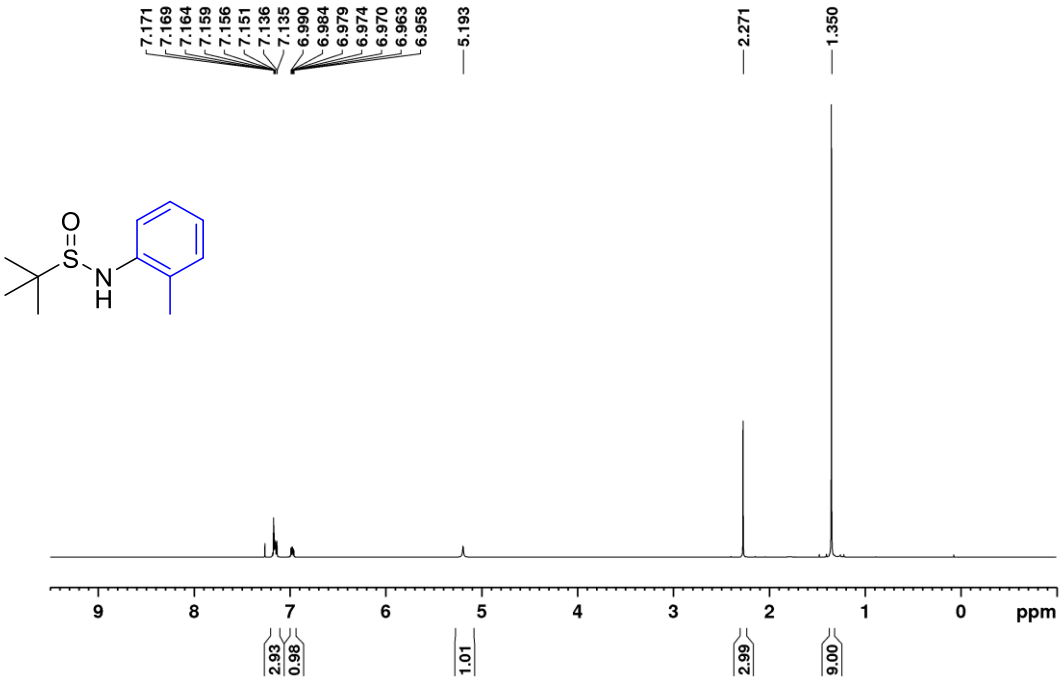

Figure A32. $^{13}C\{^{1}H\}$ UDEFT NMR Spectrum of **3h** (125.8 MHz, $CDCl_3$)

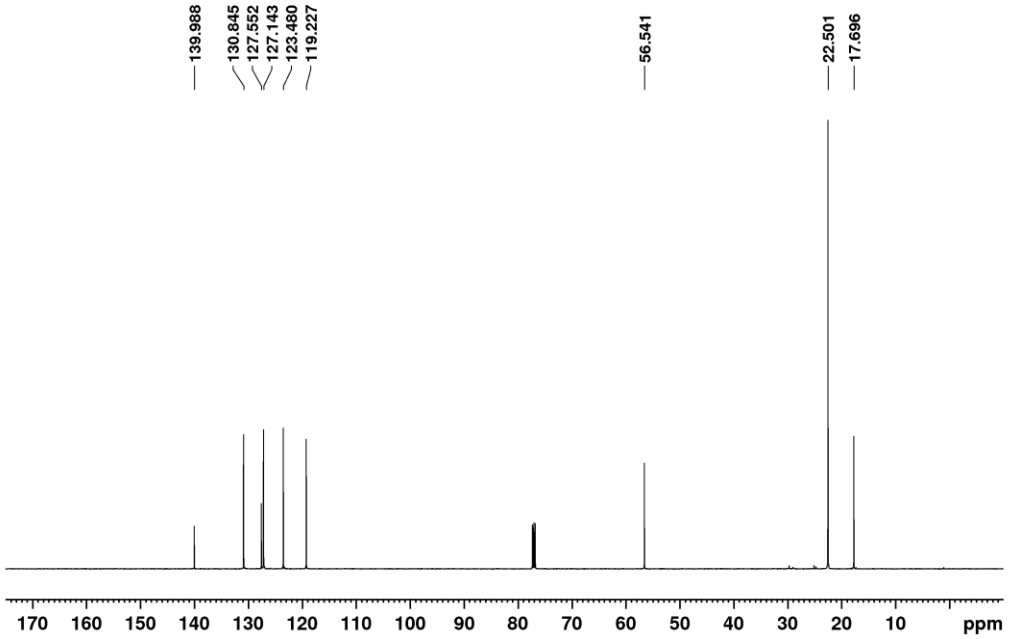

Figure A33. ^{1}H NMR Spectrum of **3i** (500.1 MHz, $CDCl_3$)

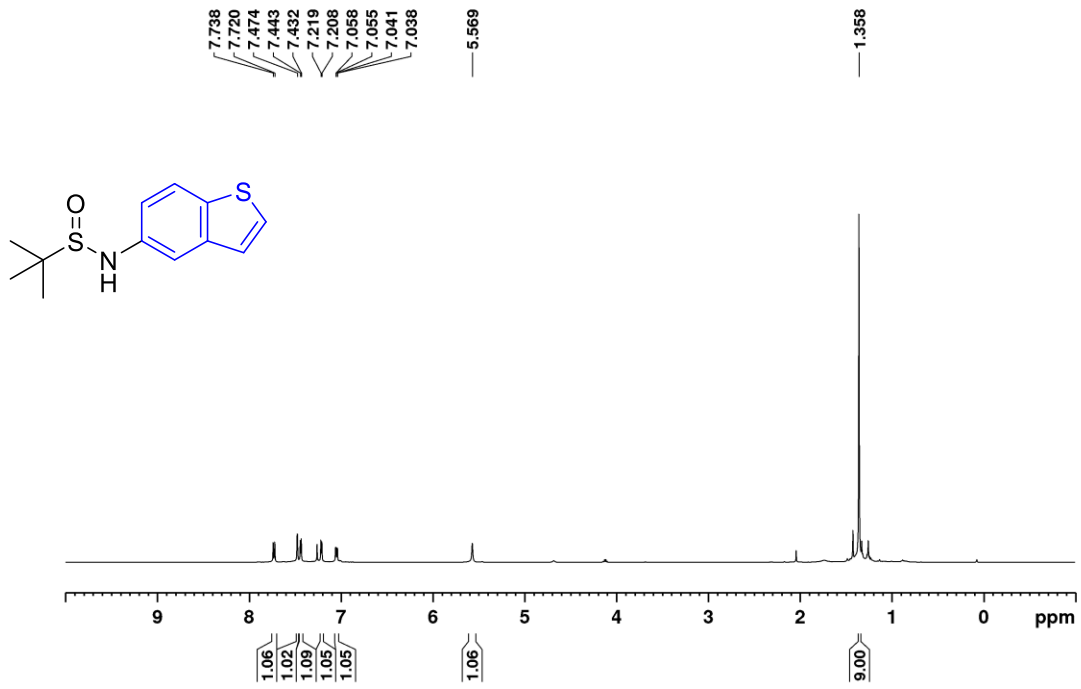

Figure A34. $^{13}C\{^{1}H\}$ UDEFT NMR Spectrum of **3i** (125.8 MHz, $CDCl_3$)

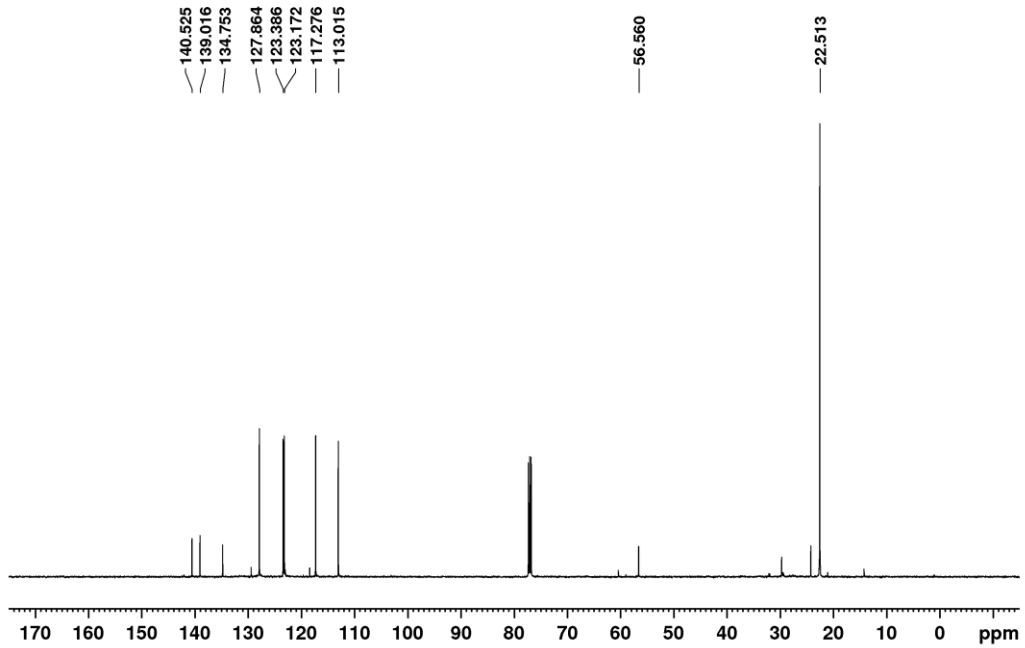

Figure A35. ^{1}H NMR Spectrum of **3j** (500.1 MHz, $CDCl_3$)

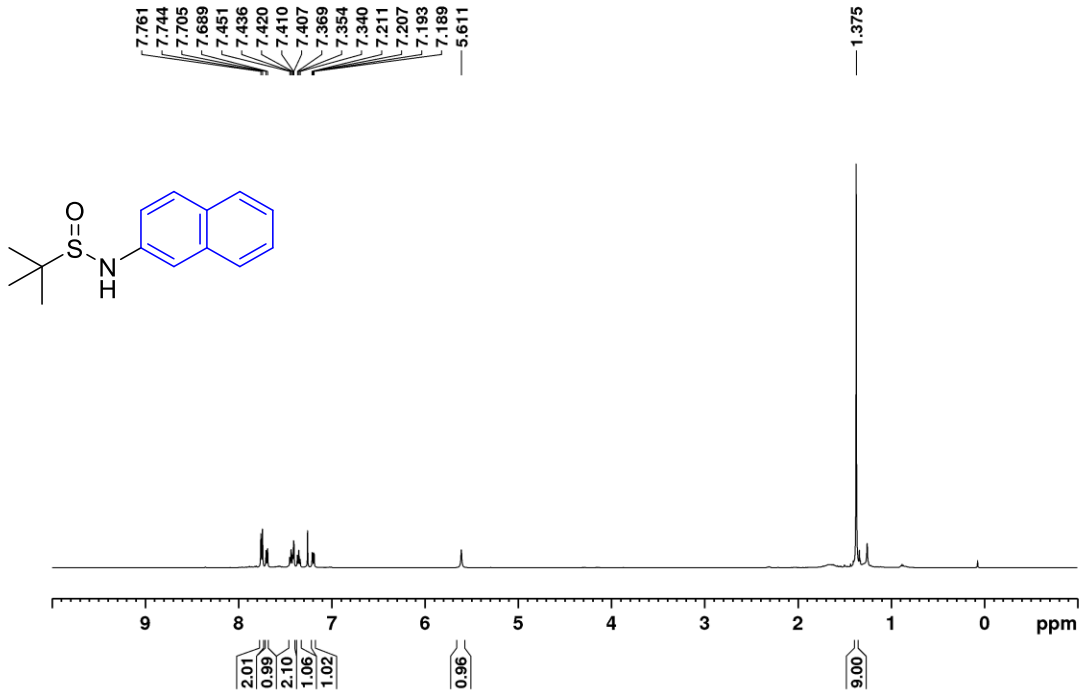

Figure A36. $^{13}C\{^{1}H\}$ UDEFT NMR Spectrum of **3j** (125.8 MHz, $CDCl_3$)

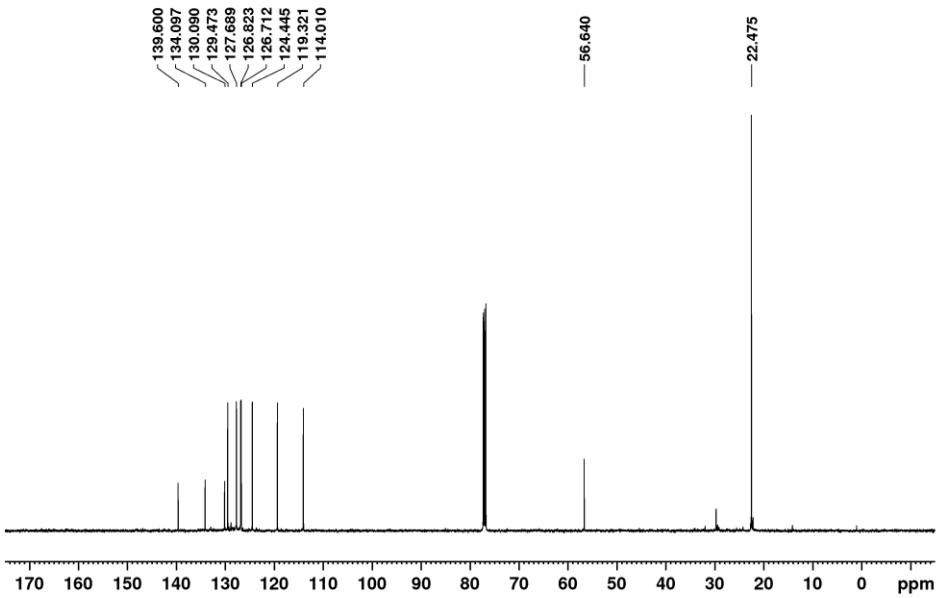

Figure A37. ^{1}H NMR Spectrum of **3k** (500.1 MHz, $CDCl_3$)

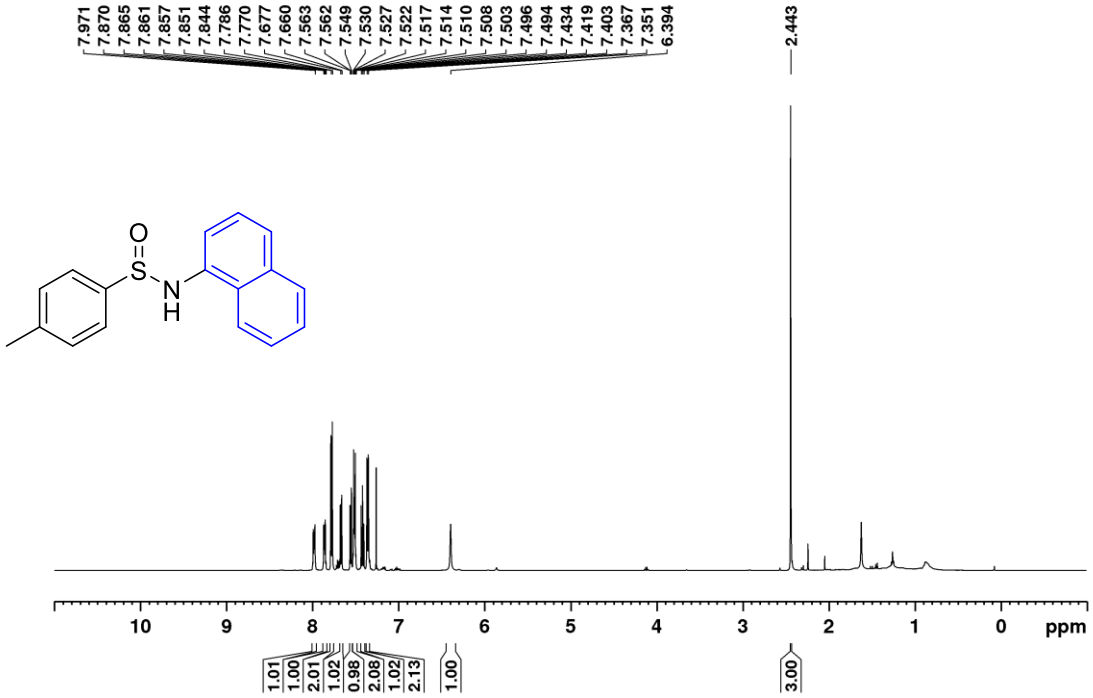

Figure A38. $^{13}C\{^{1}H\}$ UDEFT NMR Spectrum of **3k** (125.8 MHz, $CDCl_3$)

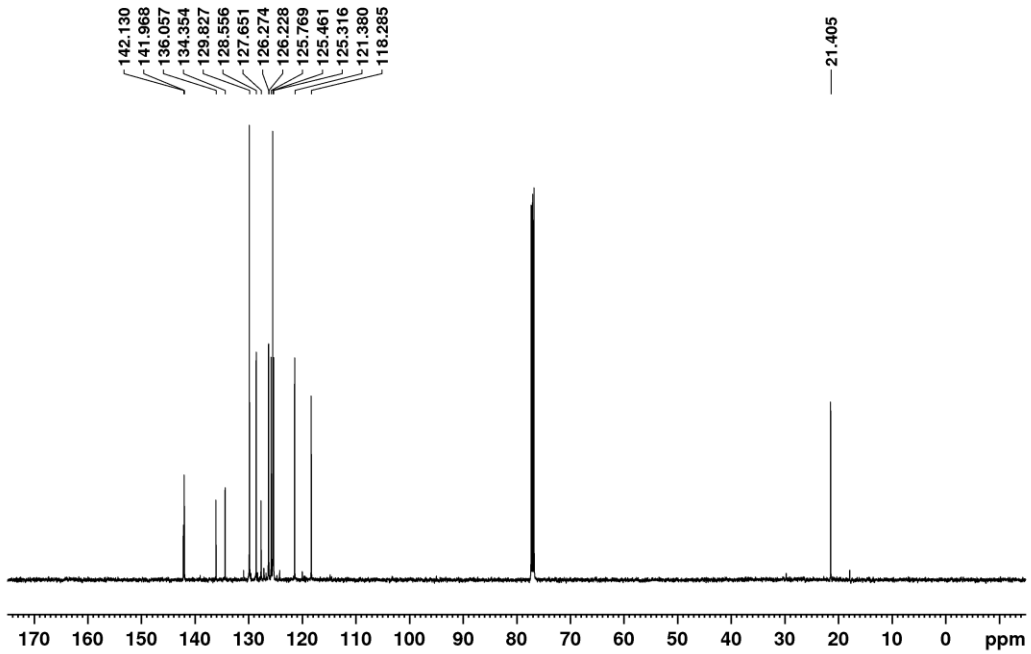

Figure A39. $^{31}P\{^{1}H\}$ NMR Spectrum of **C4** (202.5 MHz, C_6D_6)

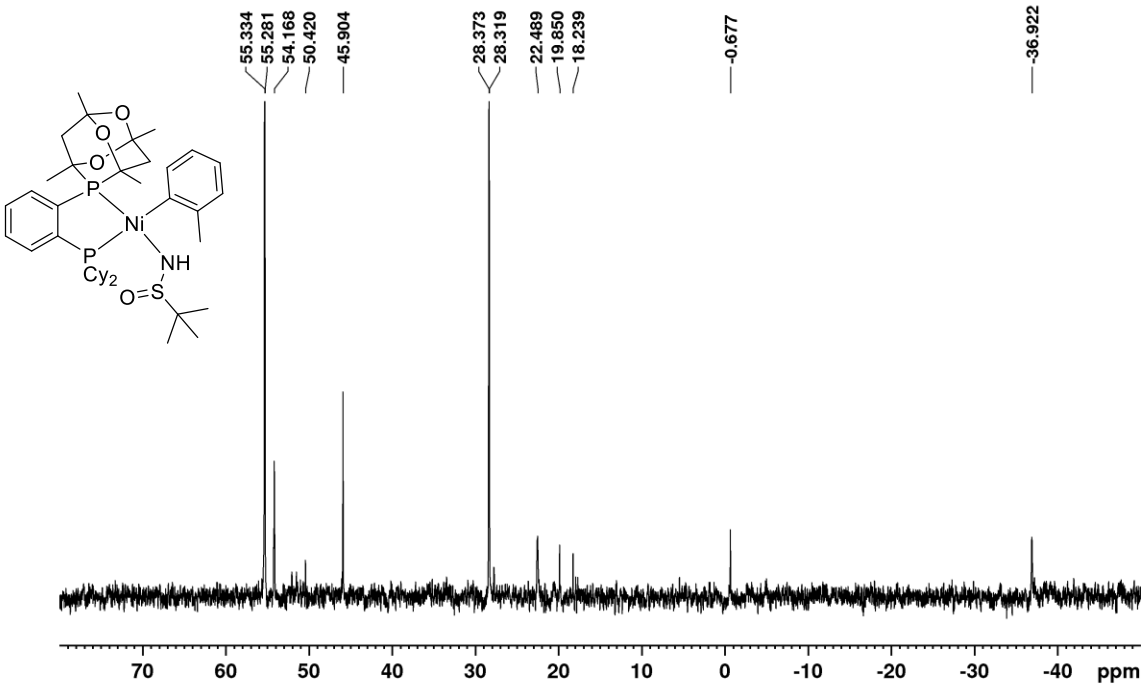

Figure A40. ^{1}H NMR Spectrum of **C4** (500.1 MHz, C_6D_6)

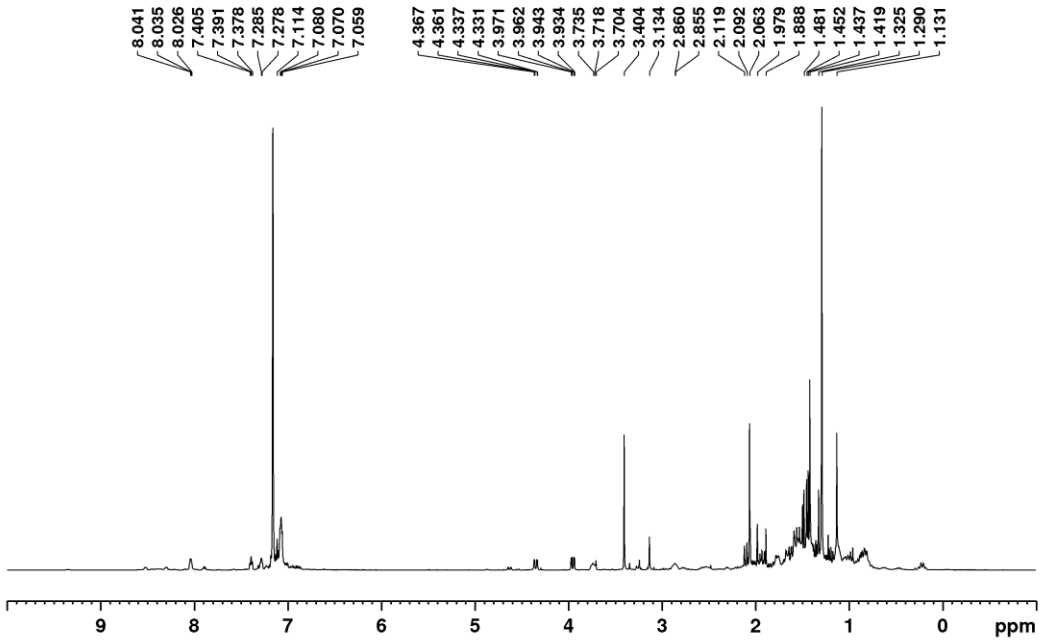

Figure A41. $^{13}C\{^{1}H\}$ UDEFT NMR Spectrum of **C4** (125.8 MHz, C_6D_6)

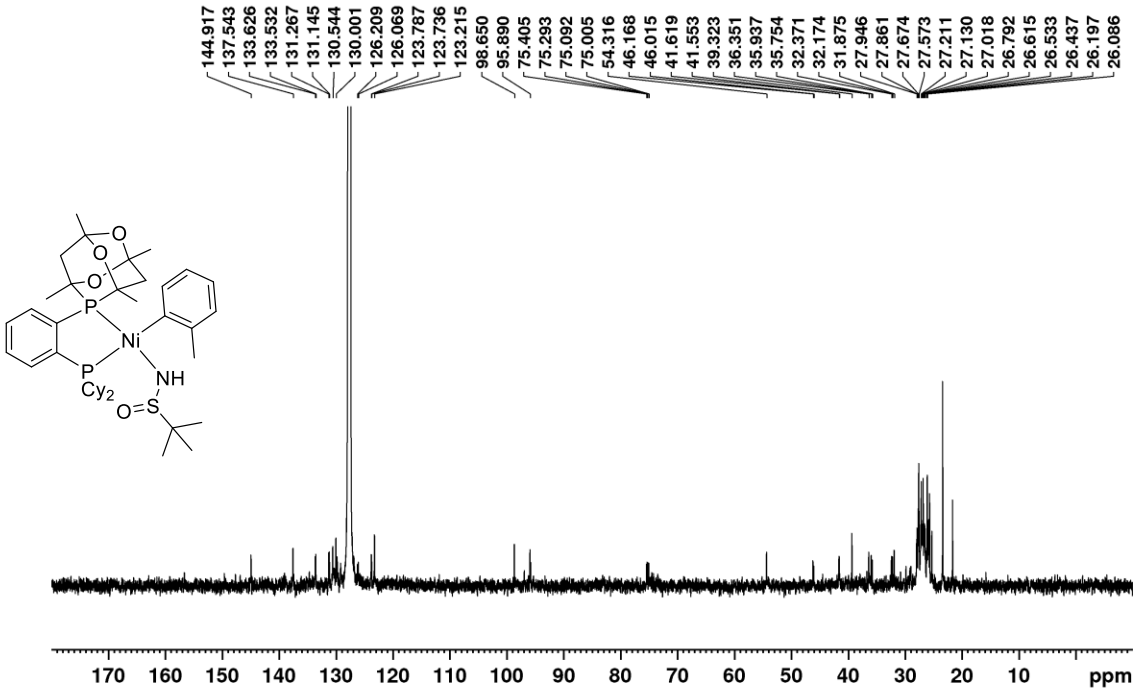

Figure A42. $^{31}P\{^{1}H\}$ NMR Spectrum of **C5** (202.5 MHz, C_6D_6)

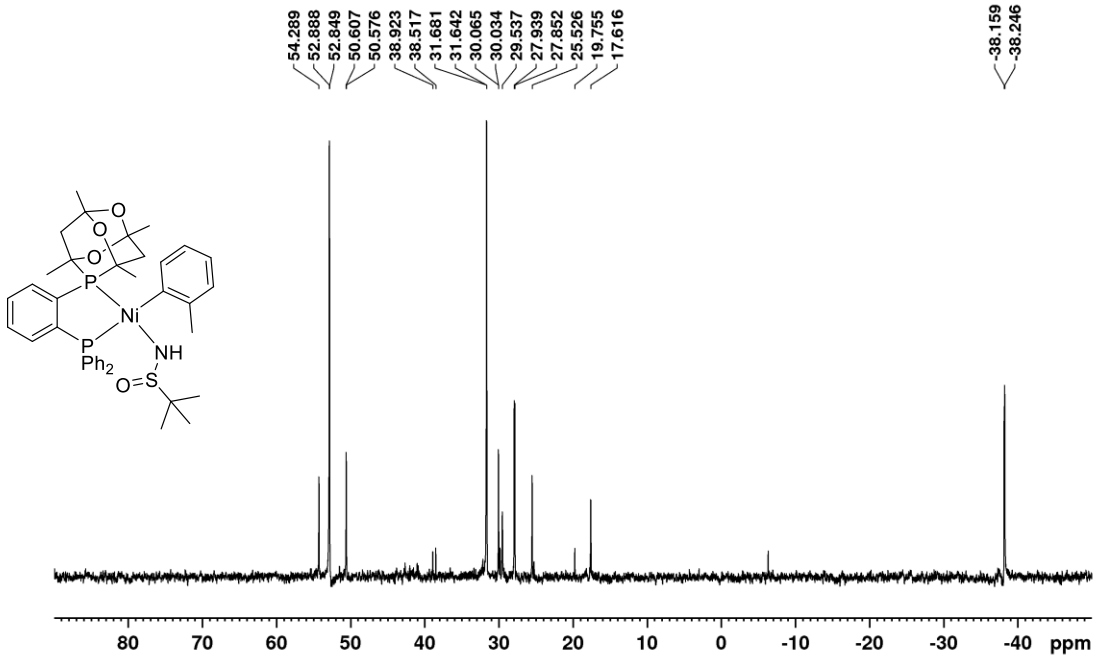

Figure A43. ^{1}H NMR Spectrum of **C5** (500.1 MHz, C_6D_6)

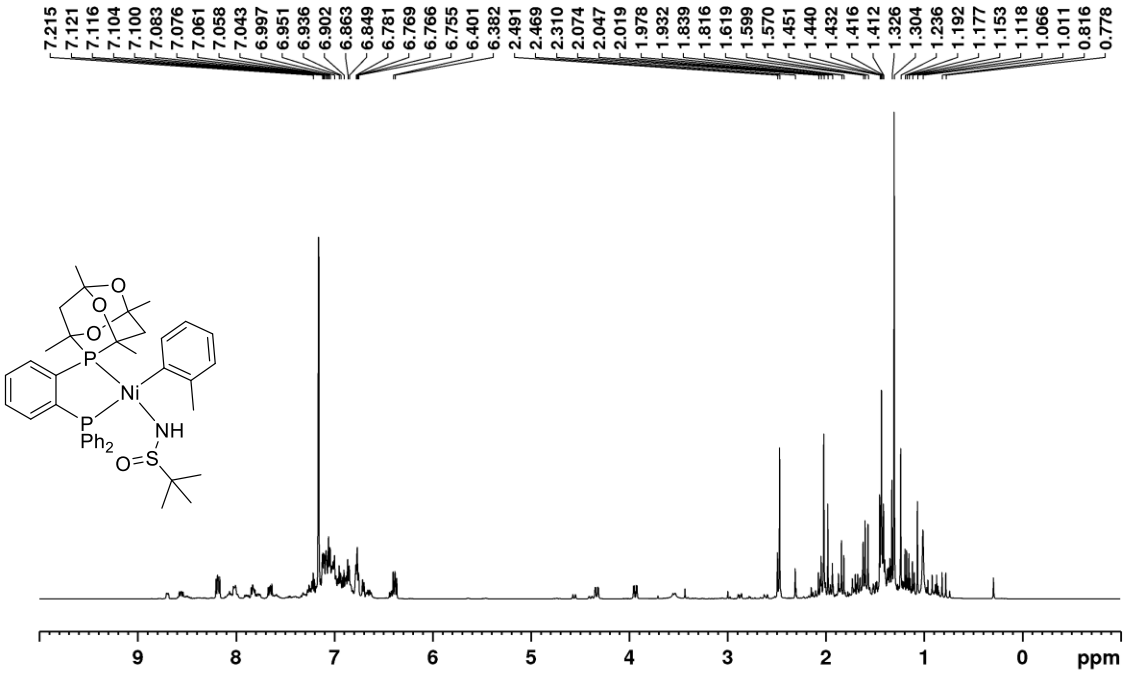

Figure A44. $^{13}C\{^{1}H\}$ UDEFT NMR Spectrum of **C5** (125.8 MHz, C_6D_6)

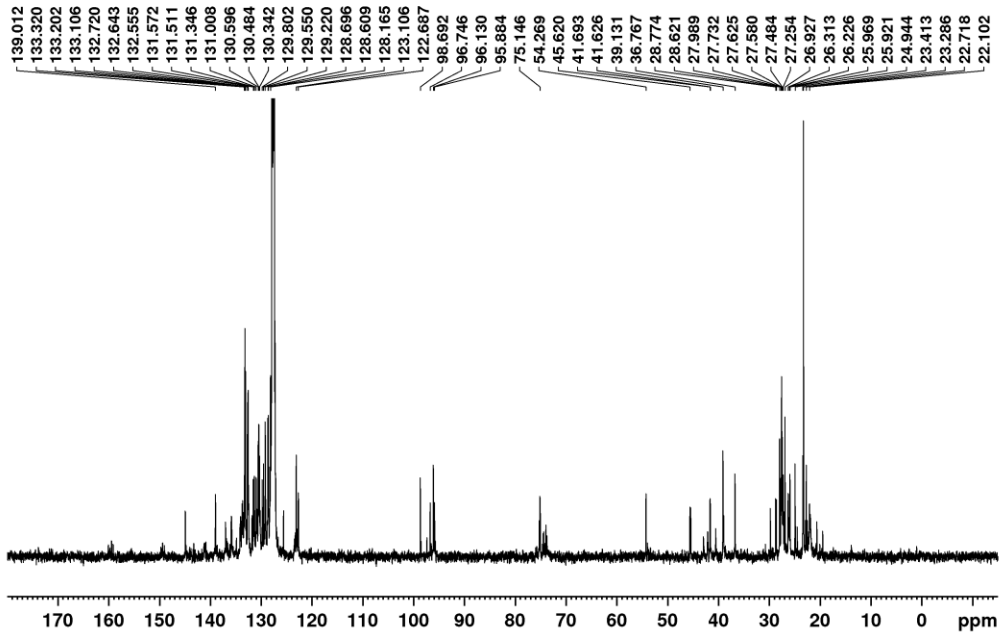

Appendix 4: Chapter 3 X-Ray Data

In each case the crystal chosen was attached to the tip of a MicroLoop with Paratone-N oil. Measurements were made on a Bruker D8 VENTURE diffractometer equipped with a PHOTON III CMOS detector using monochromated Mo Kα radiation (λ = 0.71073 Å) from an Incoatec micro-focus sealed tube at 125 K (Bruker, 2018, Brucker AXS Inc., Madison, Wisconsin, USA). The initial orientation and unit cell were indexed using a least-squares analysis of the reflections collected from a 180° phi-scan, 5 seconds per frame and 1° per frame. For data collection, a strategy was calculated to maximize data completeness and multiplicity, in a reasonable amount of time, and then implemented using the Bruker Apex 4 software suite (Bruker, 2018, Bruker AXS Inc., Madison, Wisconsin, USA). The crystal to detector distance was set to 4.0 cm and 120 second frames (0.5° per frame) were collected. Cell refinement and data reduction were performed with the Bruker SAINT (Bruker, 2016, Bruker AXS Inc., Madison, Wisconsin, USA) software, which corrects for beam inhomogeneity, possible crystal decay, Lorentz and polarisation effects. A multi-scan absorption correction was applied (SADABS, Bruker, 2016, Bruker AXS Inc., Madison, Wisconsin, USA). The structure was solved using SHELXT-2014 (Sheldrick, G.M. (2015) *Acta Cryst.,* A71, 3-8) and was refined using a full-matrix least-squares method on F^2 with SHELXL-2018 (Sheldrick, G.M. (2015) *Acta Cryst.,* C71, 3-8). The non-hydrogen atoms were refined anisotropically. The hydrogen atoms bonded to carbon were included at geometrically idealized positions and were not refined. The isotropic thermal parameters of these hydrogen atoms were fixed at $1.2U_{eq}$ of the parent carbon atom or $1.5U_{eq}$ for methyl hydrogens. The position of the hydrogen atom bonded to nitrogen was located in a near final Fourier difference map. It was added into the refinement with U_{iso}(H) equal to 1.5 U_{eq}(N) and a weak restraint on the N-H bond length.

Crystal Structure of C4·pentane (herein C4) (CCDC 2214559)

Seven reflections were removed from the refinement because of poor agreement between F_{obs}^2 and F_{calc}^2, the first five because they were almost totally or partially obscured by the beam stop. Data was collected to try and reach a maximum resolution of 0.75 Å. However, the resolution obtained was only 0.80 Å (θ_{max} = 26.39°) so the data was integrated to this limit.

The molecule was found to crystallize in the non-centrosymmetric Orthorhombic space group $P2_12_12_1$. The asymmetric unit was found to contain one complete molecule of the product plus one well ordered molecule of pentane solvent. The crystal proved to be an inversion twin so BASF was refined to give a value of 0.500(18). The program Platon was then used to calculate a value for the Hooft parameter which proved to be 0.489(4).

The structure was found to be disordered. The methylphenyl ring can be coordinated to the nickel atom with either face up, resulting in the methyl group being sometimes located on one side of the ring or the other. The disorder was defined using a two part model, with the total occupancy set to one. The geometries of each part were restrained to be similar, and the carbon atoms involved in the disorder were restrained to have similar thermal

parameters. Bond lengths from the disordered ring to nickel were restrained to be similar. The major component of the disordered model was refined to have an occupancy of 85.1(6) % leaving an occupancy of 14.9 % for the minor component. finally, bond length restraints were also imposed within the pentane solvent molecule.

Table A4. Crystallographic Experimental Details for **C4**

Identification code	MS014_CS3	
Empirical formula	$C_{44}H_{71}NNiO_4P_2S$	
Formula weight	830.72	
Temperature	125(2) K	
Wavelength	0.71073 Å	
Crystal system	Orthorhombic	
Space group	$P2_12_12_1$	
Unit cell dimensions	*a* = 12.4057(6) Å	□= 90°
	b = 18.5536(7) Å	b= 90°
	c = 19.7968(8) Å	g = 90°
Volume	4556.6(3) $Å^3$	
Z	4	
Density (calculated)	1.211 Mg/m^3	
Absorption coefficient	0.581 mm^{-1}	
F(000)	1792	
Crystal size	0.091 x 0.062 x 0.050 mm^3	
Theta range for data collection	2.227 to 26.387°	
Index ranges	-15<=h<=15, -23<=k<=23, -24<=l<=24	
Reflections collected	51962	
Independent reflections	9312 [R(int) = 0.0683]	
Completeness to theta = 25.242°	99.8 %	
Absorption correction	Semi-empirical from equivalents	
Max. and min. transmission	0.7454 and 0.6248	
Refinement method	Full-matrix least-squares on F^2	
Data / restraints / parameters	9312 / 248 / 555	
Goodness-of-fit on F^2	1.160	
Final R indices [I>2sigma(I)]	R_1 = 0.0496, wR_2 = 0.0965	
R indices (all data)	R_1 = 0.0587, wR_2 = 0.0992	
Absolute structure parameter	0.500(18)	

Extinction coefficient	n/a
Largest diff. peak and hole	0.421 and -0.338 e.Å^{-3}

Crystal Structure of C5·benzene (herein C5) (CCDC 2214560)

Three reflections were removed from the refinement because of poor agreement between F_{obs}^2 and F_{calc}^2, the first two because they were almost totally obscured by the beam stop. Data was collected to try and reach a maximum resolution of 0.50 Å. However, the resolution obtained was only 0.60 Å (θ_{max} = 36.34°) so the data was integrated to this limit.

The molecule was found to crystallize in the centrosymmetric Monoclinic space group $P2_1/n$. While enantioenriched (*R*)-*tert*-butylsulfinamide (98%) was employed in the synthesis of **C5**, the observation of a centrosymmetric space group for this compound implies that the sulfinamido moiety in the crystal structure of **C5** is racemic, which is feasible given the purity level of the (*R*)-*tert*-butylsulfinamide used.

The asymmetric unit was found to contain one complete molecule of the product plus one molecule of badly disordered benzene solvent. The solvent atoms were split over 3 positions with the total occupancy of the 3 parts refined to total to one using a SUMP instruction. The geometries of the parts were restrained to be similar, the benzene rings were restrained to be flat and the carbon atoms of the rings were restrained to have similar thermal parameters. The occupancies of the three parts of the disorder refined to values of 45.8(3) %, 34.2(3) % and 20.1(3) %.

Once the disorder of the solvent had been resolved, it became apparent that there was a small amount of disorder also present in the main molecule (as seen in the pattern of the residual density in the difference Fourier map). In particular, the largest residual electron density peak suggested a second position for the sulfur atom of the *tert*-butylsulfinamide ligand. This ligand and the central nickel atom were split over two parts, with the total occupancy set to one. The geometries of each part were restrained to be similar, and all of the atoms of the same types involved in the disorder were restrained to have similar (separate) thermal parameters. Bond lengths from the disordered parts of the molecule to the ordered parts were restrained to be similar. The major component of the disordered model was refined to have an occupancy of 97.45(9) % leaving an occupancy of only 2.55 % for the minor component. Perhaps not surprisingly, a hydrogen bond acceptor could not be located for the H(N) atom in the minor part of the disorder. The crystal structure of **C5** below is represented by 50% probability ellipsoids with selected H-atoms/solvates removed for clarity.

Table A5. Crystallographic Experimental Details for **C5**

Identification code	MS013_CS2	
Empirical formula	$C_{45}H_{53}NNiO_4P_2S$	
Formula weight	824.59	
Temperature	125(2) K	
Wavelength	0.71073 Å	
Crystal system	Monoclinic	
Space group	$P2_1/n$	
Unit cell dimensions	a = 12.4797(3) Å	a = 90°
	b = 16.9885(5) Å	b = 91.1002(10)°
	c = 20.0614(5) Å	g = 90°
Volume	4252.46(19) $Å^3$	
Z	4	
Density (calculated)	1.288 Mg/m^3	
Absorption coefficient	0.623 mm^{-1}	
F(000)	1744	
Crystal size	0.335 x 0.179 x 0.123 mm^3	
Theta range for data collection	1.939 to 36.342°	
Index ranges	-20<=h<=20, -28<=k<=28, -33<=l<=33	
Reflections collected	335016	
Independent reflections	20638 [R(int) = 0.0383]	
Completeness to theta = 25.242°	99.9 %	
Absorption correction	Semi-empirical from equivalents	
Max. and min. transmission	0.7471 and 0.6788	
Refinement method	Full-matrix least-squares on F^2	
Data / restraints / parameters	20638 / 625 / 680	
Goodness-of-fit on F^2	1.139	
Final R indices [I>2sigma(I)]	R_1 = 0.0338, wR_2 = 0.0875	
R indices (all data)	R_1 = 0.0448, wR_2 = 0.0982	
Extinction coefficient	n/a	
Largest diff. peak and hole	0.536 and -0.485 $e.Å^{-3}$	

Crystal Structure of C6 [(CyPAd)Ni(*o*-tol) dimer]

The crystal chosen was attached to the tip of a MicroLoop with Paratone-N oil. Measurements were made on a Bruker D8 VENTURE diffractometer equipped with a PHOTON III CMOS detector using monochromated Mo Kα radiation (λ = 0.71073 Å) from an Incoatec micro-focus sealed tube at 125 K APEX 4 (Bruker, 2021) Bruker AXS Inc., Madison, Wisconsin, USA.. The initial orientation and unit cell were indexed using a least-squares analysis of the reflections collected from a 180° phi-scan, 5 seconds per frame and 1° per frame. For data collection, a strategy was calculated to maximize data completeness and multiplicity, in a reasonable amount of time, and then implemented using the Bruker Apex 4 software suite APEX 4 (Bruker, 2021) Bruker AXS Inc., Madison, Wisconsin, USA.. The crystal to detector distance was set to 4.0 cm and 25 second frames (0.5° per frame) were collected. Cell refinement and data reduction were performed with the Bruker SAINT SAINT (Bruker, 2019) Bruker AXS Inc., Madison, Wisconsin, USA. software, which corrects for beam inhomogeneity, possible crystal decay, Lorentz and polarisation effects. A multi-scan absorption correction was applied (SADABS SAINT (Bruker, 2019) Bruker AXS Inc., Madison, Wisconsin, USA.). The structure was solved using SHELXT-2014 SAINT (Bruker, 2019) Bruker AXS Inc., Madison, Wisconsin, USA. and was refined using a full-matrix least-squares method on F^2 with SHELXL-2018 SAINT (Bruker, 2019) Bruker AXS Inc., Madison, Wisconsin, USA.. The non-hydrogen atoms were refined anisotropically. The hydrogen atoms bonded to carbon were included at geometrically idealized positions and were not refined. The isotropic thermal parameters of these hydrogen atoms were fixed at $1.2U_{eq}$ of the parent carbon atom or $1.5U_{eq}$ for methyl hydrogens.

Data was collected to try and reach a maximum resolution of 0.70 Å. However, the resolution obtained was only 0.80 Å (θ_{max} = 26.39°) so the data was integrated to this limit. Three reflections were removed from the refinement because of poor agreement between F_{obs}^2 and F_{calc}^2, the first two because they were almost totally or partially obscured by the beam stop.

The molecule was found to crystallize in the centrosymmetric Monoclinic space group $P2_1/c$. The asymmetric unit was found to contain one complete molecule of the dimeric product plus one disordered molecule of pentane solvent. In addition, there was a second cluster of solvent present in the asymmetric unit. Based on the peaks visible in the Fourier difference maps and the statistics of the refinement, the best model obtained was for a partially occupied mixture of benzene and pentane; the occupancy of the mixture components was refined to a total of one using a free variable.

The solvent molecules were very disordered. The first pentane molecule was split over three sets of positions, with the total occupancy of the three parts set to total one. Bond length restraints were imposed within the pentane solvent molecules and the atoms were restrained to have similar anisotropic displacement parameters. The occupancies of the three parts refined to 41.0(6), 42.5(7) and 16.6(6) %, respectively.

The second solvated region in the asymmetric unit was found to contain a mixture of benzene and pentane. The pentane was treated as described above, while the bond lengths in the benzene ring were restrained and its atoms were restrained to have similar anisotropic displacement parameters. The occupancy of the benzene molecule refined to 82.4(4) % giving 17.6 % occupancy for the pentane in the same space.

The structure of the Ni dimer was also found to be disordered, with all of the coordinated groups except the cyclohexyl rings occupying two distinct positions. In addition, all of the phosphorus atoms were included in the disorder, except for P2 which was not split. The disorder in the dimer was refined in two sections. Section 1 included P1 and the two groups bonded to it. The second section involved P3, P4 and the two groups bonded to P3. Each section was refined using a two part model for the disorder, with the total occupancy of the atoms in each section set to one. The geometries of each part were restrained to be similar, and the phosphorus and carbon atoms involved in the same disordered groups were restrained to have similar thermal parameters. Bond lengths from the disordered parts to the ordered part of the structure were restrained to be similar. Restraints were added to keep the phenyl rings in the dimer flat. Enhanced rigid bond restraints were placed over the entire structure. The major component of the disordered model for section 1 was refined to have an occupancy of 83.9(6) % leaving an occupancy of 16.1 % for the minor component. For section 2 the occupancies refined to 70.1(5) % and 19.9 %, respectively.

Finally, the dimer was bridged by something, coordinated roughly equidistant to both nickel centers, which appeared as a single peak in the original Fourier difference maps. Refinement of this atom worked best for it being a sulfur atom. For example, refining the occupancy of this atom and keeping everything else constant, near the end of this investigation, gave nearly identical statistical results for P, S and Cl. However, the respective occupancies refined to 1.039(3), 0.977(3) and 0.910(3). Fixing the occupancy at one for each of those atoms and refining, gave R1 values of 0.0373, 0.0371 and 0.0383, respectively.

While these results suggest S, or maybe P, as the bridging atom, it made more chemical sense that the bridging atom be Cl. Since the site was not completely occupied by Cl, it also made chemical sense that the minor component (which needed to be of less mass) would be oxygen. Thus, a two component model was chosen, where the occupancies of Cl and O were refined to total one. The two atoms, occupying nearly identical positions in the structure, were restrained to have the same anisotropic displacement parameters. The final occupancies refined to 84.3(6) % for chlorine and thus 15.7 % for oxygen. There was no evidence of hydrogen atoms coordinated to this oxygen in the final Fourier difference maps and no attempts were made to place hydrogen atoms of any geometry on this atom. It is still completely possible, based on the crystallographic results, that the bridging atom is sulfur and not Cl/O as has been reported here.

Table A6. Crystal data and structure refinement for **C6**

Identification code	MS015_CS4	
Empirical formula	$C_{66.83}H_{103.07}Cl_{0.84}Ni_2O_{6.16}P_4$	
Formula weight	1276.15	
Temperature	125(2) K	
Wavelength	0.71073 Å	
Crystal system	Monoclinic	
Space group	$P2_1/c$	
Unit cell dimensions	a = 19.8877(7) Å	a= 90°
	b = 12.7243(5) Å	b= 98.1374(15)°
	c = 26.6135(11) Å	g = 90°
Volume	6666.9(4) $Å^3$	
Z	4	
Density (calculated)	1.271 Mg/m^3	
Absorption coefficient	0.743 mm^{-1}	
F(000)	2734	
Crystal size	0.139 x 0.112 x 0.076 mm^3	
Theta range for data collection	1.978 to 26.385°	
Index ranges	-24<=h<=24, -15<=k<=15, -33<=l<=33	
Reflections collected	215191	
Independent reflections	13616 [R(int) = 0.0521]	
Completeness to theta = 25.242°	99.9 %	
Absorption correction	Semi-empirical from equivalents	
Max. and min. transmission	0.7454 and 0.6860	
Refinement method	Full-matrix least-squares on F^2	
Data / restraints / parameters	13616 / 2980 / 1243	
Goodness-of-fit on F^2	1.111	
Final R indices [I>2sigma(I)]	R_1 = 0.0372, wR_2 = 0.0906	
R indices (all data)	R_1 = 0.0451, wR_2 = 0.0954	
Extinction coefficient	n/a	
Largest diff. peak and hole	0.525 and -0.466 e.$Å^{-3}$	

Figure A45. Solved solid state structure of **C6** represented by 50% probability ellipsoids with selected H-atoms/solvates removed for clarity.